MODERN PROCESS PLANNING FOR ADDITIVE MANUFACTURING ASSISTED A356 ALUMINUM CASTING

By

MIKAEL ANDREW GARCIA

Bachelor of Science in Metallurgical and Materials Engineering

University of Texas at El Paso

El Paso, TX

2017

Bachelor of Science in Mechanical Engineering

University of Texas at El Paso

El Paso, TX

2019

Submitted to the Faculty of the
Graduate College of the
Oklahoma State University
in partial fulfillment of
the requirements for
the Degree of
MASTER OF SCIENCE
May, 2023

MODERN PROCESS PLANNING FOR

ADDITIVE MANUFACTURING ASSISTED

A356 ALUMINUM CASTING

Thesis Approved:

Vaidyanathan, Ranji, Ph.D.

Thesis Adviser

Bair, Jacob, Ph.D.

Connor, Joseph, Ph.D.

ACKNOWLEDGEMENTS

Dr. Vaidyanathan, for advisory through my graduate career
Dr. Bair, for the guidance on simulations
Dr. Conner, for the direction for experimental practice

I would like to extend a warming thanks to my advisor, Dr. Vaidyanathan, for forming the casting research group at Oklahoma State University. His direction and counseling helped me gather the insight to organize and share this information as a collaborative effort of the research circle.

I would like to thank Dr. Bair for the guidance with simulations and design modifications that reinforced this project. I started off completely new to the phase field technique and gained working knowledge to use it as a powerful tool for process development.

I would like to thank the research team including Jefferson Harrison, Michael Costa, and John Gage for the background information from the original casting sessions that were performed at the Design and Manufacturing Lab at Stillwater, OK.

This project was funded by the Air Force. Lastly, I would like to thank Michael Thompson, Ryan Fowler, and Ryan Hill, the engineers from Tinker Air Force Base that supported the team with molds sand casting.

Name: MIKAEL ANDREW GARCIA

Date of Degree: MAY, 2023

Title of Study: MODERN PROCESS PLANNING FOR ADDITIVE MANUFACTURING ASSISTED A356 ALUMINUM CASTING

Major Field: MATERIALS SCIENCE AND ENGINEERING

Abstract: Foundry engineering integrates mechanical design, thermal-fluid dynamics, and material science to cast components of a unique design. This project was intended to apply these concepts to optimize the casting process of an aircraft Bearing Housing by applying the design flexibility obtained from additive manufacturing (AM). The two AM processes that were studied include 3D sand printing and 3D wax printing to determine their advantages when applied to sand and investment casting, respectively. For efficiency, generative design (GD), computational fluid dynamic (CFD), and phase field (PF) simulation were used to rapidly compare the outcomes of multiple rigging systems prior to 3D printing molds. Once verifying the optimal design based on the part's geometry, the mold prototypes were printed and casted in controlled laboratory conditions. The material properties were tested and characterized at critical cross sections to verify consistency of results to the simulated environments.

TABLE OF CONTENTS

Chapter Page

LIST OF TABLES

Table Page

LIST OF FIGURES

Figure Page

Figure Page

CHAPTER I

INTRODUCTION

Scope

Metal casting is a manufacturing process where liquid metal is poured into a cavity, referred to as a mold, to form a final shape after solidification. Numerous casting methods have long been accepted for production of components with acceptable properties that allows designers to optimize functionality, obtain net or near-net shape, and produce intricate components as a single cast part with grew restrictions on weight or size [1] . In recent years, strength-to-weight ratios of entire mechanical assemblies have been significantly increased by using components of highly complex geometries, often developed through artificial intelligence [2]–[4]. The demand for design complexity in aviation and automotive industries has risen drastically because it decreases costs and increases efficiency and performance of their products[5], [6].

This has damaged many traditional casting companies. Foundries across the world have gone under due to the inability to create molds of such intricate designs. This may have been due to the cost of custom-made tooling to produce molds, or the molds are deemed physically impossible to create by conventional methods [7]. When geometric complexity is in demand, AM is widely known as a golden ticket to deliver

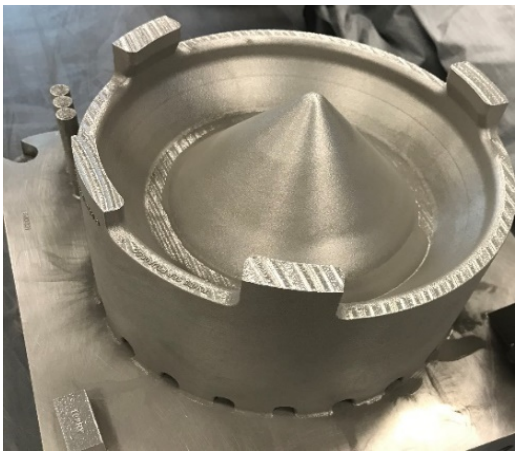

(a)

(b)

Figure 1: AM Produced GE Components . Additive Manufactured (a) Sump Cover for the F110 Engine and (b) Fuel Nozzle for the LEEP Engine, courtesy of General Electric

The most practiced AM method for metal components is laser powder bed fusion (LPBF). Unfortunately, these parts have very low fatigue resistance due to LPBF-related defects such as porosity, unwanted anomalies, surface roughness, and powder contamination [8], [9]. LPBF may also be costly due to powder contamination and yield undesirable microstructures that can result in inferior mechanical properties, decreased performance, and be of high risk for failure [10], [11]. In aviation, this makes it very difficult and time-consuming to accept LPBF parts for critical, high load bearing applications. Only recently has General Electric developed a proprietary LPBF process to produce components that are deemed air worthy, such as the F110 Sump Cover and Fuel Nozzles for the LEAP engine shown in Figure 1 [12]–[14]. Accepting of LPBF parts on aircraft assemblies is a breakthrough for the aerospace industry. However, casting will always be the preferred manufacturing method for most critical components, such as Housings for Bearings, due to cost and material properties [15]. This project serves as a comprehensive foundation that describes how to use AM to keep the casting industry alive.

There are numerous forms of AM techniques available on the market apart from LPBF. Binder jet deposition is a form of which a liquid is deposited in 2D profiles along a layer-by-layer powder bed of a

selected material as shown in Figure 2 [16]. This is the technique used for sand and wax printing used to produce molds for metal casting, which has enabled foundries to produce complex components with the desirable material properties that are only obtained from casting processes [7], [16]–[18].

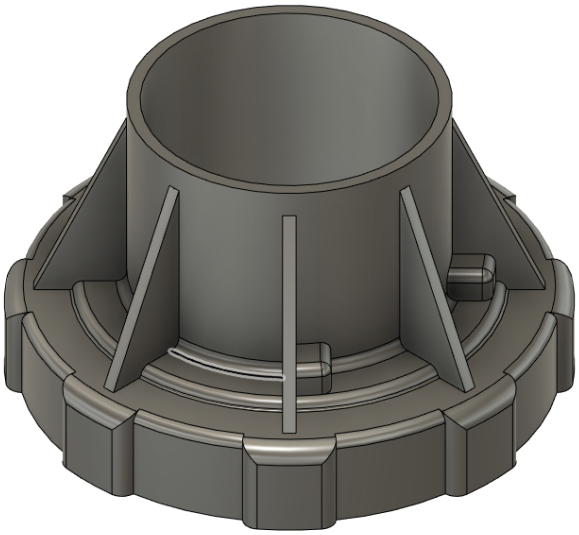

Figure 2: Bearing Housing. Bearing Housing - Designed in Fusion360

Background

In this study Binder/Wax jet deposition will be referred to as AM and will be applied to sand and investment casting of the Bearing Housing shown in Figure 2. Experimenting with this design was approved by the Air Force after verifying the physical dimensions were modified in such a way that it does not match the original part used in jet engine assembly. Even though the experimental design dimensions are far different from the original design, the geometric features are the same. The design team uses the geometric features to generate rapid modifications to the rigging system that produces an improved mold design.

In traditional sand casting, the components that make up the mold are shown in both exploded and assembled views in Figure 3 [18]. It comprises of a cope and a drag with the associated features for metal flow that include the sprue, runners, gates, and risers. A process flow chart for investment casting is shown in Figure 4, which starts with the creation of multiple wax patterns of the desired design. The wax patterns are assembled onto a wax tree that is submerged into a high refractory ceramic slurry that is then coated with high refractory particles. Once the liquid covering the wax tree solidifies, the processes is repeated multiple times that results in a thick high refractory ceramic casing. The ceramic casing is then inverted and placed in a heated environment, such as a furnace or autoclave, where the wax melts out leaving an

empty shell containing a cavity of the desired shape as the mold for pouring. After solidification, the ceramic shell is broken, and the parts undergo required post processing [19]. The advantages and disadvantages to the two casting techniques help manufacturers stipulate the appropriate process based on the component in consideration. After addressing the critical elements of casting materials, processes, and geometries, AM will be discussed as to how advanced mold configurations brings about ample improvements and cost savings to the casting industry.

Foundries are constantly looking for ways to increase their profit margins [7] so this study focuses on applying GD, CFD, and PF simulations to design an optimal rigging system. The proceeding sections will address design and processing problems that are encountered in traditional casting.

In practical foundries, a team is required to meet regularly to discuss what changes need to be implemented for improvement based on geometry, process, and material interactions [19]. This is essential considering every casted component has a unique geometry, so mold production needs to be modified to tailor to the final product. Therefore, special focus will be taken to typical design features of a part that present concern for casting defects and how they can be circumvented.

Figure 3: Investment Casting. Investment Casting Process. The process starts with the production of wax patterns and assembling them onto a “tree”. The tree is submerged (invested) into a ceramic slurry and coated with refractory particles at least 5 times and cured to produce a thick shell around the tree. The assembly is inverted and placed in an autoclave to remove the wax and inverted again for pouring of metal into the empty shell. Once solidified, the shell is cracked, parts are removed, and post processing ensues.

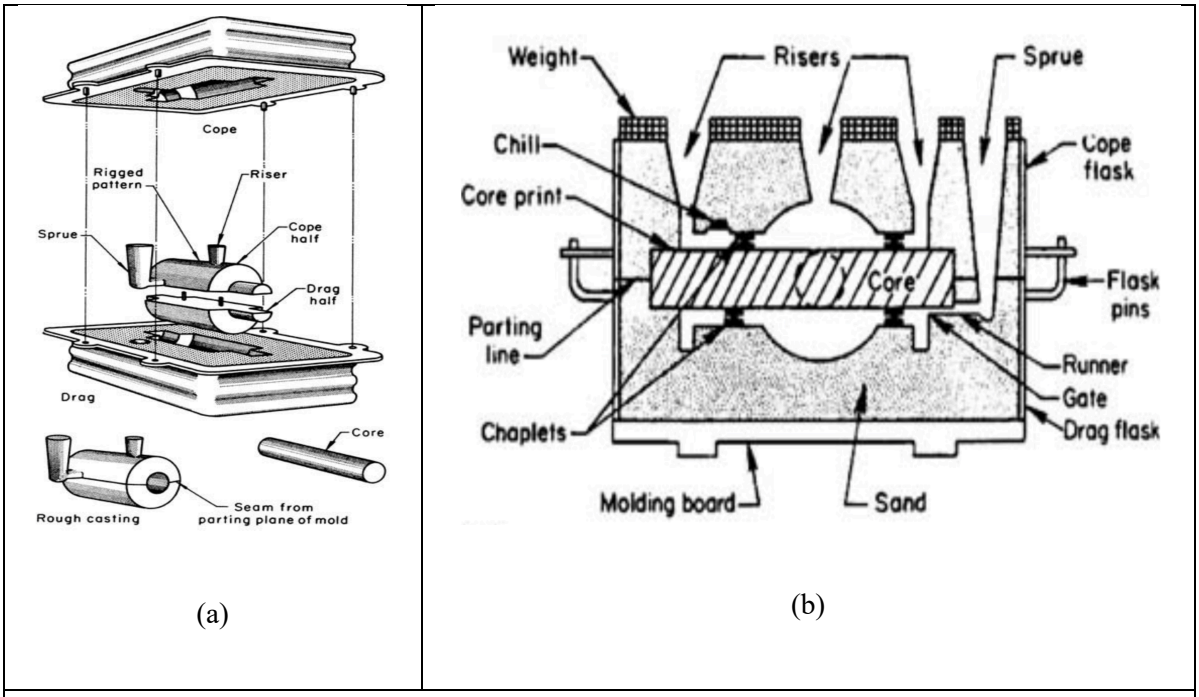

Figure 4: Sand Casting. (a) Exploded view of sand mold components. The top part is called the cope and the bottom part is called the drag. A core is used to select areas where molten metal is not to flow, which helps minimize post processing. (b) Assembled Cross Sectional View. A cross sectional view is the best way to envision where the liquid metal enters the mold through the sprue, fills the cavity in desired areas, and exits the mold at the risers. This model represents a simple design that is easily produced using traditional preparation procedures of filling the cope and drag portions of the flask with sand, packing around a pattern up to the parting plane, removing the pattern and assembling the flask halves. AM assisted sand casting will be discussed later.

Additionally, it is crucial to know original casting techniques that are commonly practiced in traditional foundry operations, which takes year of hands-on practice. The following theory section has been taken from ASM Handbook Volume 15 (Casting) and will be used as a guide to reason the rigging design and casting process for the Bearing Housing. In the casting industry, this helps identify the limitations of conventional casting, which offers a better vision of how AM can be used to improve the design of novel rigging systems [7], [19].

CHAPTER II

THEORY

Bearing Housing: Geometric Evaluation

This section defines traditional casting operations and challenges commonly encountered in traditional mold preparation and processes planning that pertain to the Bearing Housing. This was necessary before using design tactics that effect the outcomes of a casting. Figure 5 identifies the locations and types of geometric features that are classically known to present problems during the casting process.

Preliminary Design Challenges

To be clear, the aim of this project is to develop an "initial" rigging design that can be produced using AM. It was tempting to take liberty with design complexity because it is not limited to simple geometries. To finalize an initial design, numerous iterations and total redesign cycles may be necessary, depending on discussion and/or results obtained from simulations. Minor modifications for optimization will be discussed on the initial design that is produced from this project, which demonstrates how the process eliminates the need for long collaboration sessions for total redesigning for any casted product [20][20].

Design Parameters

Several factors are considered when designing a rigging system. First is fluid life, also called fluidity, which is a physical property of a metal to retain its liquid state. It is influenced by the material and surface characteristics of the mold, alloy composition, surface tension, gas content, suspended inclusions, degree of superheat, flow rate, heat transfer, heat of fusion, and viscosity [17]. It is helpful to consider these when constructing CFD and PF simulations. A356 aluminum has been metallurgically designed to have enhanced fluidity compared to other alloys. Table 1 presents a table comparing A356 to A201, A206, and a couple of superalloys. A356 is a eutectic alloy has excellent fluid life and exhibits little amounts of solidification shrinkage. It has a pouring range of 1300-1400°F, has a high tendency for gas porosity, and is moderately susceptible to slag/dross formation [21]. It melts between 675 and 815°C, which is a freezing

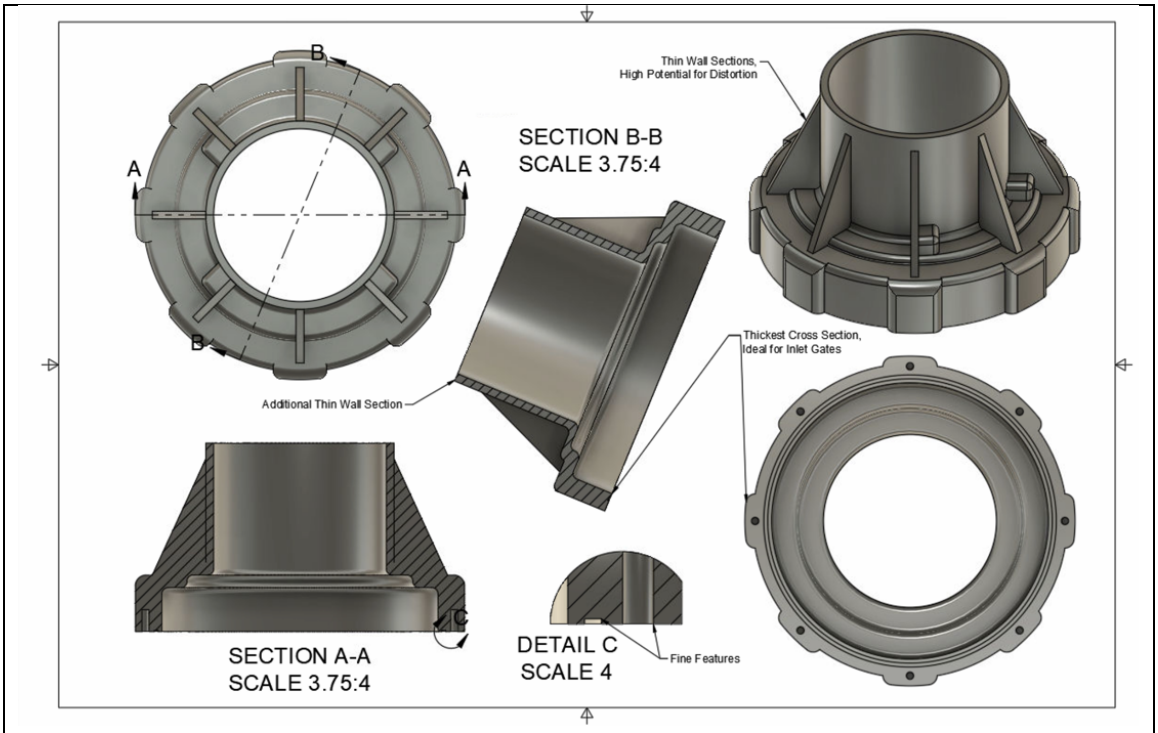

Figure 5: Bearing Housing Design Features. Bearing Housing Design features.

Table 1: Physical Properties of A356. List of physical properties of A356 and A357 in comparison to A201, A206, and a couple of superalloys. These values will be needed later in the design section of this paper.

Alloys are further classified based on their solidification type: directional, eutectic-type, and equiaxed.

Alloy group	Fluid life	Solidification shrinkage		Pour temperature	Gas microporosity	Slag/dross
		Type	Amount			
Superalloys						
Nickel base	Poor	Directional	Moderate	2600–2800 °F	Moderate(+) tendency	Moderate
Cobalt base	Excellent	Directional	Little	2600–2800 °F	Moderate(+) tendency	Little/moderate
Nonferrous						
Aluminum 356, 357	Excellent	Eutectic-type	Little	1300–1400 °F	High tendency	Moderate
Aluminum 201, 206	Good/fair	Equiaxed	Moderate	1300–1400 °F	High tendency	Moderate/large

range of 114°C [22]. These are favorable properties for casting. However, favorable properties can be diminished due to poorly designed rigging systems that can lead to subpar first articles. Casting engineers stay alert to the design parameters and processing conditions to fully utilized the benefits of these properties.

Design Problems

Loss of fluidity occurs from temperature loss and surface tension from oxide films that form at the flow front during filling. This contributes to incomplete filling of the mold cavity, especially in thin sections making it a determining factor for wall thickness and length of thin walled sections [20]. There are ways for designers to compensate for loss of fluidity such as modifying part features to softer shapes, larger lettering, finer detail in the bottom portion of the mold inlet and tapering toward thin sections. A356 has excellent fluidity, but the main concern will be gas porosity and slag/dross formation as listed in the table shown in Table 1.

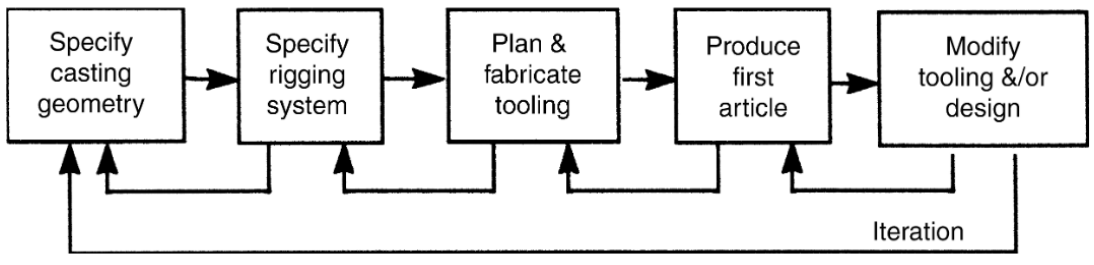

Figure 6: Process Improvement. An example of a 5-Step Approach to Traditional Sand Casting Process Improvement.

The design parameters mentioned above are closely considered when monitoring the material geometry and process interactions. Additional considerations shape optimization and process simulation that pave the way for casting design improvement strategies. To effectively assess problems associated with a design, a team must formulate an evaluation structure to the preliminary designs for the rigging system to determine if they are acceptable or not before carrying on with the course of action. It is an iterative process that is shown by the flow chart in

Figure 6 [20]. The creation of an initial design is the longest part because it requires consideration of unforeseeable problems that the geometry is prone to.

There are many approaches for improving traditional casting processes. A better constructed, 5-Step approach is shown in Figure 7 [20]. Each provides a sufficient description of what is required from a casting manufacturer. These steps were closely followed through the duration of this project. They are listed with connected details as follows:

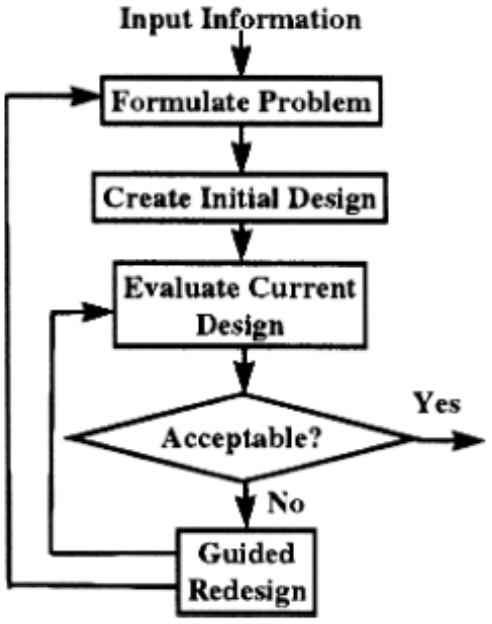

Figure 7: Iterative Design Process. Iterative Model of the Design Process. With this model, confirmation of an initial design ensues the evaluation process for iteration after iteration.

Step 1: Specify Casting Geometry – Combine geometric design and process planning into one concurrent process that integrates shape optimization and rigging system design. Considers geometry, material, process interactions, and cost from start to finish.

Step 2: Specify Rigging System – Establish the customer needs and downstream processing requirements before starting the design.

Step 3: Plan and Fabricate Tooling – Put emphasis on an acceptable initial design that is carried on

with minor adjustments to avoid long evaluation sessions and total redesign. When analyzing iterations, it should be to confirm the design, not produce it.

Step 4: Produce First Article – Use casting simulations and other CAD packages that enable quick optimization.

Step 5: Modify Tooling and/or Design – Keep a database for consistent and well defined troubleshooting techniques for future designs.

Geometric Considerations

Design Problems Involving Distortion

Distortion is a detrimental defect caused by nonuniform contraction of solids at high risk cross sections [23], [24]. Distortion zones are most susceptible to hot tearing, a very common and casting defect, that can result in high rejection rates of casted products . The main causes for normal contraction are solidification time differences and mold resistance [24]. Physical features can be added to a mold such as tie bars and chills, to combat distortion. Several examples for distortion were presented and explained in ASM Handbook Volume 15, which will be discussed and connected to how they can affect the Bearing Housing.

Effects of Solidification Rate on Distortion

For the first example, a thin walled, L-shaped cast fitting exhibited severe distortion due to higher temperatures encountered at a thicker cross section. This was due to a junction between two thin

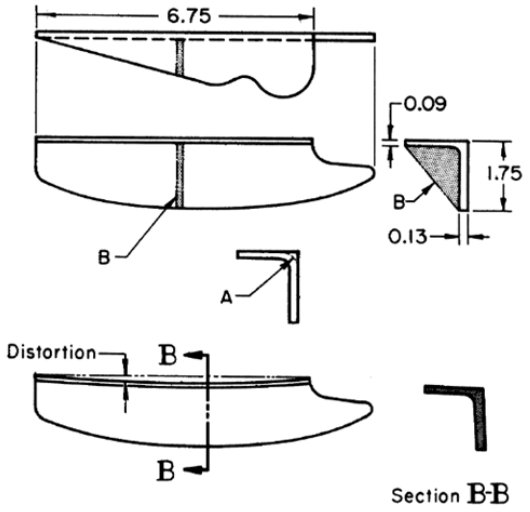

Figure 8: Distortion by Solidification Rate. Effects of Solidification Rate on Distortion: Distortion due to various solidification rates at different cross sections. Cross section B-B indicates a thicker area that caused distortion of the adjacent thin walls due to gradual solidification.

walls shown by the phantom lines in the arbitrary shown in Figure 8 [24]. A riser adjacent to the junction was required to produce sound metal but resulted in hot corners causing the walls away from the corners to solidify first causing the surface of the fillet to freeze later. Even though the fitting can be deformed to the desired shape in the as-cast condition, the distortion reappeared after a required heat treatment. In this case, it is crucial to avoid distortion in the as-cast condition.

Two solutions to minimize distortion were suggested. First was to introduce a fillet at the outside corner, indicated by "A", and the second was to add gussets, indicated by "B" in Figure 8. This

example identifies the flanges featured on the Bearing Housing shown in Figure 2 should behave as gussets minimizing distortion that can occur around the ring.

Another example entailed a flat casting, shown in Figure 9, with a thicker cross section in the center that served as a helpful example that explains distortion from solidification time. Same as the previous example, faster solidification occurred in the thin sections that caused the distortion identified by the phantom lines on the right side of Figure 9. The original cross section had an unsuitable bulky center and redesigning was considered with five iterations as shown in Figure 10.

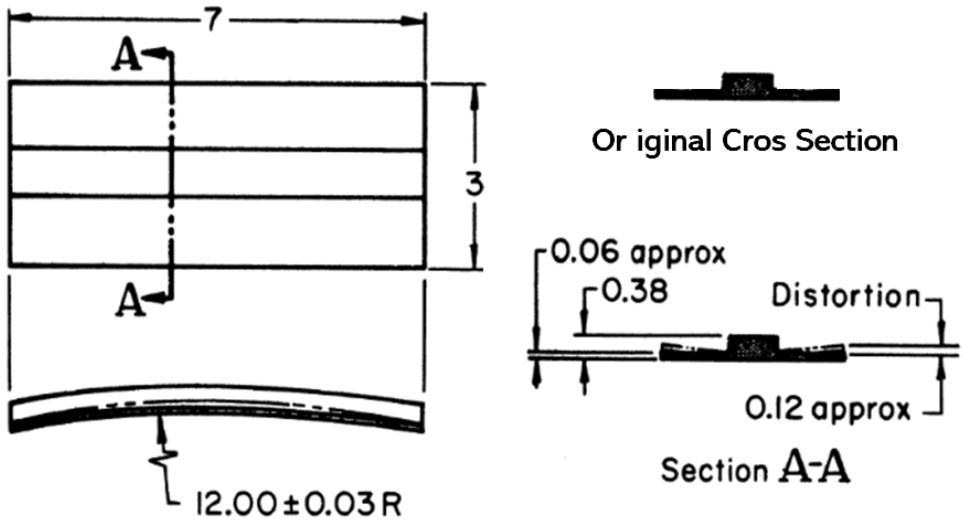

Figure 9: Distortion of Flat Member. Effects of Solidification Rate on Distortion: Distortion of flat member with varying cross sectional area. The center cross section solidified slowly causing distortion as identified by Section A-A. Redesigning of the cross section was considered for this case.

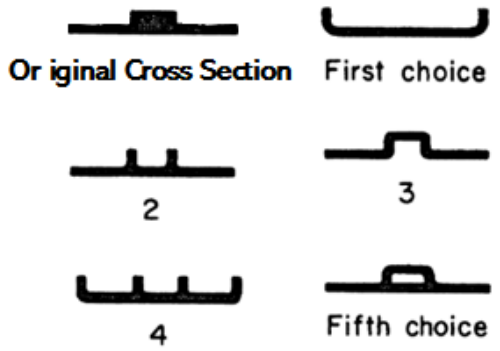

Figure 10: Varying Cross Sections. Effects of Solidification Rate on Distortion: Cross sectional redesign options that were approved to regulate thermal distribution to achieve a more uniform solidification reaction throughout the part. Iterations were numbered in order based on difficulty to produce mold by traditional methods but easily produced using AM.

The iterations were numbered in a sequence based on the complexity for traditional mold preparation, which is not an issue for AM preparation.

A sand casted Hub served as a highly applicable example that contained six radial ribs shown in Figure 11 [24]. Judging by the circular symmetry connected by radial ribs, the geometry is not much different from the Bearing Housing. Since the original hub design exhibited hot tearing at the rib junctions, it is something to expect when casting the Bearing Housing and will be taken into consideration during the simulations. The original Hub design exhibited hot tearing at the rib junctions but was redesigned replacing the external ribs with internal ribs

and inserting internal gate pads. Redesigning a military aircraft component, such as the Bearing Housing, would require a long line of clearance to authorize such a drastic modification in

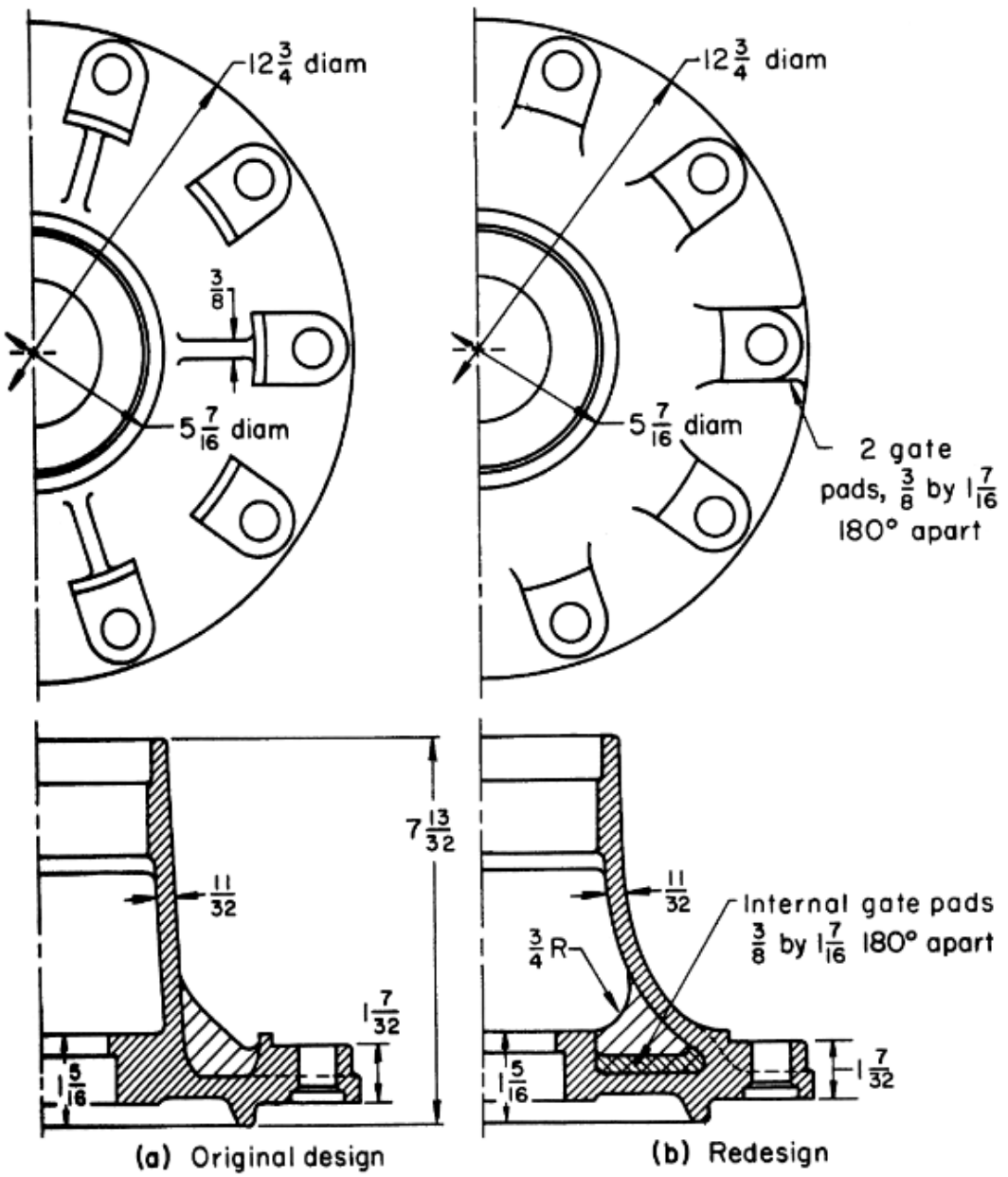

Figure 11: Sand Cast Hub. Effects of Solidification Rate on Distortion: Sand Cast Hub: Distortion occured at the rib junctions of the original design (left). The approved redesign (right) resulted in even heat transfer throughout the mold, which eliminated the distortion.

geometry. We are limited to the redesigning of the rigging system alone, which presents its own line of challenges that will be addressed when discussing distortion from mold restraint. Considering what is presented by the casted Hub, it is reasonable to expect hot tearing to occur at the rib junctions. The designers of the rigging system remained alert to this problem during CAD and simulation trials.

An example for an investment casted Gimbal Ring was presented that had a high rejection rate due to hot tearing in a web connecting two heavy sections shown in Figure 12 [24]. To accelerate the solidification of the thick section, the webs were extended outward from the enclosed area. This is a potential problem that can result in the investment casted components because the geometry of

the Bearing Housing also has webs connected to the base, which is a heavy section as was shown in Figure 11. In this component, the webs are expected to freeze before the heavy section, which, will be investigated in thermal-fluid CFD simulations in the results section of this paper.

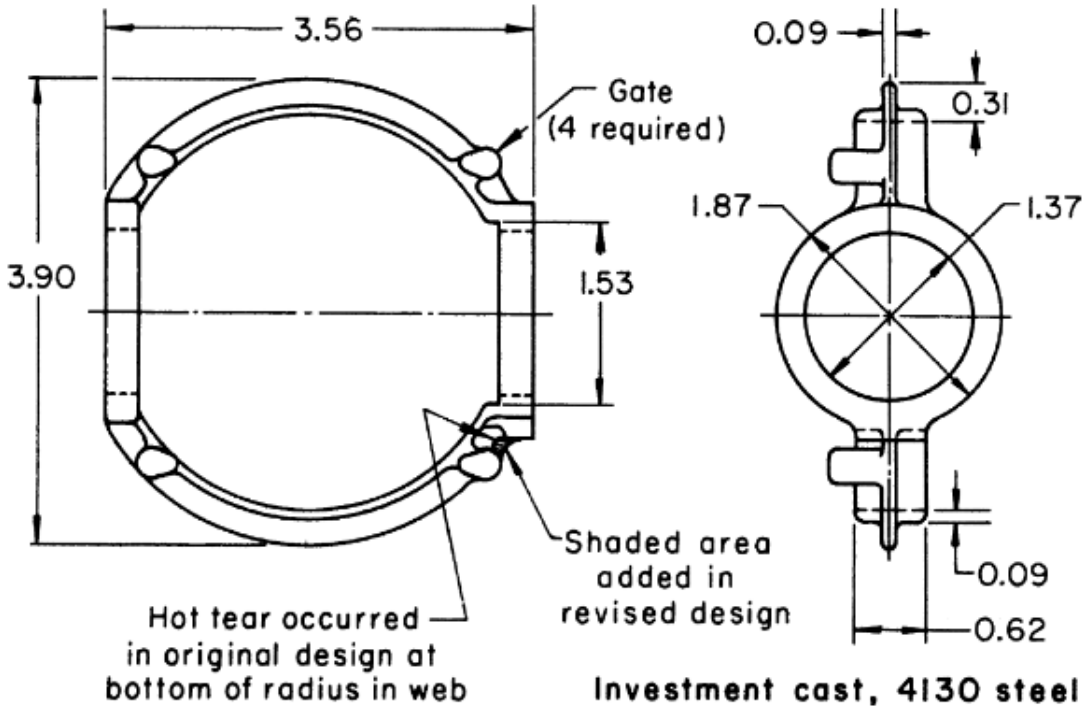

Figure 12: Gimbal Ring. Gimbal Ring Hot Tearing: Rejection rate was high. The solution was to extend the web out from the enclosed area, which accelerated solidification in the thick section.

Effects of Mold Restraint on Distortion

This form of distortion is based on a molds ability to resist the distortion that occurs during cooling and contraction of the casting [24]. It is difficult to eliminate because it is done by modifying the rigging system, which is what this project is limited to since redesigning geometric features of the casting is not allowed. However, mold restraint can be improved by inserting expendable features such as tie bars and chills [24].

An example of distortion from mold restraint was showed by two vertical flanges that repositioned outward as the base plate contracted upon cooling. This distortion is shown in Figure 13(a) [24]. The two flanges were separated by mold sand can result in contraction of base metal pointing the flanges outward, despite complete filling and sound metal were achieved. Figure 13(b), (c) shows

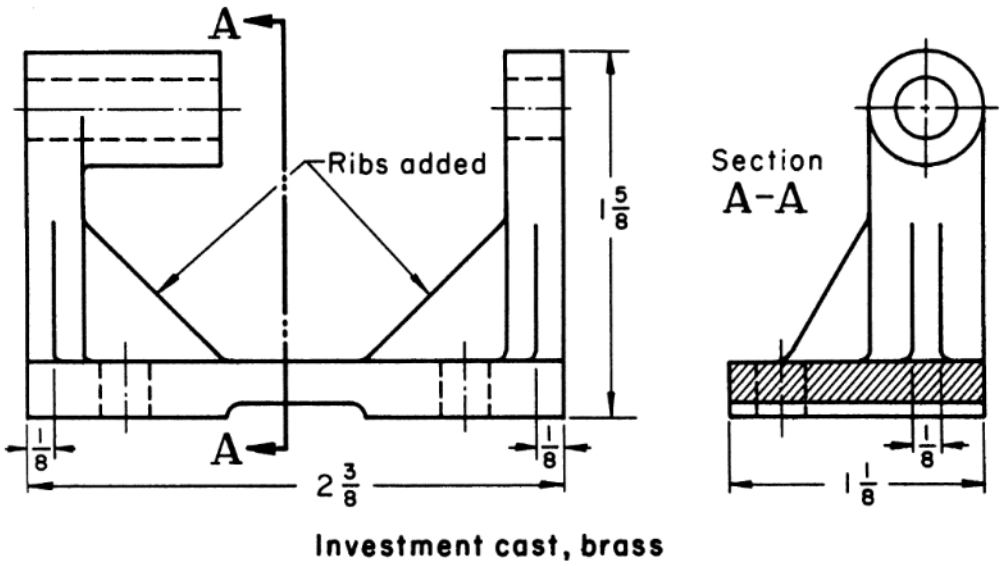

Figure 13: Brass Investment Casting. Brass Investment Casting. Ribs were used to stabilize the positions of the upright members.

the two solutions that were considered. The first was insertion of a removable cross member between the flanges, which was a preferred method due to minimized post processing. The second was to apply gussets to the flanges, which was not preferred [24].

An example of a brass investment casting was presented where mold restraint prevented two upright sections from displacing as the base material cooled to room temperature. Instead, the upright sections bent outward, which rendered the final product out of tolerance. Ribs were incorporated to accommodate mold restraint which yielded acceptable tolerances as shown in Figure 14 [24]. It was noted that proportions of ribs to joining members must be closely considered during designing because poor design can promote distortion and hot tearing instead of preventing it [24]. Again, the designers remained alert of this during the design process for investment casting.

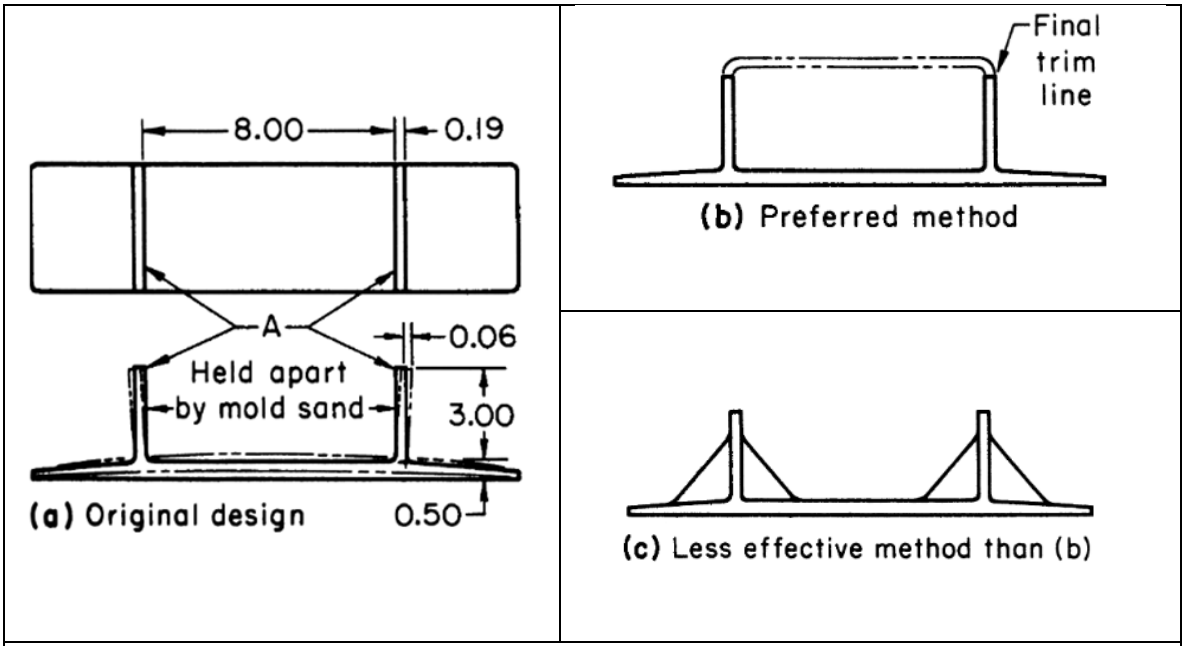

Figure 14: Sand Casting with Flanges. Sand casted part with flanges separated by mold sand. (a) Distortion occurred when the base plate contracted at cooling. Addition of (b) removable member or (c) gussets are two techniques that can minimize/eliminate distortion.

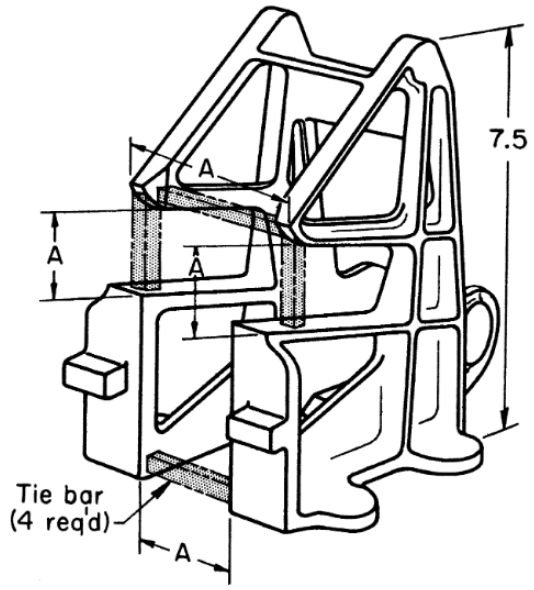

Figure 15: Tie Bars. Strategic placement of tie bars to minimize and/or eliminate distortion due to mold restraint.

Tie Bars and Chills

Tie bars are expendable volumes that can be inserted to reinforce the mold, which resists mold restraint that can eliminate distortion. Strategic placement of tie bars is key to improving the effectiveness of this technique as shown in Figure 15 [24]. Chills can be added to select sections of a mold which provides thermodynamic control of the solidification rate of localized areas of a casting. This could simply be a material with a higher specific heat that can absorb heat from a cross section that takes more time to solidify [25], [26].

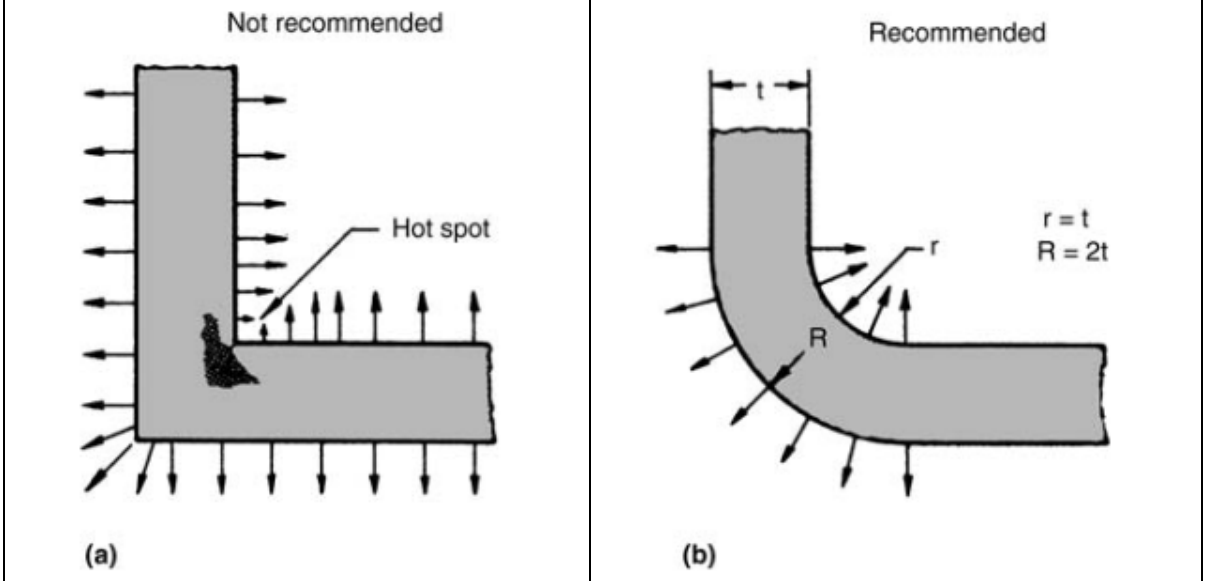

(a) (b)

Figure 16: Fillet Effects on Junctions. Comparison of two L-shaped junctions that show the effect (a) without and (b) with a fillet.

Design Problems Involving Junctions

Junctions are used to redirect metal flow into or out of component members. The nature of flow is dependent on the junction's geometry. Fillets are a junction's best friend, which will be demonstrated later in the design section of this paper. Figure 16 shows how the junction can influence how heat transfers to the mold [27]. The arbitrary indicates how a significant about of heat is lost to the mold when there is no fillet. Figure 17(a) shows how sharp corners lead to hot spots at the inside of the corner, which would be the last to solidify leaning to shrinkage defects upon solidification. By applying a fillet radius equal to the wall thickness of the junction, as shown in Figure 17(b), the heat is distributed uniformly, which typically eliminates shrinkage voids [27].

Five junction shapes including L-, T-, Y-, V-, and X-junctions were used in real-world experiments to determine their influence on fluid flow based on resultant shrinkage that was exhibited [27].

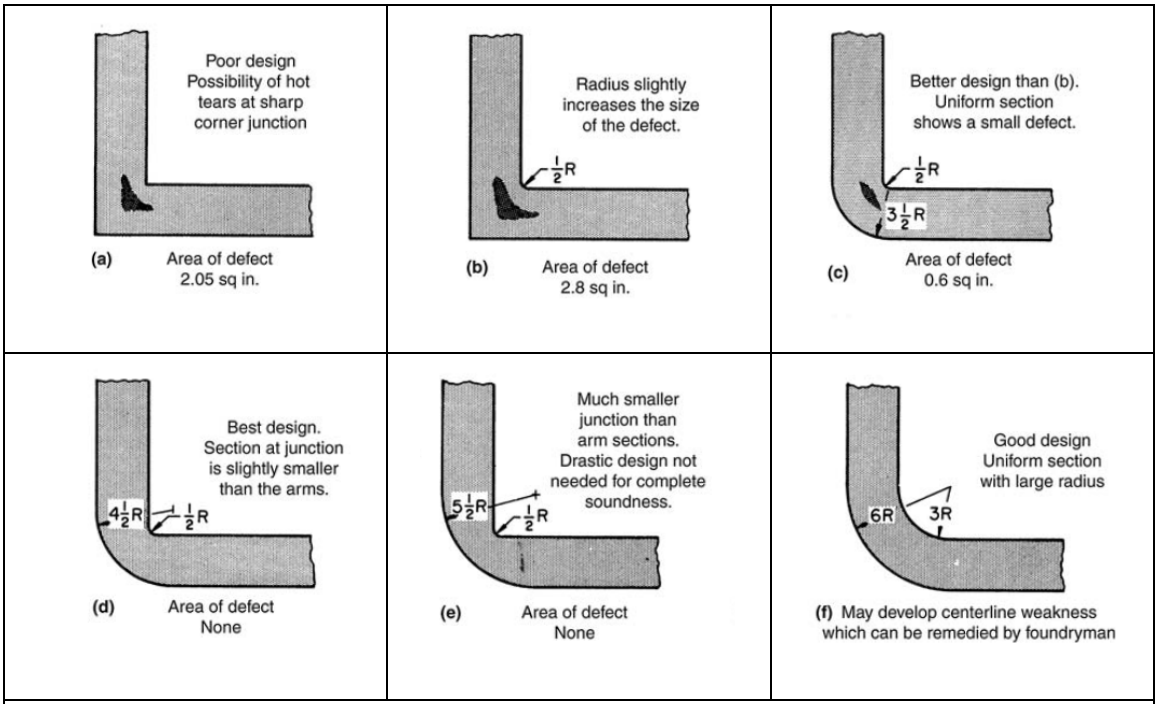

Figure 17: L-Type Junctions. These exhibited varying fillet radii sizes. Smaller fillets exhibited larger shrinkage voids.

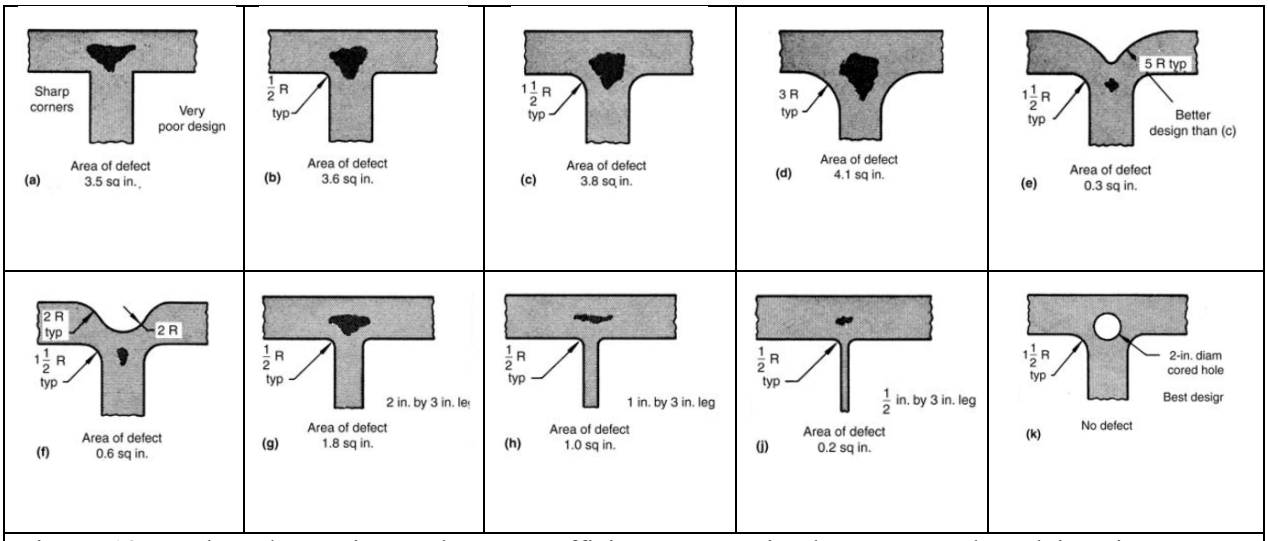

Figure 18: T-Shaped Junctions. The most efficient way to implement a T-shaped junction was to implement a core at the center of each intersection as shown in the final iteration.

Cross sectional thickness was selected to be 3 inches because it was large enough to identify defects using radiography. Junctions were compared on a horizontal plane and based on varying thicknesses of cross sections and/or sizes of fillet radii. This information was useful in designing the initial rigging system.

L-Shaped Junctions

The first three iterations shown in Figure 17 exhibited pronounced shrinkage when only one small fillet was applied or not present at all. The best designs were that of Figure 17(d), (e), which applied a larger radius on the outside and a small radius on the inside. As mentioned earlier, no defects typically do not occur in L-junctions with fillet radii equal to the wall thickness as shown in Figure 17(f), however, it was susceptible to centerline weakness [27].

T-Shaped Junctions

In summary, the only way to minimize shrinkage in these junctions was to insert a core at the center of a T-shaped junction as shown in Figure 18 [27]. This type of junction was experimented with at gate inlets in CFD simulations to predict its efficiency when entering the cavity.

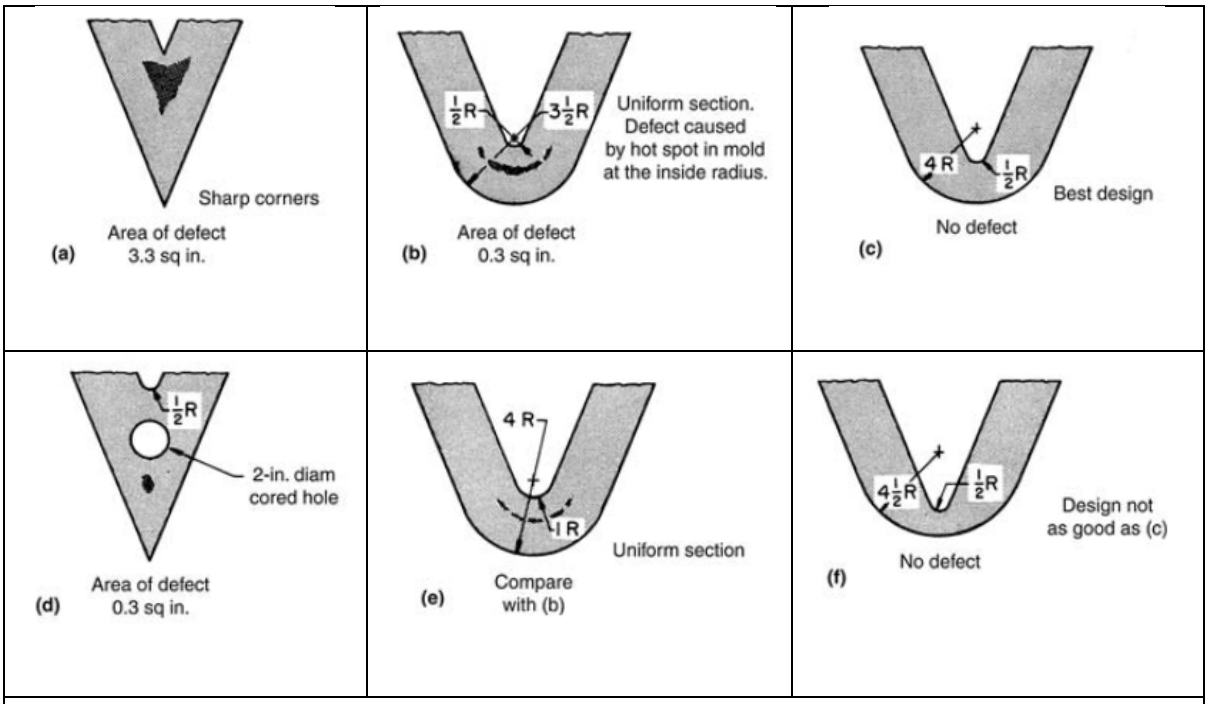

Figure 19: V-Shaped Junctions. These are unfavorable and result in pronounce defects in the inner sides of the corners.

V-Shaped Junctions

Hot spots are easily formed inside the mold because mold sand is a poor conductor of heat. This makes it difficult to draw heat away from the sand. This results to retarding the solidification of the adjacent metal and the acute V-angle causes this condition to become more server. Examples of V-shaped junctions are shown in Figure 19 [27].

X-Shaped Junctions

There was no way to eliminate defects that occurred with these junctions as shown in Figure 20 [27]. Addition of a core, as with T-shaped junctions, can help minimize. Out of curiosity, X-shaped junctions were taken to CFD simulation for the investment casting portion and will be briefly identified in the Design and Processing Section.

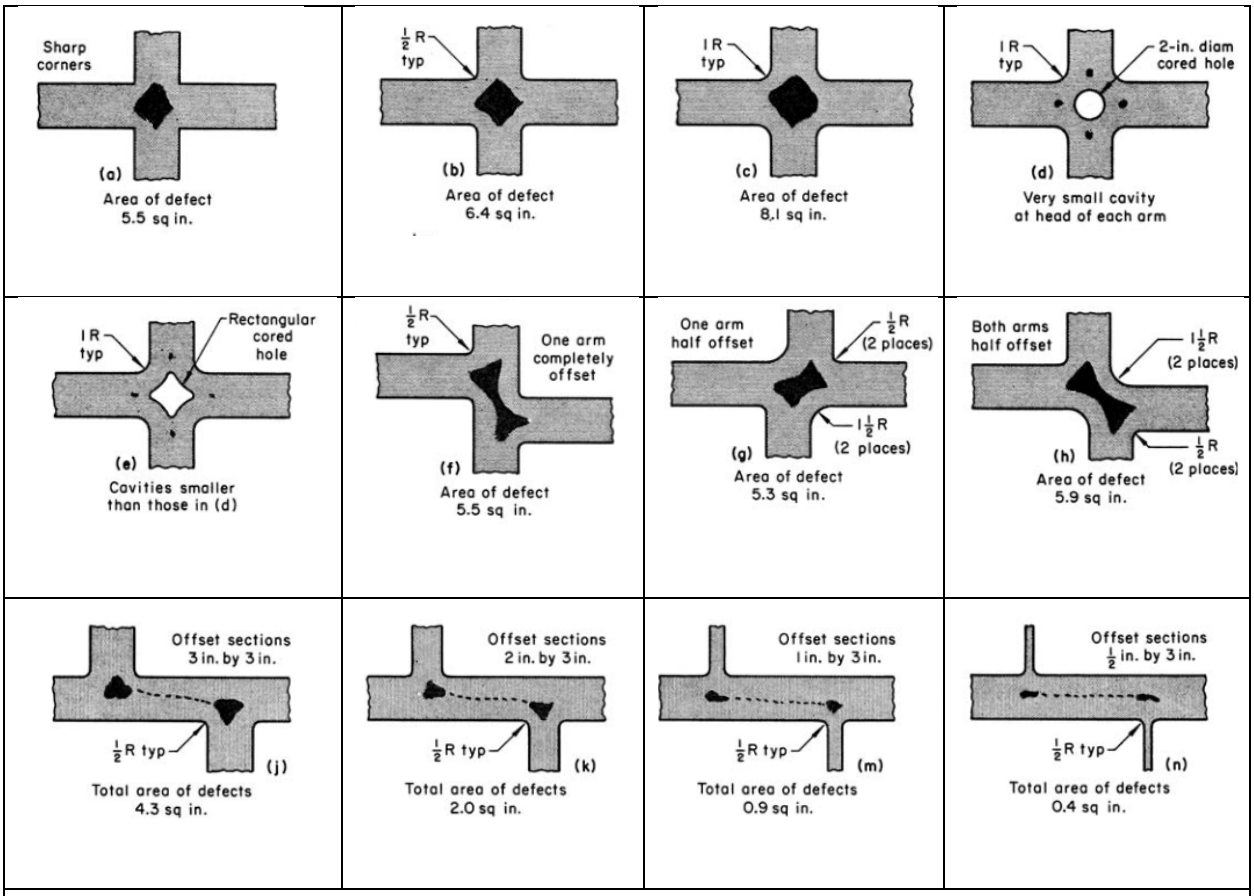

Figure 20: X-Shaped Junctions. There was no way to avoid defects using this type of junction. These junctions were avoided in all design iterations except for one simulated in InspireCast for training and curiosity.

Y-Shaped Junctions

Figure 21 [27] shows that applying a triangular core was an effective way to eliminate defects for Y-shaped junctions. Each of the iterations showed that defects would occur in Y-shaped junctions regardless of dimensional changes.

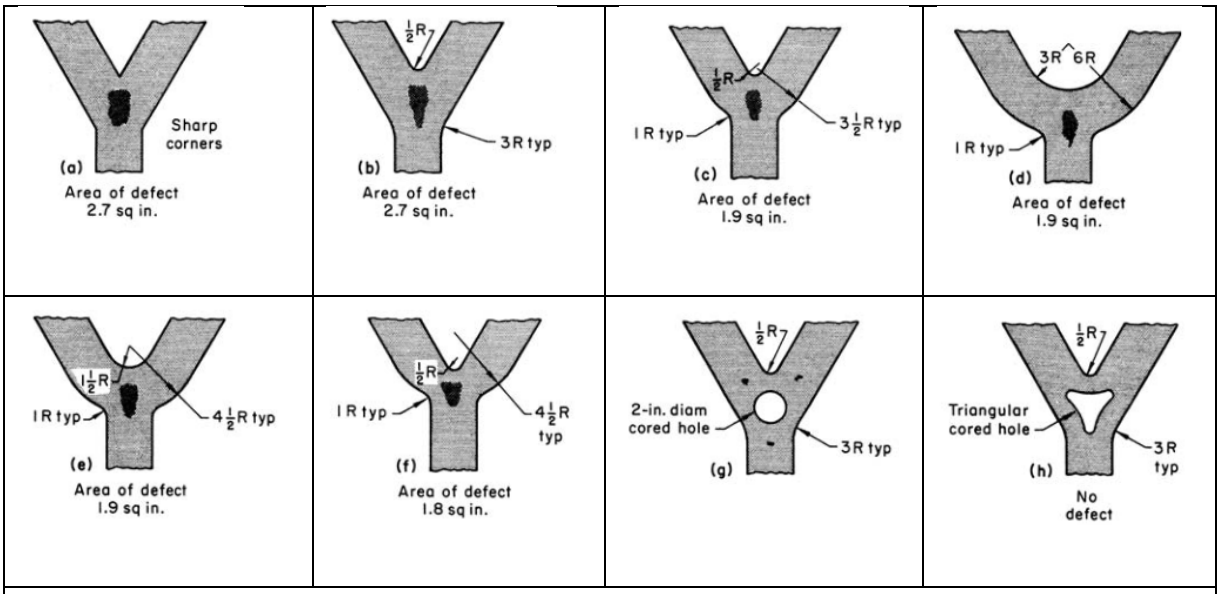

Figure 21: Y-Shaped Junctions. Applying a triangular shaped core at the center of the junction was the only way to eliminate defects with these types of junctions.

Design Problems Involving Thin Sections

This is an important topic for the Bearing Housing. They are useful because they save a significant amount of weight in a cast part, which contributes to the strength-to-weight ratio [28]. However, the designers need to stay alert to the fluid dynamic factors that are involved that differ based on the selected alloy and process conditions. It is very relevant to distortion, heat treatment, and overall cost of engineering design and development. Data was provided that specified minimum thickness requirements of castings based on alloy types and casting process are identified in the table showed in Table 2 [28]. This indicated that the minimum

Table 2: Minimum Thickness Requirements. Minimum thickness requirements of casted components. This presented restrictions of how small the experimental castings are allowed to be to facilitate a credible experiment.

	Minimum section thickness, in.		
Casting method	**Aluminum**	**Magnesiu**	**Steel**
Sand	0.125 ± 0.031	0.156 ± 0.031	0.187 ± 0.031
Permanent mold	0.093 ± 0.015	0.125 ± 0.015	...
Investment	0.062 ± 0.010	0.062 ± 0.010	0.093 ± 0.010
Die casting	0.062 ± 0.010	0.093 ± 0.010	...
Plaster mold	0.080 ± 0.015	...	...

(a) For compatibility with economical production. Not the thinnest producible by the processes.

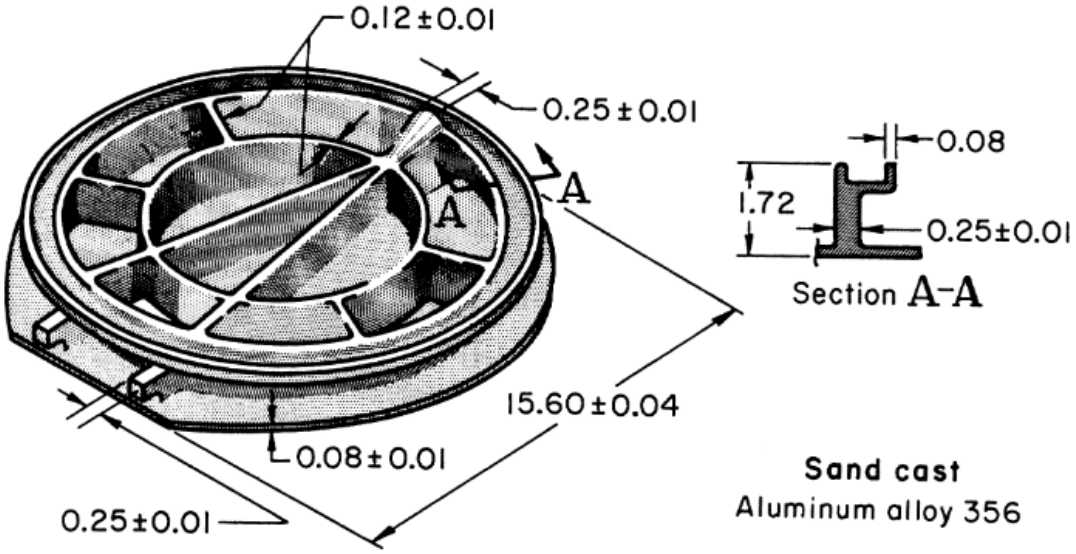

Figure 22: Fuselage Access Door. A356 Sand Casted Fuselage Access Door. The minimum wall thickness was 0.08 +/- 0.01 in. The ribs were designed with a wall thickness of 0.12 +/- 0.01in to assist filling the thin walls, which lead to successful production batch with acceptable number of rejected first articles due to misruns and cold shuts.

thickness requirements for casting the Bearing Housing will have to be 0.0994 in for sand casting and 0.052 in for investment casting.

An example of a good design for a thin walled casting of A356 was explained by an arbitrary shown in Figure 22 [28]. It was a sand casted thin-walled fuselage access door on an aircraft with a minimum wall thickness of 0.08 +/- 0.01 in. It featured ribs that were modified to a thickness of 0.12 +/- 0.01 in to accommodate for complete filling of the thin sections. Despite that increasing the cross sectional thicknesses of one area of a profile presents risks for distortion and hot tearing, a successful batch resulted with an acceptable range of rejections mainly due to misruns and cold shuts [28].

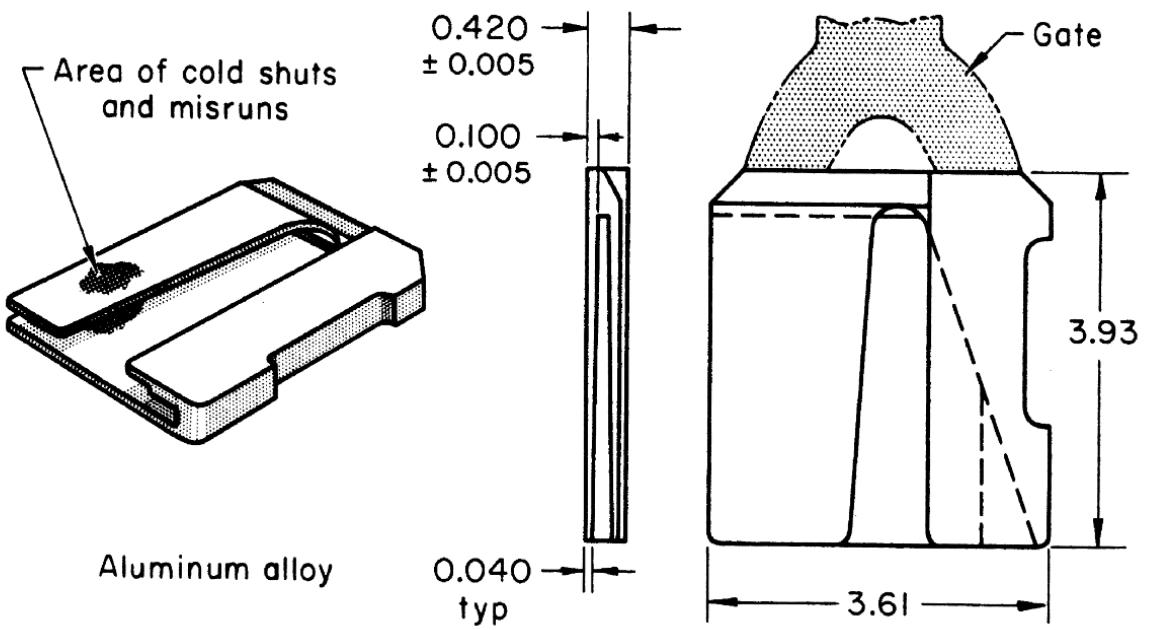

Figure 23: Fin-Shoe Slide Casting. Fin-Shoe Slide Casting. A195 preferred for mechanical properties sacrificing castability. The yield resulted in 100% rejection rate due to misruns and cold shuts.

It was noted that thin walled castings of certain designs can cause aluminum to fail in providing sufficient metallostatic pressure to force the metal into these tight spaces. In this situation, a process that provides more pressure to the melt upon pouring can be selected to do this [28]. In this project, we will consider pressure effects in investment casting to sand casting during the simulations.

A Fin-Shoe Slide casting that required maintenance of thin-walled sections, maximum surface roughness of 250 micro-in, and a minimum tensile strength of 32 ksi, minimum yield strength of 20 ksi, and minimum elongation of 5% verified by witness coupons that were casted with the same pour used to cast the Fin-Shoe Slide [28]. Investment casting with gravity pouring was the selected process. The selected alloy was A195 in leu of A356. It is known that the castability of A195 is inferior to A356, but it possesses better mechanical properties that was the central focus for this casting. Unfortunately, the rejection rate was 100% due to cold shuts and misruns as shown in Figure 23 [28]. It was demonstrated earlier that core holes can be useful for

mitigating or even eliminating casting defects. However, cores can shift during the pouring process, which will reduce wall thickness to the point were thin recesses do not fill completely. This is where the designers need to improve core stability.

Design Problems Involving Uniform Sections

During pouring, premature freezing of the metal often happens before completion of mold filling of uniform sections for various reasons such as centerline shrinkage. Two geometric modifications to mold walls can be made to overcome problems uniform sections. These include tapered walls or ribs that enable the metal to fill the extreme recesses as shown in Figure 24 [21]. Specifically, the arbitrary of a flat plate casting with a uniform wall thickness in Figure 24(a) shows how the liquid tends to flow in all directions leading to casting defects, lack of sound metal, and incomplete filling. Figure 24(b) shows how a network of ribs helps direct the metal to reach the ends of the plate, producing a complete casting. Applying a uniform and continuous taper toward the end of the plate confirmed that it is best for the metal to enter through the thickest sections as shown in Figure 24(c). These dimensional modifications are easy to apply since AM will be taking course of mold production, where design complexity can be introduced without a significant increase in cost [7].

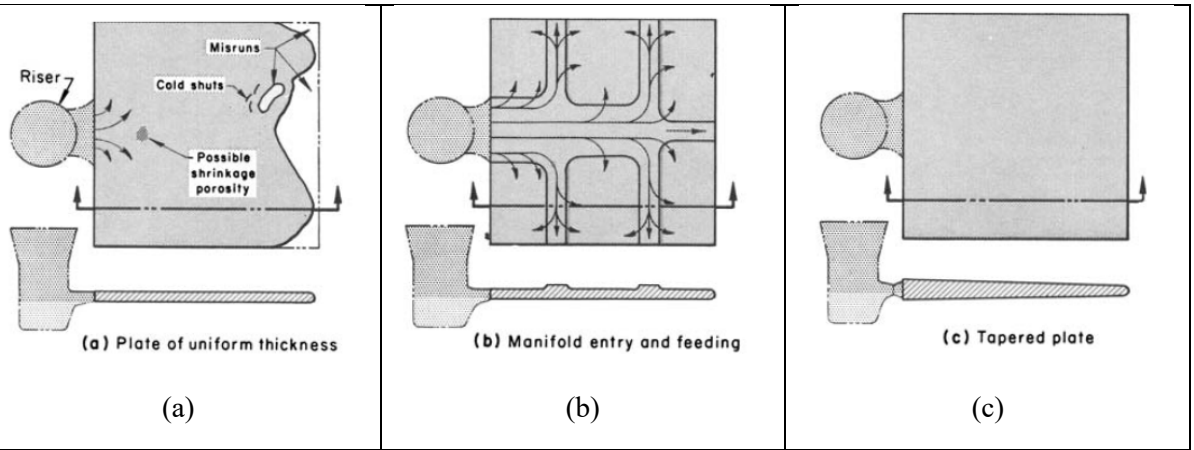

Figure 24: Effects of Uniform Cross Section. Example of a flat plate with uniform walls was difficult to fill completely for a sound casting. Introducing ribs provided feed paths for the liquid to flow. The example on the right shows how tapering allows the fluid to enter a thicker section, which is generally favorable for fluid flow.

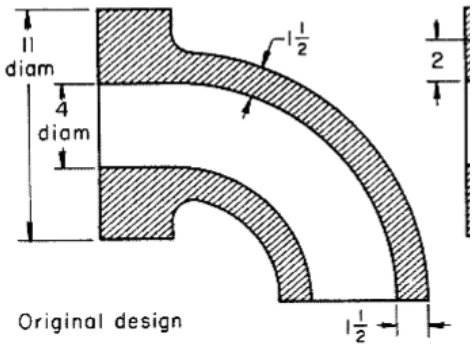

(a)

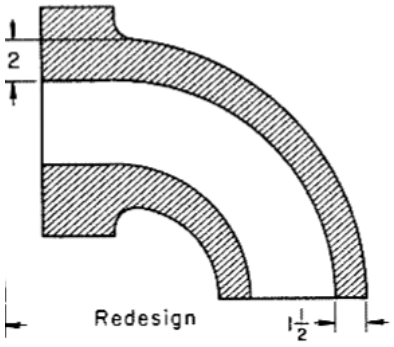

(b)

Figure 25: Elbow Fittings. The acceptance rate of casted Elbow Fittings was increased from 84% to 96% by thickening the inlet walls by half an inch. The Elbow Fitting was sand casted.

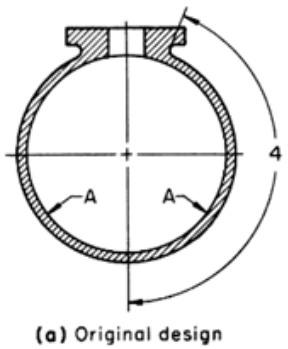

(a)

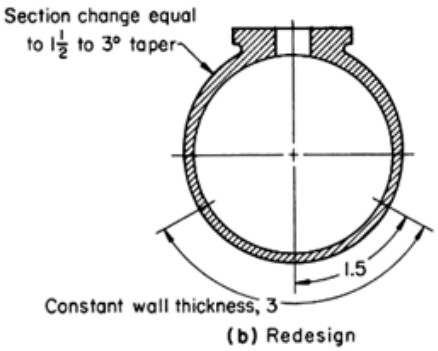

(b)

Figure 26: Flanged Spheric Casting. Flanged Spherical Casting. The original design (right) that exhibited feeding restrictions due to uniform wall thickness. The redesigned component enabled better metal flow. This component was produced by a shell mold.

Figures 25 and 26 are examples how tapering can be applied to casting an Elbow Fitting and a flanged spherical casting, respectively. Acceptability of the castings increased from 84% to 94% by simply increasing the wall thickness of the entry point by half an inch [21].

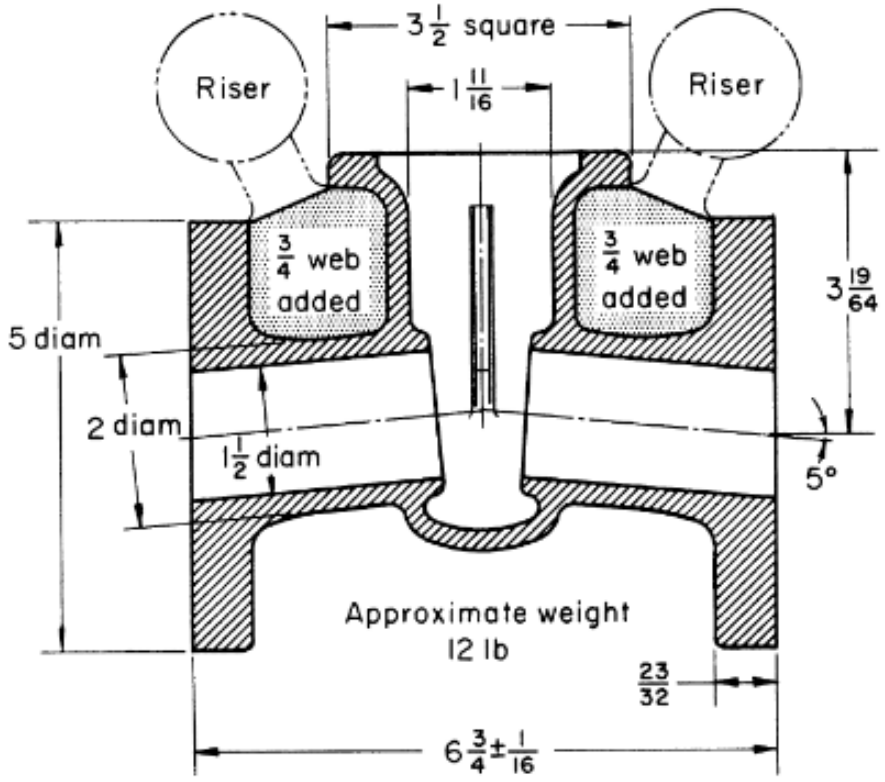

Figure 27: Nuclear Gate Valve. Nuclear Gate Valve. Shrinkage and porosity were greatly reduced by reducing the distance the liquid needed to travel to fill the mold entirely.

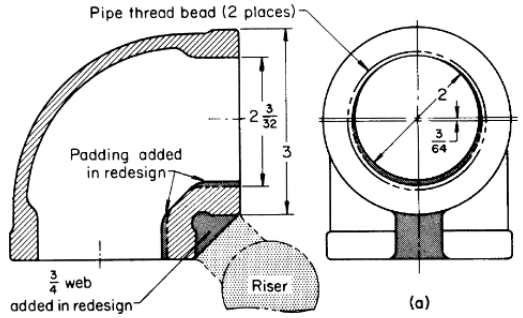

(a)

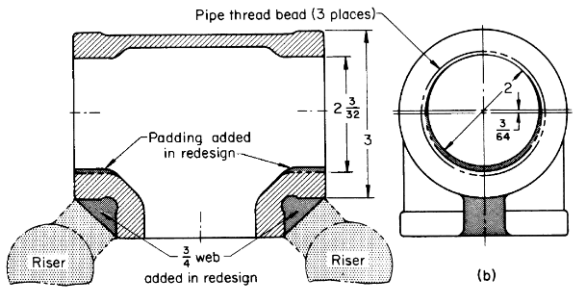

(b)

Figure 28: Combination of Tapers and Webs. Combination of tapers and webs for sand casted (a) Elbow Fitting and (b) Tee Fitting. Addition of webs and tapering greatly improved the flow of metal, yielding optimal freezing patterns.

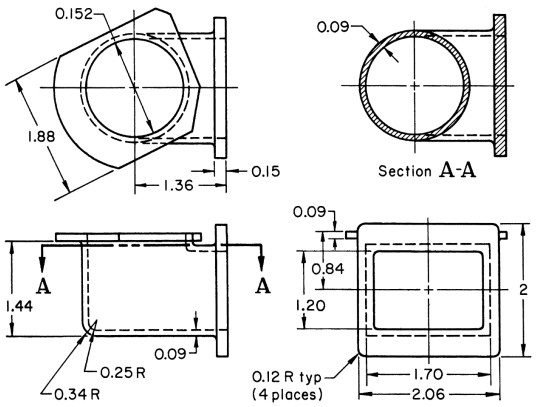

Figure 29: Aluminum Investment Casting. Aluminum Investment Casting. Well-designed rigging system that accommodated uniform walls by incorporating efficient gating areas.

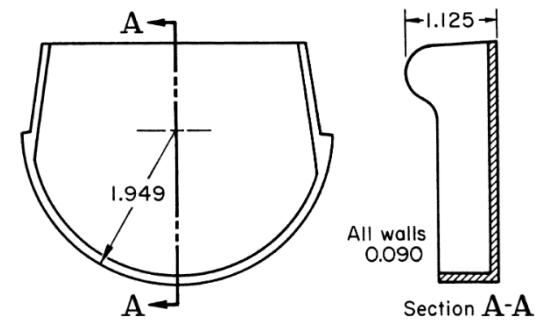

Figure 30: Thin Walled Investment Casting. A356 Investment casted A356 with uniform thin walls. Minimum thickness is dependent on alloy selection as well as process selection.

Webs are a favorable addition to castings when a feed path is needed. Figure 27 [21] is an example of how webs are used for a sand casted Gate Valve used in nuclear reactors to provide more effective distribution of the liquid upon filling. In this component, any detectible defects observed by radiography is causable for rejection. A combination of tapering and webbing can also be useful as shown by the two Fittings in Figure 28 [21].

The challenges of uniform sections may also be encountered for investment castings as shown in Figure 29 [21]. Even though uniform walls were present in the design, a carefully designed rigging system based on gating areas was able to circumvent misruns and cold shuts of the final products. Last mention for uniform sections, particular to investment casting is the factor involving minimum wall thickness for the shape, process, and alloy selection as shown in Figure 30 [21].

Processing Problems - Gasses in Metals

It is widely known that the solubility of gas increases with rising temperatures [29]. Gas evolution in liquid metal typically occurs when a gas is more soluble in the liquid phase than the solid phase, which is exactly the case for hydrogen and aluminum. This is easier to understand at a solid-liquid

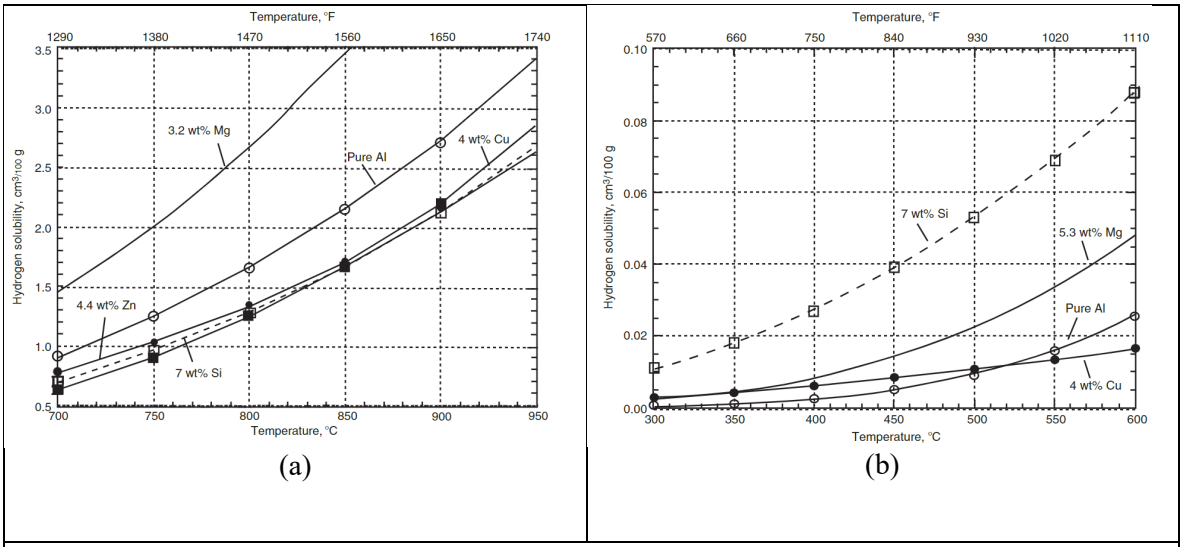

Figure 31: Hydrogen Solubility Curves. Hydrogen solubility in various aluminum alloys in the (a) liquid and (b) solid state. The dashed line represents A356 because it contains 7% silicon. Although hydrogen solubility is lowest in the liquid range, it is the highest in the solidus range. Special care must be taken to the environment of which the casting takes place. It may be advantageous to have a dehumidifier in the casting lab to minimize water vapor in the air while it solidifies.

interface of a solidifying alloy. The difference in solubility pushes hydrogen away from the solid liquid interface, causing the gas to agglomerate during solidification. The evolution of gas in molten metal is based on its concentration in the air, the alloy being casted, and chemical kinetics [30]. These factors are useful considerations when modeling the solidification behavior and dendrite formation of aluminum using phase field simulations.

Taking things back to the first principles of statistical thermodynamics, hydrogen is readily absorbed in aluminum. This makes it the most

susceptible to hydrogen related defects, primarily gas porosity [30], [31]. This can be easily explained by Equation 1,

$$2\mathrm{Al(l)} + 3\mathrm{H_2O(v)} \rightarrow \mathrm{Al_2O_3(s)} + 3\mathrm{H_2(in\ Al)} \qquad \text{Eq.1}$$

because the free energy of the above reaction in is very high which is calculated in Equation 2,

$$\Delta G^\circ = -979{,}100 - 719\mathrm{T}\log_{10}\mathrm{T} + 413\mathrm{T} \qquad \text{Eq. 2}$$

Table 3: Empirical Constants. Empirical constants used to plot curves shown in Figure 31, representing the solubility of hydrogen in aluminum at various temperatures.

Alloy	Solubility constants, $\log_{10}S, cm^3/100\,g = \frac{A}{T} + B$ A	B
Al-Mg alloys		
Al-3.2wt%Mg	2735.6	2.9752
Al-6wt%Mg	2695.5	3.1452
Al-Zn alloys		
Al-1.8wt%Zn	3193.9	3.1392
Al-3.5wt%Zn	3058.1	3.0382
Al-6wt%Zn	2957.7	2.8602
Al-Si alloys		
Al-2wt%Si	2777.8	2.7702
Al-4wt%Si	2941.3	2.9032
Al-7wt%Si	2731.0	2.6562
Al-Cu alloys		
Al-2wt%Cu	2955.3	2.9060
Al-4wt%Cu	3047.7	2.9392
Al-Li alloys		
Al-1wt%Li	2141.4	2.5952
Al-2wt%Li	2850.7	3.3832
Al-3wt%Li	2869.7	3.4862

Source: Ref 14

Additionally, the partition coefficient (k) of aluminum is very small which affirms that hydrogen is more soluble in the liquid state than the solid state. Such a low partition coefficient is unique to aluminum and its alloys compared to its counterpart nonferrous metals [30].

The solubility of hydrogen in the solid state is far lower than that in the liquid state. However, different alloying elements affect solubility. For example, silicon, coper, zinc, and iron decrease the solubility while lithium, magnesium, and titanium increase it. A356 is a 7%Si alloy and referencing Figure 31 [30] shows the solubility A356 is one of the lowest in the liquidous range but highest in the solidus range. This means that the environment of which the casting is solidifying should be as dry as possible. For reference purposes, a table containing the empirical constants for calculating hydrogen solubility in the liquid sate was provided in the handbook, which is shown in Table 3 (et. al. Richard J. Fruehan) [30].

Final remarks on "Gases in Metals", hydrogen can be removed from the melt by a process called inert gas flushing. It is when an inert gas that binds with hydrogen is pumped into the liquid aluminum, which removes a great deal of hydrogen content dissolved in the melt. It is possible to calculate the minimum amount of gas required to do so by Equation 3,

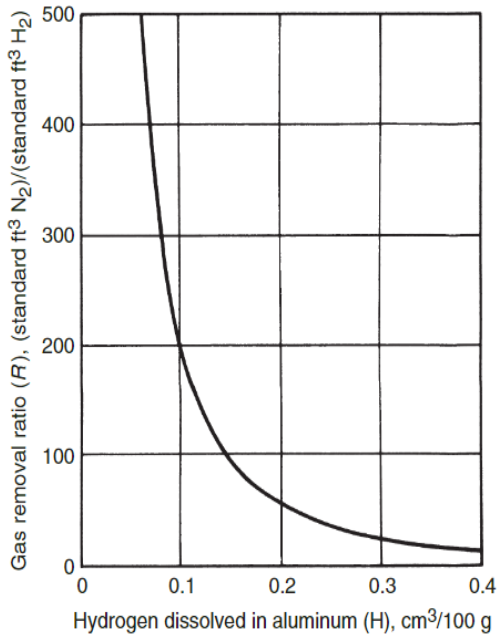

Figure 32: Inert Gas Flushing Rate. Inert Gas Flushing Rate. Sample equation 3 can be used to plot this graph. Removal of H gas within the melt increases acceptability of casted components.

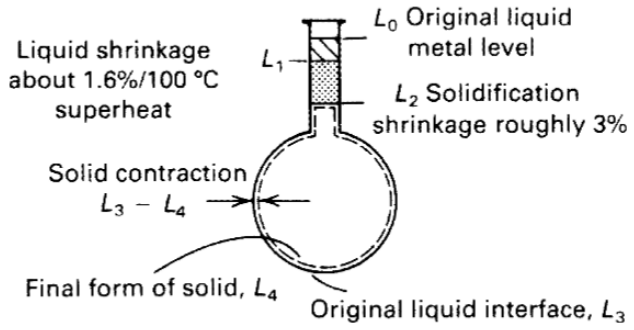

Figure 33: Types of Shrinkage. Three types of shrinkage that occurs in casting. Liquid shrinkage occurs between a superheated condition to the solidus temperature. Solidification shrinkage is typically a temperature range based on the alloy. Solid shrinkage takes place when cooling to room temperature.

$$\frac{1}{[H]} - \frac{1}{[H_0]} = \frac{k_H V t}{W} \qquad \text{Eq. 3}$$

Where t is the timestep, [H] is the hydrogen content at set timestep, $[H_0]$ is the initial content, W is the weight of the melt, and k_H is a constant related to solubility. This is a marvelous relation that can be plotted into a curve shown in Figure 32 [30]. These parameters are simple and possible to implement into a phase field analysis or molecular dynamic simulation.

Shrinkage and Porosity (Riser Design)

Shrinkage and porosity lead to lower quality castings that are costly due to an increased need for nondestructive evaluation (NDE) [32]. There are three types of shrinkage that occur in metal casting including liquid shrinkage, solidification shrinkage, and solid shrinkage (pattern makers shrinkage) [33]. The three differ based on temperature ranges of which they occur, and Figure 33 shows an arbitrary that provides a visual representation of the three. Liquid shrinkage results in loss of

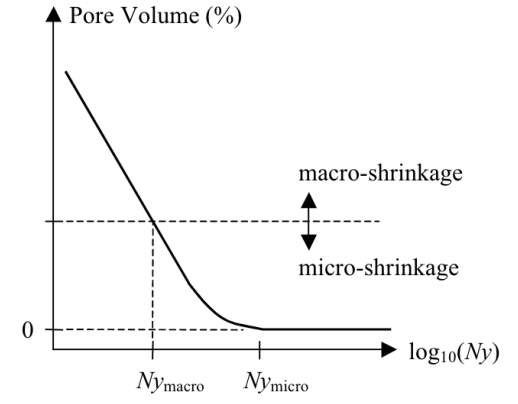

Figure 34: Niyama Criterion Curve. Effect of Niyama value on simulation shrinkage/porosity.

volume as the melt loses superheat while cooling to the solidification temperature, which is 555°C for A356 [33], [34]. Solidification shrinkage results when metal gains higher density as a solid and takes place at a single temperature for pure metals but for a given temperature range for noneutectic alloys [33], which can differ for A356 since it is a hypoeutectic alloy.

Solidification shrinkage was sectioned into three categories: directional, eutectic, and equiaxed. Solidification shrinkage occurs at freezing when the material transforms from liquid to high density solid and takes place over a specific temperature range depending on the alloy [19], [35]. Solid shrinkage is a uniform contraction that can that takes place between its solidification temperature to room temperature, which can be compensated by modifying the scale factor of the casted component [19]. This is considered by the coefficient of thermal expansion for Al-Si alloys, such as A356, is roughly $20.5(10^{-6})\ °C^{-1}$. With this, thermal contraction from the melting point, 600°C, to room temperature, 25°C, can be predicted by 20.5(10-6) *635 = 0.0130, which is 1.3% [23].

Proper use of risers is important because it can influence the extent of directional solidification for some alloys. A356, a hypoeutectic alloy, can exhibit microstructures that vary vastly based on its processing conditions [36]–[38]. For risers, the designer has to keep three things in mind: the right time, the right place, and the right amount [33]. For the experimental portion of this project, piles of InspireCast simulations were conducted with various riser designs.

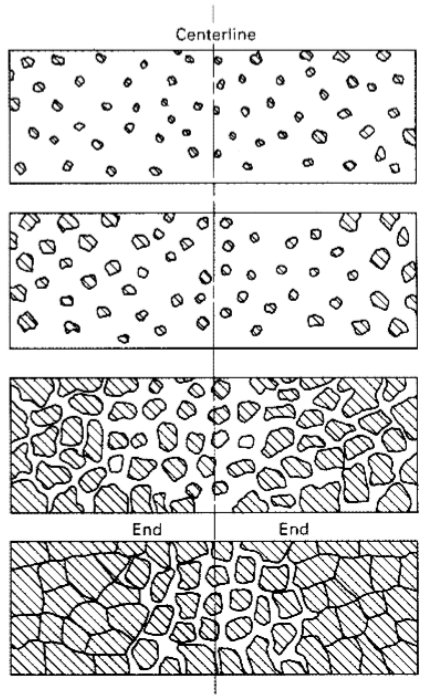

Fig. 7 Schematic of mode of freezing in alloys having a long freezing range

Figure 35: Long Solidification Behavior. Solidification behavior of alloys with long freezing ranges. A356 has a freezing range of 114°C , as discussed earlier.

Niyama criterion is a simulation technique that are used to predict solidification shrinkage in castings [32], [39], [40]. This criterion is integrated in Altair's InspireCast software and was extensively used to determine the efficacy of preliminary designs to develop the initial design. This can be used to predict cases for hot tearing, which is a casting defect of which cracks form at critical cross sections during solidification [35]. The Niyama value (Ny) is obtained by dividing the local thermal gradient (G) by the square root of the cooling rate ($\dot{T}$) as shown in Equation 4,

$$Ny = \frac{G}{\sqrt{\dot{T}}} \qquad \text{Eq. 4}$$

A sufficiently large value for Niyama value is favorable because higher values indicated that no shrinkage or porosity will form. A study showed that macro-shrinkage and micro-shrinkage will occur at a critical Ny value as shown in Figure 34 [40].

The freezing range of the alloy is an additional factor that determines the solidification behavior of the solid, such as the formation of dendrites. For metals of short freezing ranges, a solid-like character is developed by nucleation forming at random points within the bulk liquid. For long freezing ranges , the solid will exhibit dendrite formation [24], [25]. A356 has a long freezing range of 114°C, which is likely to exhibit a combination of the two as shown in Figure 35 [26], [27], [33]. Solidification behavior of alloys can predict the microstructure of a metal, such as one that contains a combination of dendritic and equiaxed grains can be expected [22], [33]. Being aware of these factors throughout the design process can help the design team combat distortion as well as the possibility of hot tearing, even though A356 is resistant to hot tearing [18].

Experimental methods that have been covered so far only address design criteria that can predict the results of a casting process at a macroscopic scale. These cannot predict microstructural evolution and phase transformations that govern material properties. Physical metallurgy and phase transformation can be taken to computational methods to simulate microstructural development in casting such as nucleation and grown of crystal structures as well as dendrite formation [37], [41]–[55]. To keep a sequence, nucleation will be discussed before approaching solid state transformations.

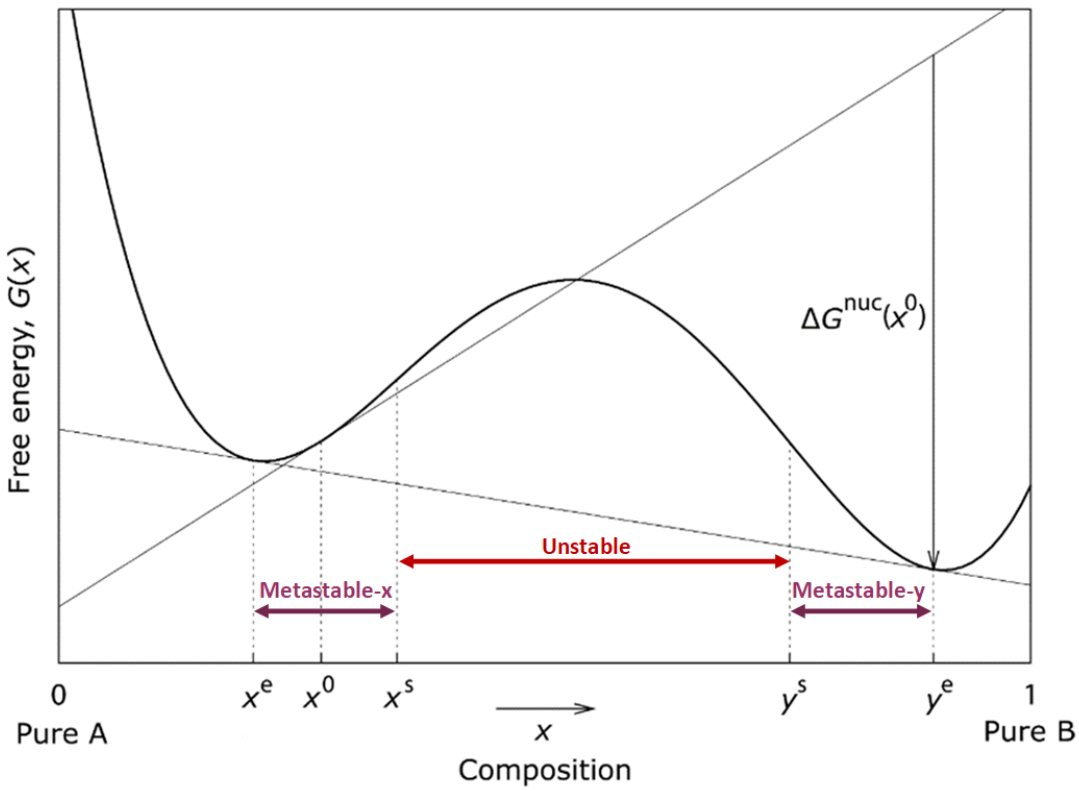

Figure 36: Gibbs Free Energy Curve. A common tangent between the two equilibrium composition values of phase x (x^e) and phase y (y^e) determines the limits of isothermal equilibrium for the respective phases. The intersection between the tangent line of the system composition (x^0) and the equilibrium composition of phase y (y^e) indicates the change of free energy of nucleation in the homogenous region of the system in a metastable state. The limits for spinodal decomposition are identified by x^s and y^s, which are the zones where nucleation cannot occur.

Nucleation reactions happen when a thermally stable homogeneous liquid is exposed to a temperature gradient that drives it toward a metastable state. In a metastable state, the liquid will interact with its surroundings to lower its free energy that establishes the equilibrium requirements for a solid phase [41], [49]. Spinodal decomposition is a phenomenon that occurs when a parent phase is stable that prevents this transformation from occurring. Thermodynamic considerations in binary systems indicate differences between nucleation and spinodal decomposition as well as metastable and unstable phases [49], [54].

It is easy to remember that the decrease of free energy is the driving force for transformation in all materials [54], [56]. Consider the free energy curve of a binary system of composition (x^0) associated with a phase fraction (f) in an isothermal state shown in Figure 36. A second order differential equation can determine if the second derivative free energy (G'') is negative or positive based on Equation 5,

$$\Delta G = \frac{1}{2}(f dx_1^2 + (1-f)dx_2^2)G''(x^0) + o(dx_1^2) \qquad \text{Eq. 5}$$

where x_1 and x_2 are the concentrations of element A in phases 1 and 2, respectively. In Figure 36, x^e and y^e represent the equilibrium compositions while x^s and y^s identify spinodal compositions of

phase A and phase B, respectively. This is essentially the change of free energy (ΔG), which determines if the melt compositions (x^0) is going to be metastable or unstable.

If the change of free energy (ΔG) negative, spinodal decomposition occurs and designates that the system has reached a two phase equilibrium state as shown in Figure 37(a). On the other hand, when the change of free energy (ΔG) is positive, nucleation occurs as shown Figure 37(b).

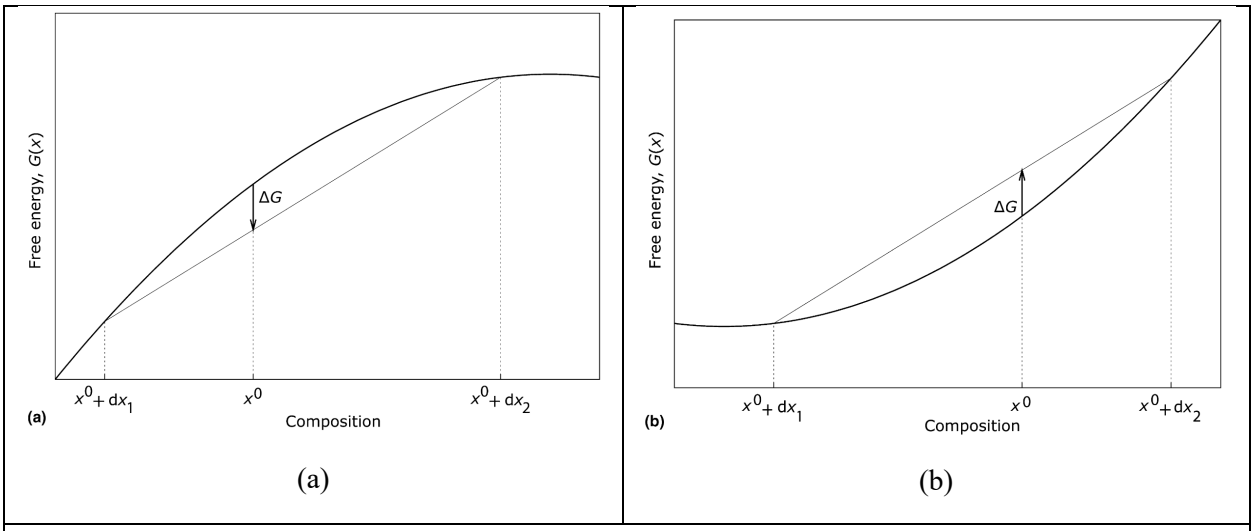

(a) (b)

Figure 37: Spinodal and Nucleation Reactions. Free energy curves representing the criteria for (a) spinodal reactions in the unstable region where change of free energy decreases and (b) nucleation reactions in the metastable region where change of free energy increases. The unstable and metastable regions are identified in Figure 39. These curves are based on composition of the melt (x^0) and composition of equilibrium compositions of phase A (x^1) and phase B (x^2).

It is understood that the change of free energy determines the type of reaction that will occur in a binary mixture. In phase field simulations, the free energy change is plotted as a function of time. Again, a temperature gradient drives a liquid to a metastable state. Therefore, time and temperature are conserved variable that will be included for simulating the anisotropic free energy of solidifying aluminum [52].

To model solidification and dendrite growth, only metastable conditions will be considered in this project. These two models are depended on anisotropic free energy that can be computed using a new method that involves classical nucleation theory (CNT) and kinetic equations of crystal-melt interfaces [47].

CHAPTER III

METHODOLOGY

Additive Manufacturing

The solid models designed by CAD and GD are difficult, if not impossible, to produce by traditional methods. especially when it comes to spherical shapes applied to the upper sections of risers. This is not the case for AM produced molds . However, before rapid prototyping and casting in laboratory conditions, the influences of the component's geometric features needed to be thoroughly understood through referencing industrial literature, modeled using GD, and simulated using sophisticated CFD tools, each of which have been described above. The AM method used for mold production are liquid jet deposition processes.

Sand Molds

Traditional sand mold preparation is usually performed by packing of binder-bonded sand of a given material around a pattern to create the expendable mold assembly that was presented in Figure 3. The process is limited to simple patters due to tooling cost and physical reality that some geometries are too complex to be prepared by manual mold packing and assembly. It is widely known that AM has enabled manufacturers to produce objects of complexed geometry from varying fields of industry. Printing a sand

mold can enable novel designs of the rigging systems of complex shapes that satisfy a desired geometry of the casted component [7]. At each layer of the build, fused silica sand is layered into a flat plane and bound together with liquid binder that is deposited from a liquid jet head, similar to that of an ink jet printer, instead of using energy from a laser as in LPBF process. This enables designers to produce novel geometries for a rigging system of complex shapes to best support the fluid flow for the geometry of the component [7].

Investment Shells

Production of molds for investment casting entails the same layer-by-layer process of binder jet printing, except it deposits wax on the print bed instead. Two types of wax are used, support wax and printing wax. The support wax is highly soluble in isopropyl alcohol so that it can be dissolved away from the printing wax, which leaves the wax pattern of a desired shape. The printed parts are then taken to the shell production process as was described in Figure 4.

Material Selection

Casting Material: A356 Aluminum-Silicon Alloy

A356 is a eutectoid aluminum-silicon alloy that is resistant to hot tearing, has a low-pressure tightness, excellent fluid life, low shrinkage tendency, adequate corrosion resistance, weldability, and moderate machinability compared to other aluminum alloys [15]. Physical properties of the melt and mold materials are crucial considerations in the design process because they affect the likelihood of prevalent defects that occur based on the casting material. For example, the fluid properties of steel are not the same as those of aluminum, which makes one more susceptible to specific casting defects [27].

Mold Materials

Molds for expendable casting processes, such as sand and investment casting, need to meet four requirements. These include formability into a desired shape, ability to hold the shape of which the molten metal is introduced, ability to maintain the shape during solidification, and ability to break down after solidification to remove the part [15]. For sand casting, silica sand has excellent dimensional and thermal stability with suitable particle shape and size it is chemically and physically inert with molten metal and has low wettability [57]. For investment casting, an expendable shell mold was produced by multiple coats produced from submerging a disposable pattern into a ceramic slurry of fused silica (Ransom & Randolph, SuspendaSlurry) and coating with the dry particles. There are two grades of the slurry that vary based on coarseness. The first coat that interfaces the wax must be the finer grade to ensure smoother cast surface.

CHAPTER IV

PROCEDURE

Computer Aided Design

Autodesk Fusion 360 was the preferred CAD package for designing the rigging system. This was due to the need for numerous iterations that are saved on a cloud server instead of the computer storage drives as SolidWorks does unless one chooses to pay extra for cloud capabilities. The cloud server is also convenient such that it can be accessed from any device and uses less computation power. This allowed the designer to collaborate easier and allocate computer storage and processing power to save and run simulations using Altair's InspireCast. Fusion360 also contains multiple "workspaces", such as generative design and finite element analysis, on a single desktop application instead of multiple packages that end up on the computer desktop, like SolidWorks. Additionally, it requires far less steps to execute commands making complicated tasks, such as shape forming, far easier to complete. When comparing SolidWorks to Fusion360, it is nonsensical to walk and swim from Tokyo, Japan to Tulsa, OK when one can board an airplane (for free).

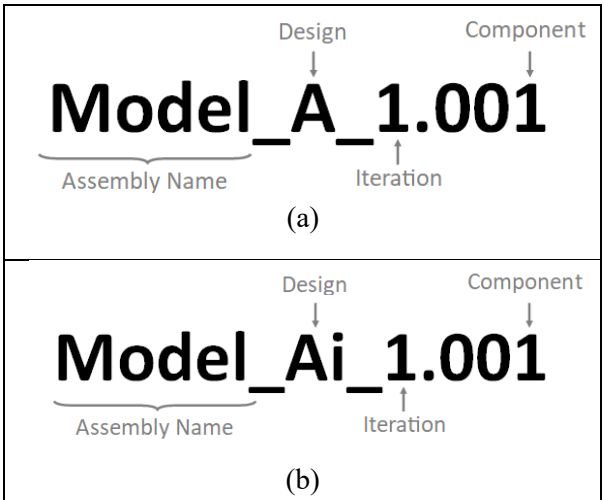

Figure 38: Naming Convention. Naming convention that referred to design development for (a) sand casting and (b) investment casting. "Model" referred to the rigging assembly intended for casting the Bearing Housing. The multiple designs were organized in by alphabetical number. Each design entailed several iterations that were numerically listed, each number representing an improved iteration. The last number represents the components in the assembly; assembly -1, sprue-3, and risers-5.

Rigging Design – Inlet

This portion of the rigging design comprises of sprues, runners, and gates. As mentioned before, the rigging system to be tailored to geometric features of the casting so there were numerous iterations to keep record of. To keep track of the design iterations, a naming convention was developed for each iteration as described in Figure 38. This was necessary for keeping track of which designs are being casted as they will be identified as a part number that can be printed into the actual molds. In the nomenclature, assembly names referred to rigging system assemblies that were sequenced in alphabetical order. A new design letter denotes that the rigging system that was totally redesigned either manually or generatively. Figure 39 shows three preliminary designs and their design problems. Model_A_1.003 and Model_A_2.003 in Figure 39(a),(b) showed that the using multiple Y-junctions was a high risk for shrinkage with or without fillets. Additionally, feeding the cavity from the base plane were not efficient for the Bearing Housing. Bottom feeding the cavity from the sides was more effective as shown in Figure 39(c), (d). However, abrupt changes in cross sectional thickness were present that can cause pressure differentials in the runners and yield entrainment of air. Abrupt changes and the presence of Y-Junctions called for total redesign that wasn't incorporated until the 6th iteration of Model B. The final iterations of Model B incorporated T-junctions at the sprue-runner transition and were decided to be the initial design with minor modifications that will be compared later with casting simulations.

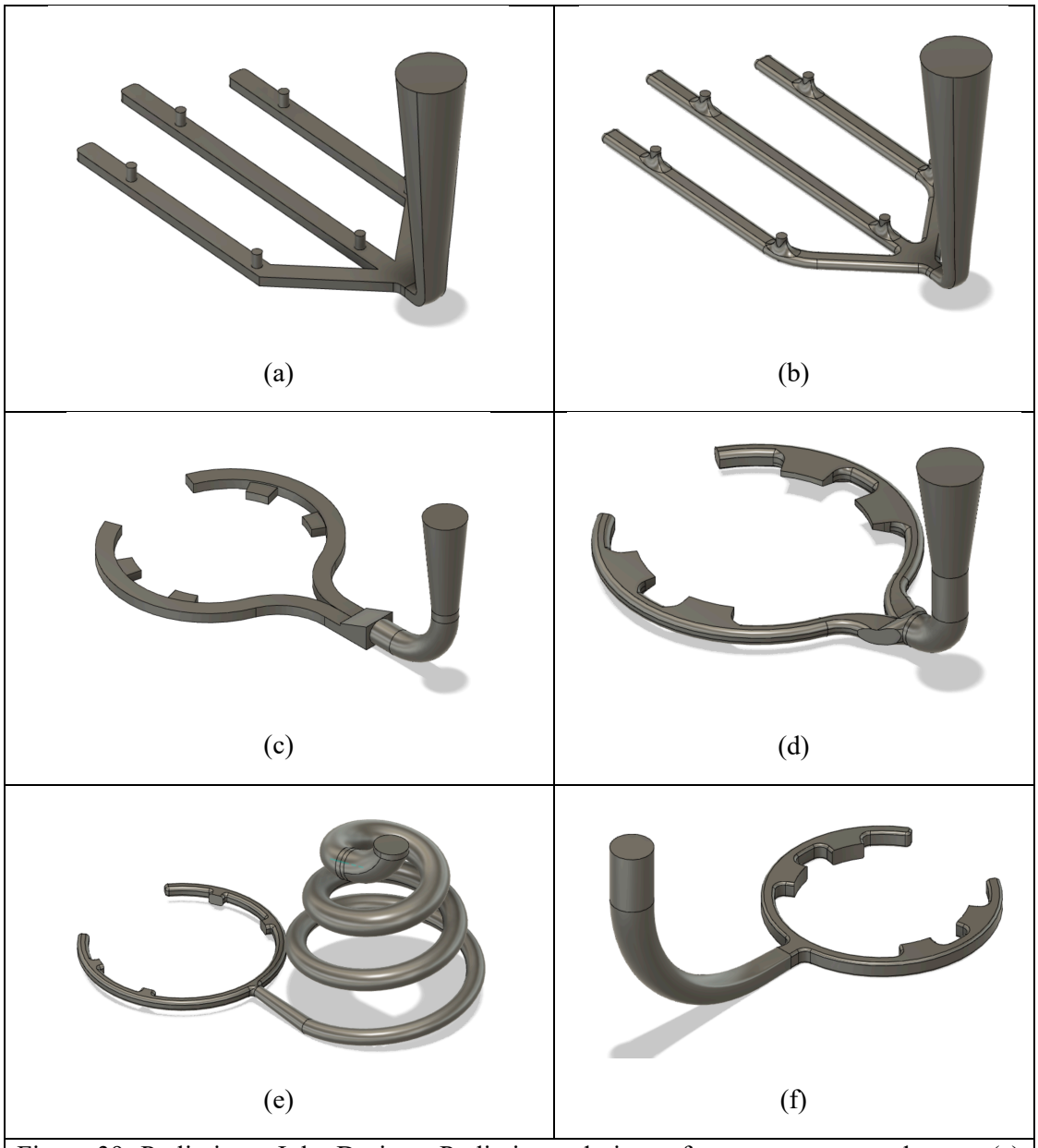

Figure 39: Preliminary Inlet Designs. Preliminary designs of sprue, runners, and gates. (a) Model_A_1.003 contained a triple Y-junction, which was a risk for shrinkage. (b) Model_A_2.003 introduced fillets that made little difference, so it was decided that the bottom feeding was not effective. (c) Model_B_1.003 incorporated ring shaped runners that fed the cavity at the bottom but from the sides with wider gates. However, this design featured abrupt changes in cross sectional area that promote air entrainment and the creation of pressure differentials within the runner system [35]. (d) Model_B_5.003 kept the same set up but introduced fillets with tapered gates but the splitting point was still not favorable for fluid flow. Since the ring shaped runner was most favorable, it was decided that the sprue-runner transition needed to be changed to a T-junction, which was finalized as the initial design. Minor variations of this design will be compared with casting simulations. (e) Model_C_1.003 and (f) Model_G_1.003 were ambitious techniques for lowering flow velocity (et. al Sama S, Badamo T) [7] but the molds were deemed too large for printing.

(a)

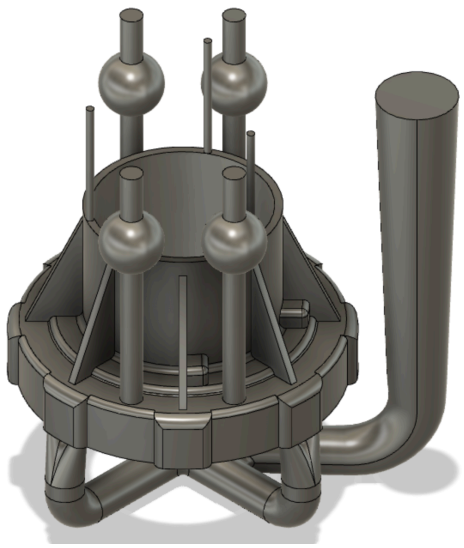

(b)

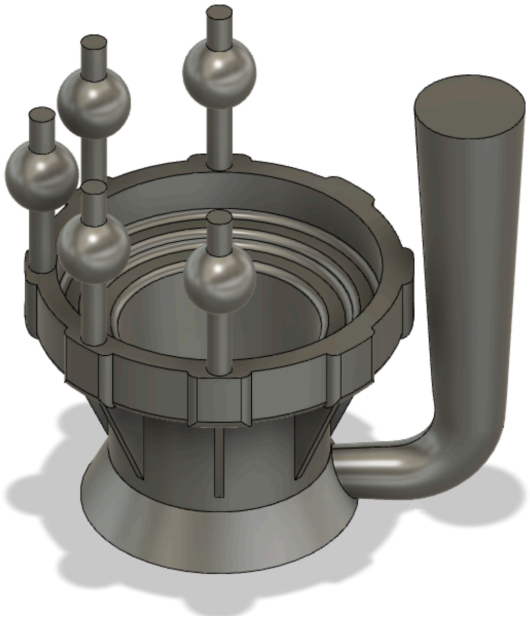

(c)

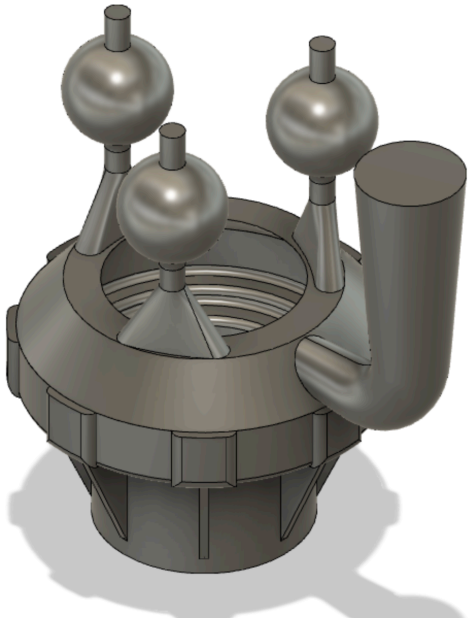

(d)

Figure 40: Preliminary Riser Designs. Preliminary designs of rigging systems for investment castings. (a) Model_Ai_1.001 featured as wax tree but was too large for the scope of this project. (b) Model_Ci_1.001 featured an X-shaped junction at the base, which is widely known to cause unavoidable shrinkage [27]. (c) Model_Di_1.001 and (d) Model_Ei_1.001 featured ring-shaped inlets that were tested from bottom fed and top fed methods, respectively, and were taken to generative design

Preliminary inlet rigging designs for investment casting were also developed shown in Figure 40. Model_Ai_1.001 shown in Figure 40(a) was intended to feed multiple components using a tree-like structure, as in a practical investment casting practice. However, it was too large to print multiple full sized castings for the scope of this project. Model_Ci_1.001 introduced a bottom fed rigging system as shown in Figure 40(b). Tiny risers were placed at the top of the rims intended for ventilation. However, they were predicted to break off easily during handling. The main issue with this design was the X-junction at the

base, which is a junction shape that results in unavoidable shrinkage defects upon solidification in sand castings, which may be the case for investment castings as well [27]. X-shaped junctions were not worth the risk, so a ring-shaped inlet was then considered in Model_Di_1.001 shown in Figure 40(c). Multiple risers were placed at the opposite end of the sprue due to excessive microporosity observed in casting simulations. A top fed inlet was finally introduced in Model_E_1.001 shown in Figure 40(d). Since the inlet was placed at the top, attaching risers at the top was an option that did not increase post-processing requirements. Model D and Model E were taken to generative design to create Model F and Model G, respectively, which will be shown in the GD section.

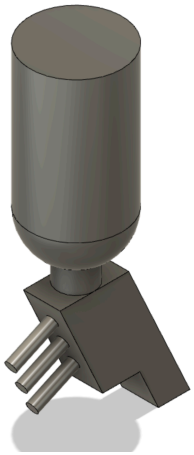

(a)

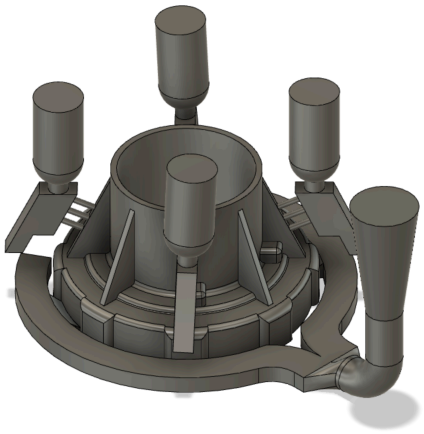

(b)

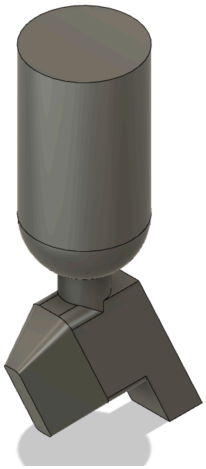

(c)

(d)

Figure 41: Poorly Designed Risers. Poorly designed and risers and inadequate riser locations. (a) An incredibly complex design was produced to introduce (b) gates that connect to the casting flanges. (c),(d) More simplified designs were developed to improve fluid flow into the riser but there was a call for total redesign.

Rigging Design – Risers

Most attention was drawn to the sprue, runners, and gating design of the rigging system for sand molds to which little attention was given to the design and placement of risers. The first attempt of riser designing was centered around taking AM to its fullest potential in mold production. Even though AM does offer the capability of producing complex designs, fancy shapes can lead to ruin, which was a worthy simulation to run since it only took a few minutes. The Figure 41 shows the preliminary riser designs that were

compensated at an angle and were to be placed at the flanges of the Bearing Housing. These riser designs and locations were a high risk for mold erosion, which is proven by the mold erosion analysis in Figure 42. Although the earliest risers were horribly designed, the problem was avoided, and the lesson was learned the easy way.

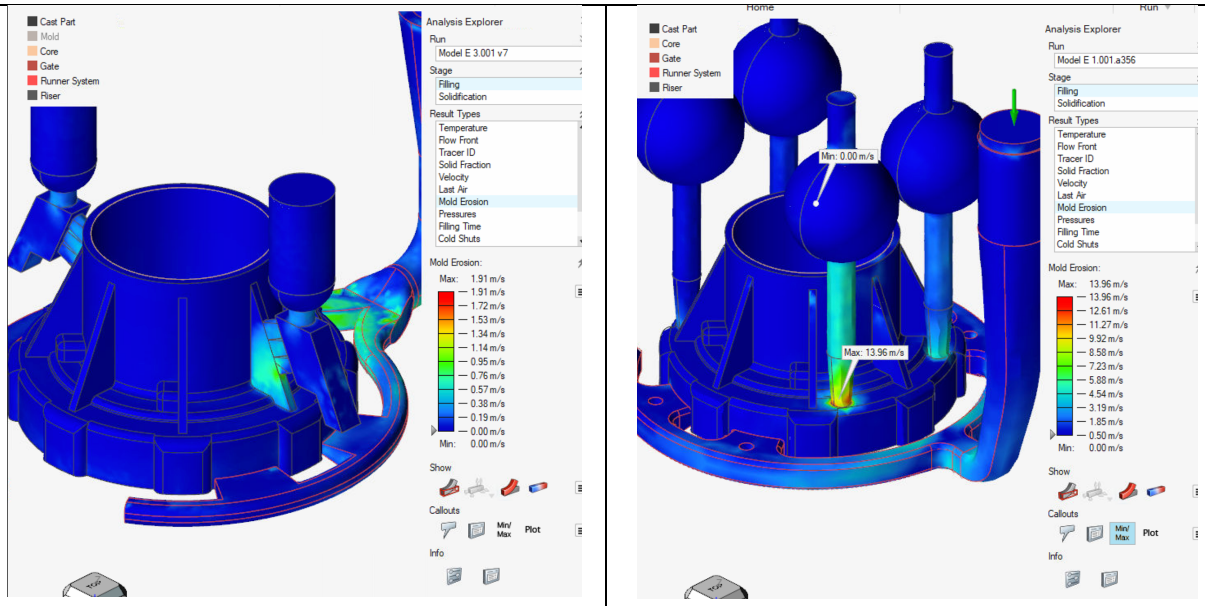

(a) (b)

Figure 42: Improper use of Risers. Niyama simulations were used to compare mold erosion from (e) improper to (f) proper use of risers. This resulted in discontinuing this placement and design of risers due to the risk of substantial shrinkage and sand entrainment [39], [40], [58]. This is also problematic due to potential distortion [24], [59].

Spherical risers were highly recommendation (et. al. Sama S, Badamo T) if AM production was possible as they cannot be produced by traditional methods [7]. Figure 43 shows the spherical riser designs that were finalized for both sand and investment casting processes. Complexity to riser geometries was possible for top fed rigging systems in investment casting because the risers in this adjacent to the runners instead of the part, which also minimizes post processing requirements.

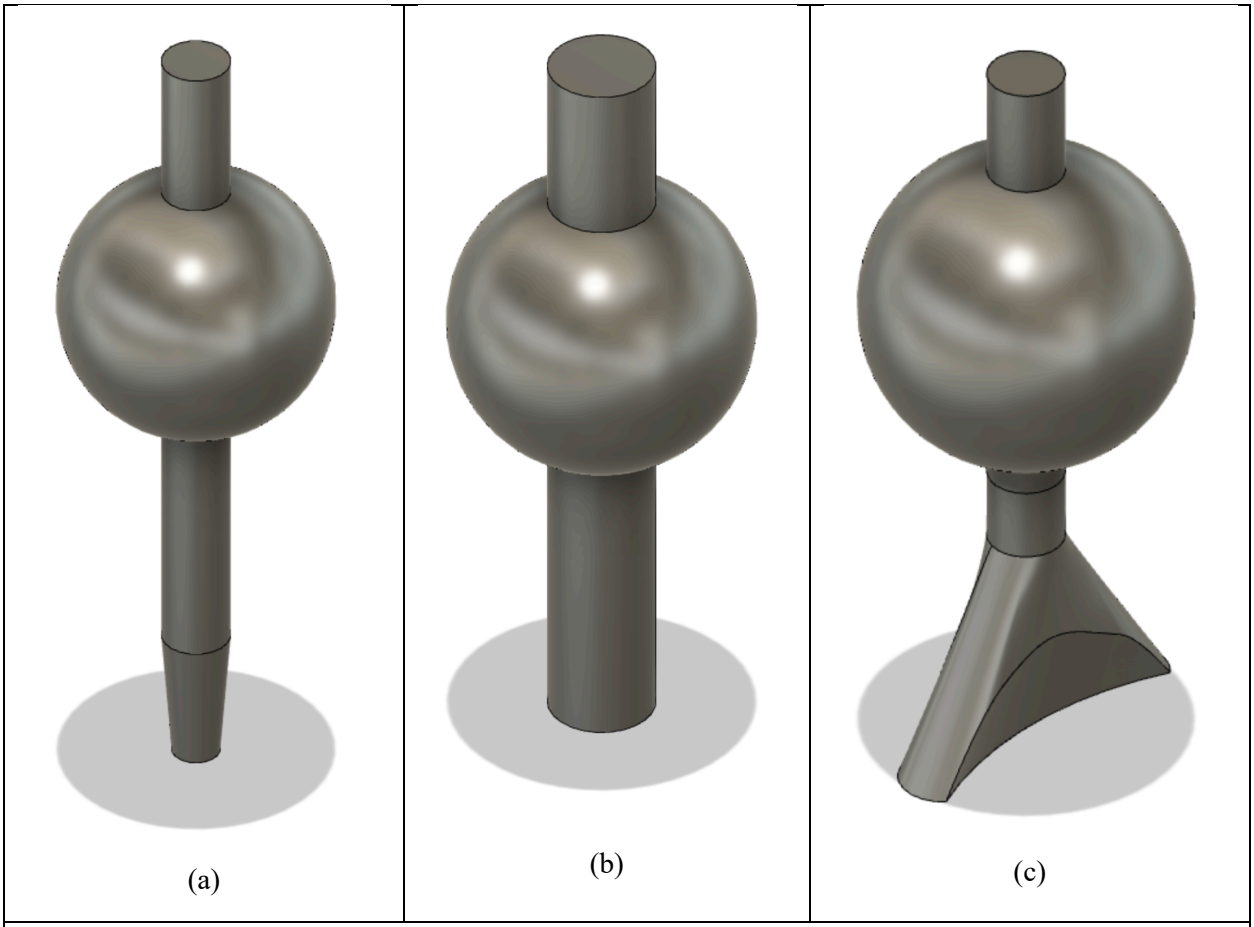

(a) (b) (c)

Figure 43: Spherical Risers. Spherical risers for (a) sand casting molds and (b) investment casting molds. (c) The investment riser on the right utilized the available area from the curvature of the runners given they do not need to be detached from the part during post processing.

Finite Element Analysis – GD Structural Component

GD is a virtual workspace in Fusion360 created by Autodesk in 2018 intended to maximize strength-to-weight ratios of mechanical components. It is done by combining the bases of finite element analysis (FEA)

case was with machine learning that recognizes critical cross sections resulting from constraints and loading conditions. Before diving into GD, a simple FEA simulation for a Journal Bracket is shown in Figure 44. The original design is shown in Figure 44(a) that has the basic volume and density. The setup and results of the FEA simulation is shown in Figure 44(b). The black arrows represent constraint locations for two pins and a fixed base where a faster is placed.

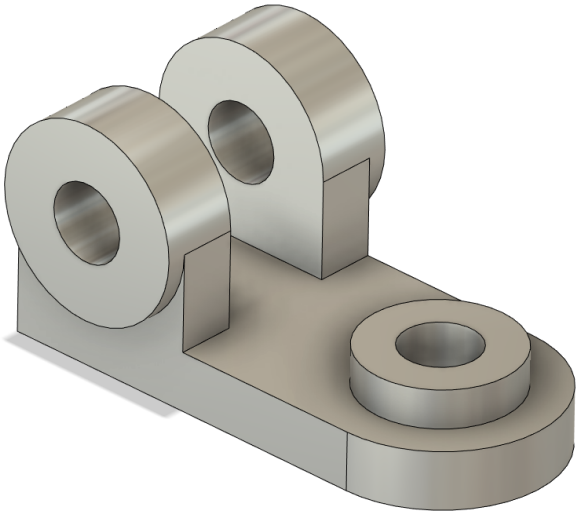

(a)

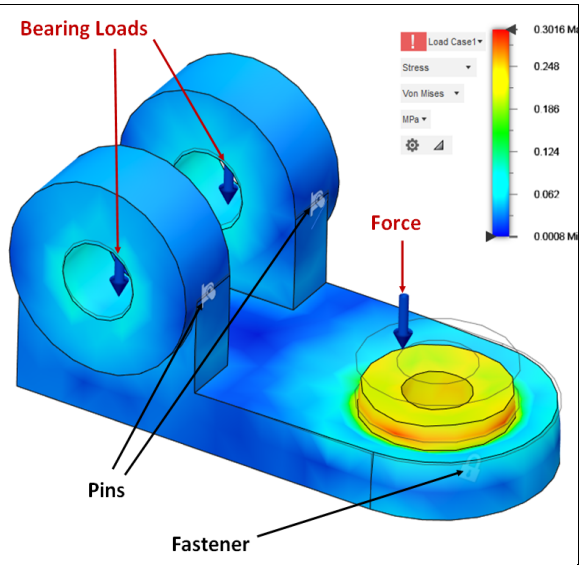

(b)

Figure 44: Finite Element Analysis Basics. A Basic FEA Simulation of (a) the Journal Bracket and (b) the loads and constrains, and deflection it would encounter while in service.

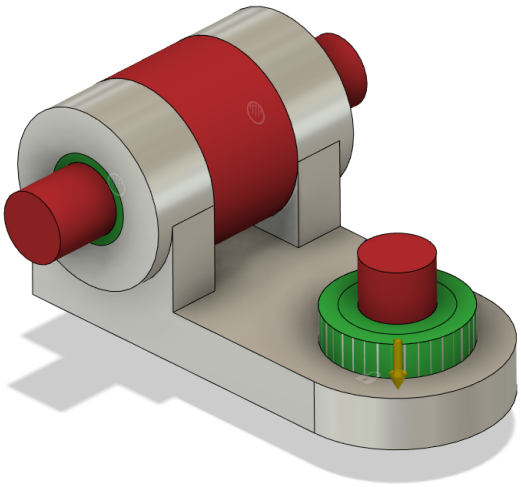

(a)

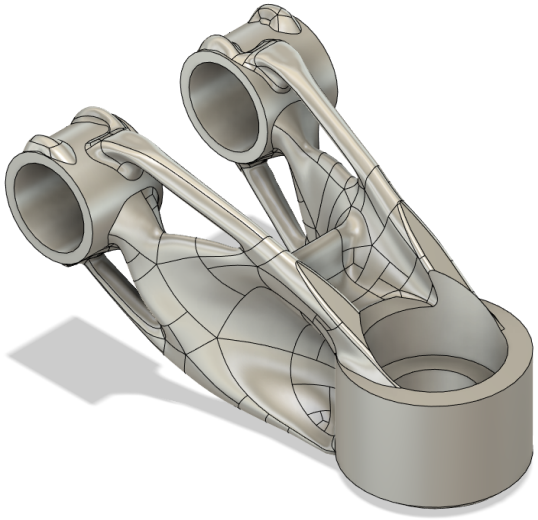

(b)

Figure 45: Generative Design for Solid Modeling. (a) The GD set up showing obstacle geometries in red. The structural loads and constrains are the same as defined in the FEA simulation. (b) The resultant geometrically optimized Journal Bracket with far better strength to weight ratio would be incredibly difficult for a human to create.

Their red arrows represent the loading conditions for two bearings and a normal force, respectively. For GD, the machine was assigned to take the FEA model and add material to high critical cross sections shown by the brighter regions while subtracting material to low critical cross sections shown by darker regions. The set up for a GD study is shown in Figure 45. The model had to be edited with new geometries that designate preserve geometries in green, where forces interact with the component and obstacle geometries in red, where material is not supposed to be added as shown in Figure 45(a) and the geometrically optimized design for increasing the Journal Bracket's strength-to-weight ratio is shown in Figure 45(b). GD presents a groundbreaking method for design optimization by surpassing human cognition and has been used extensively in numerous design projects [2]–[6]. GD can also be used to optimize fluid paths as will be explained.

GD Fluid Path

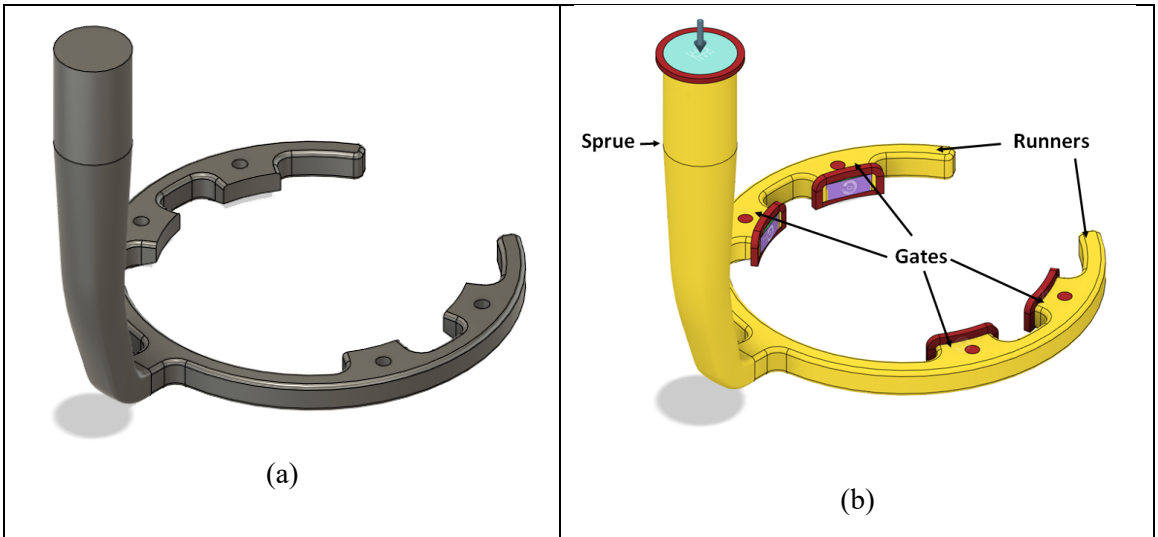

(a) (b)

Figure 46: Generative Design for Fluids. Set up of a GD fluid path for (a) an initial rigging design. (b) Yellow represents the rigging system comprising of the sprue, runners, and gates.

In 2021, Autodesk integrated CFD into Fusion's GD workspace that enabled designers to optimize geometries that manipulate fluid dynamic factors including output pressure and flow rate. For a casting process, these variables need to be at their absolute minimum to produce sound metal [27]. Explaining a GD study for a structural component helps to understand setting up GD for fluid paths, which were significantly more complex but were very effective for advancing the design criteria for this project.

Figure 46 shows the setup for one preliminary rigging system that was tested. The yellow bulk defines the starting shape of the fluid, which included the sprue, runners, and gates in this rigging system. Figure 47 shows the obstacle and preserved geometries in an isolated condition for clarity. The obstacle geometries were used to define the shapes of the cores, inlets, and outlets. The preserve geometries were shapes used to define fluid conditions including the inlet surface (cyan) at the top of the sprue, the outlet (purple), and the fluid pressure (purple) before the fluid exits the

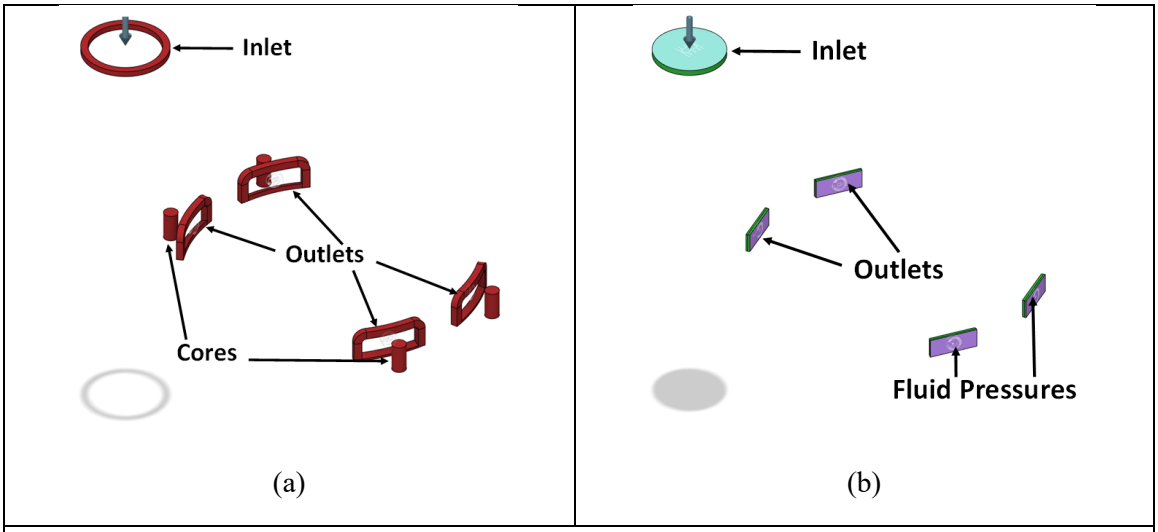

Figure 47: Geometries for Generative Design. (a) Obstacle Geometries were used to define shapes of inlets, outlets, and cores. (b) Preserve geometries were used to define areas of inlet, outlets, and fluid pressures. Inlet required a flow rate of 10 gallons per minute and the fluid pressures were defined to be 20 psi.

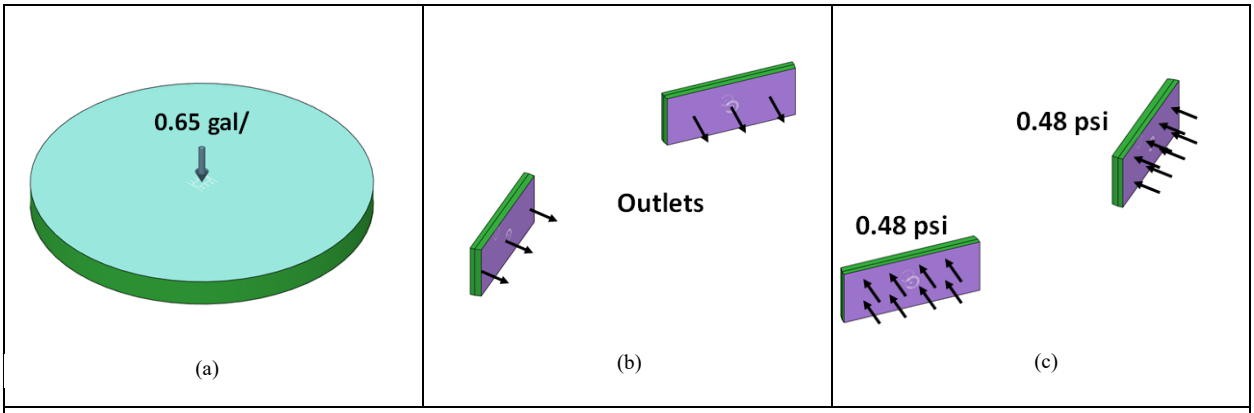

Figure 48: Preserve Geometries. (a) The inlet was set to 0.65 gallons per minute (GPM), (b) the outlet surfaces were faced toward the cavity, and (c) the fluid pressures were set to 0.48psi for each study. Note, the initial trials for learning GD were done at 10GPM and 20psi.

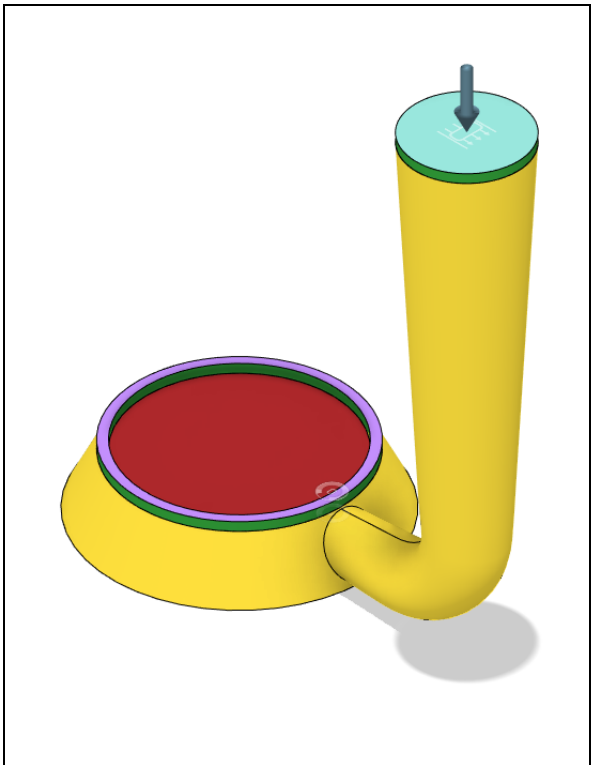

Figure 49: Improper Generative Design Set Up. Improper setup of a GD fluid path for investment casting rigging system. Proper setup will be displayed in RESULTS.

system. It should be noted that even though the outlets and fluid pressures are adjacent, they required their own preserve geometries. The surfaces where outlet and fluid pressures are defined needed to be positioned at opposite ends as shown in Figure 48. For consistent results, the variables for the inlet flowrate and fluid pressures were 0.65 gallons per minute and 0.48 psi, respectively. These values were based on simple calculations from Bernoulli Principles [35]. Equation 5 was used to calculate flow rate ($\dot{L}$),

$$\dot{L} = \frac{V}{t} = \frac{0.011\ \text{gal}}{0.5\ \text{s}} \left(\frac{60\text{s}}{1\text{min}}\right) = 1.32\ \text{GPM} \qquad \text{Eq. 5}$$

where volume of the rigging system is 0.011 gallons (41,623mm^3), determined in Fusion360, and time to complete filling was 0.5s, determined by InspireCast.

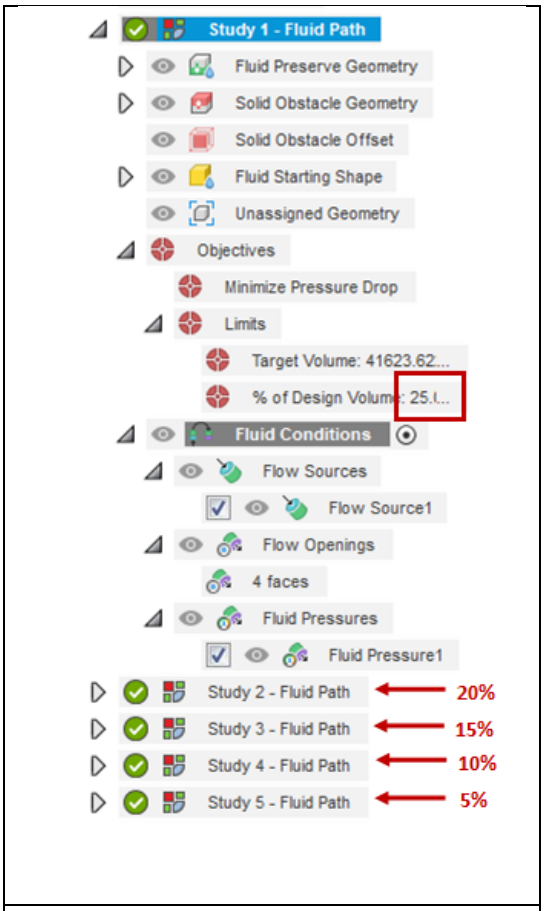

Figure 50: Design Criteria. The target volume was measured to be 41,623mm^3 and the GD set up was cloned into 5 studies that compared the anticipated efficiencies of each iterated design.

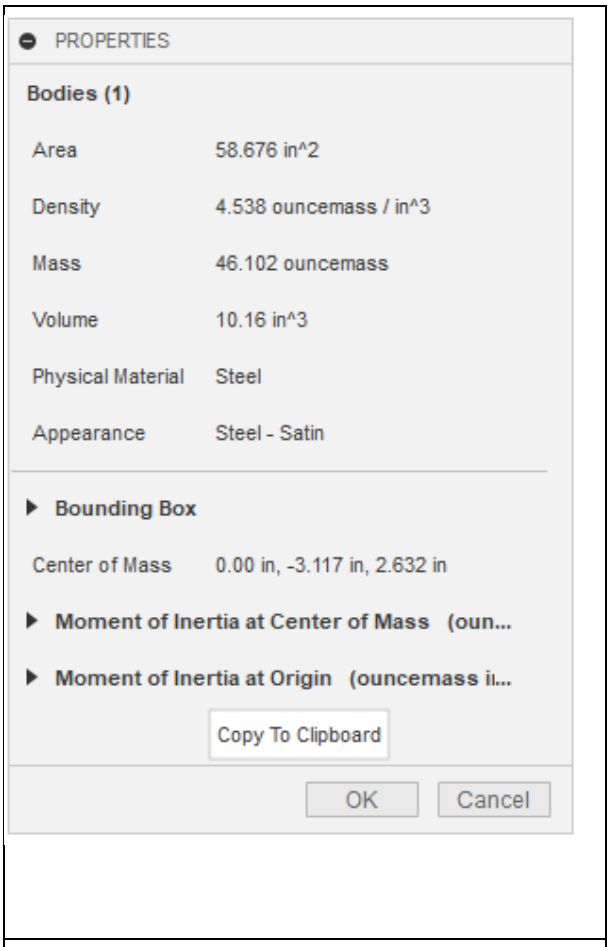

Figure 51: Filling Volume. Design of rigging system and the properties that Fusion360 calculates. The total volume of the rigging system was 10.16 in^3 (166,492.57 mm^3)

Equation 6 was used to calculate output pressure based on a height (h) of 5in and the density (ρ) of A356 is 0.0975 lb/in^3 (2700 kg/mm^3).

$$P = \rho h = 0.0975 \frac{\text{lb}}{\text{in}^3} * 5\text{in} = 0.48 \text{ psi} \qquad \text{Eq. 6}$$

The outlets did not require a specified flow rate because it will be determined in the study. Side note, a sample GD setup for the investment casting is shown in Figure 49. It will be addressed now that this is not an effective setup for a GD fluid simulation due to the obstacle geometry present in the center of the ring. It should be centered around the inlet as will be demonstrated later.

Finally, five clones of each study were created to compare different design criteria that varied based on percentage values of the target volume starting from 25% decreasing by 5% for each study, as shown in Figure 50. The total volume of the rigging system was determined to be 10 in^3 as shown in Figure 51. This was essential for providing variation to gauge a final GD model. The data for output velocities and pressure differentials were plotted as a function of time, which will be compared in the RESULTS section. At this point, the simulation can be submitted for processing to obtain geometrically optimized designs to lower fluid outlet pressures and velocities.

Thermal Fluid Simulations

InspireCast is a simulation software by Altair specially intended for metal casting. It was an efficient way to test numerous designs, verify theoretical design considerations are applicable, and gather fluid data based on rigging geometry and thermal data based on processing conditions. InspireCast provides ample information that was narrowed down to focus on thermal distribution, flow velocities, solidification time, microporosity, niyama criterion, and mold erosion in relation to timesteps.

Material Specification

Before setting up InspireCast simulations for sand and investment cast processes, the physical properties of A356 and dimensions of the Bearing Housing were required for better accuracy. Starting with fluid properties, values for the dynamic viscosity of the melt were calculated and plotted with respect to the Arrhenius-type relation shown in Equation 7, which determines the viscosity of an element past its melting point [60].

$$\eta(T) = \eta_0 \exp\left(\frac{E}{RT}\right) \qquad \text{Eq. 7}$$

where E is the activation energy, η_0 is the pre-exponential viscosity, and R is the gas constant. For aluminum, these values are 13.08 kJ/mol, 0.257 mPa*s, and 8.314 J/mol*K, respectively. The values for fluid properties that were logged into A356 custom material are shown in Figure 52.

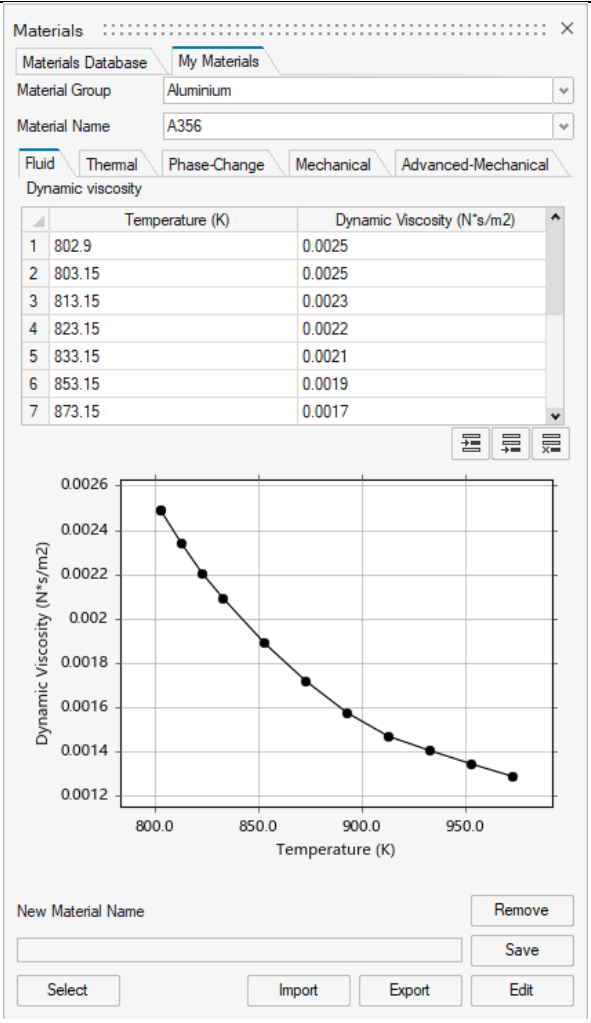

Figure 53: InspireCast Fluid Properties

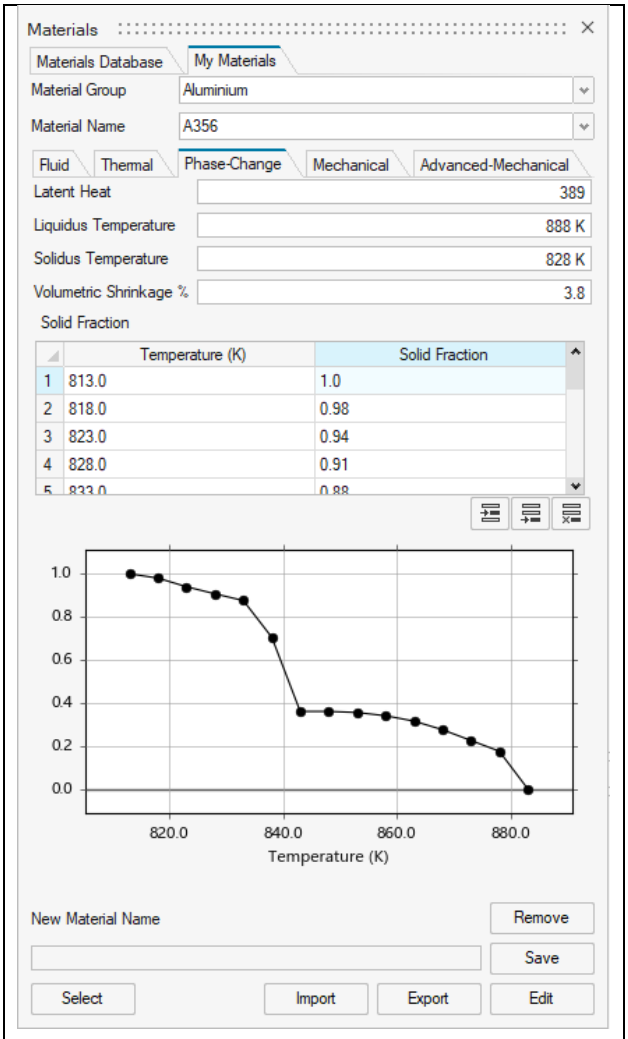

Figure 52: InspireCast Phase-Change Properties

The phase change properties were determined shown in Figure 53. The liquidous and solidus temperatures were set to 888 K and 828 K, respectively. The latent heat of fusion was set to 389 J/kg [61]. Solid fraction percentages per solution temperature were assigned based on experimental values (et. al. Birol, Y) [62] and the percentage of volumetric shrinkage was kept at the default value of 3.8% [33]. Thermal and mechanical properties were kept at their default values for aluminum.

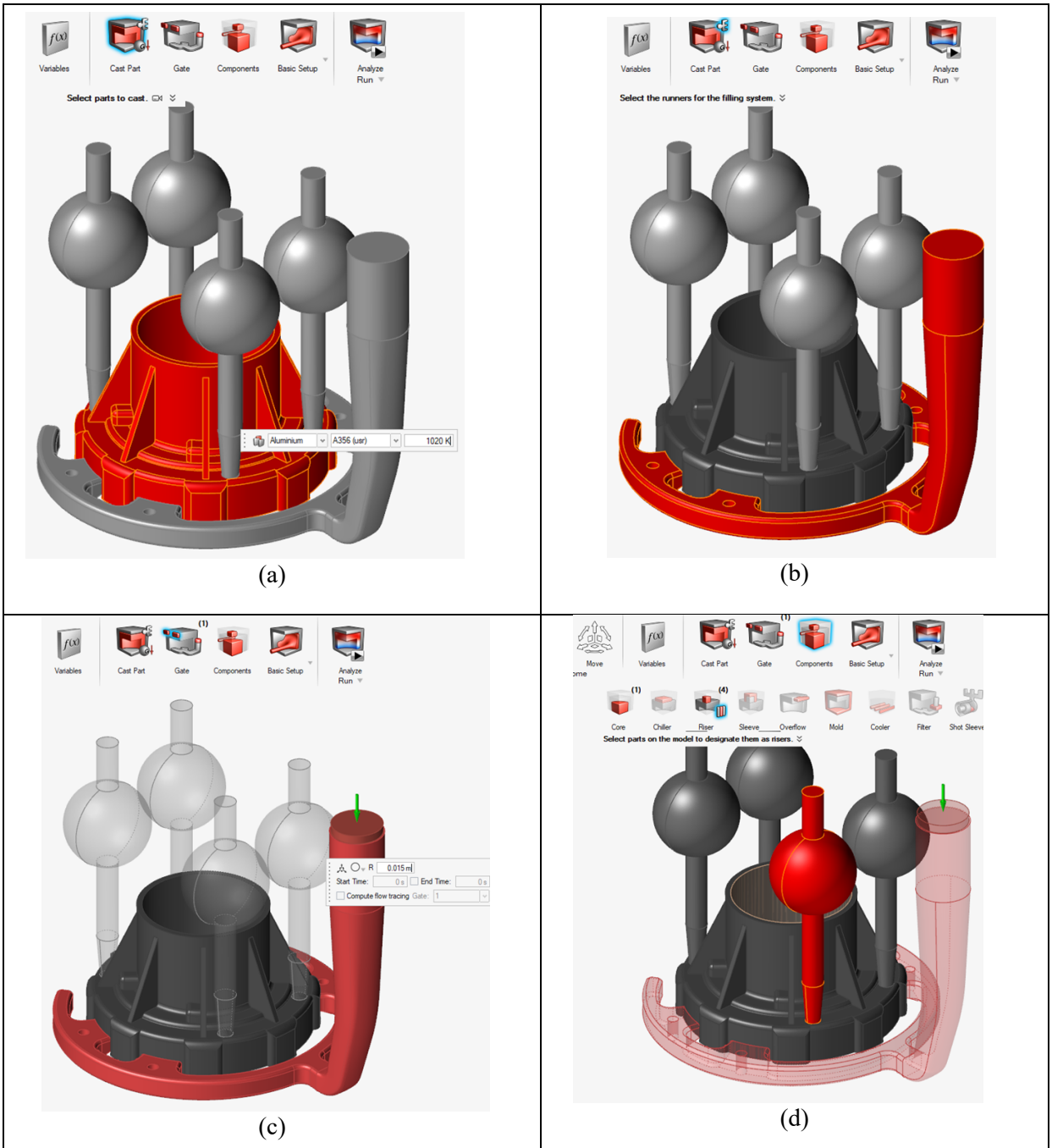

Figure 54: Inspire Cast Rigging Setup. InspireCast rigging setup. (a) Cast part with selected material was defined. (d) Defining rigging system from CAD design, which could be a GD optimized design. (c) The inlet location indicates where the metal is to be poured. (d) InspireCast automatically generates a core for the empty space and the risers are selected based on CAD design.

Process Planning

Once material specification was complete, defining the gates, inlet, cast part, core, and risers was effortless as shown in Figure 54. The gravity process was then selected with the option of investment casting as shown in Figure 55(a). The final and most important step is dimensional specifications in Run Analysis tab shown in Figure 55(b),(c), where the average thickness and minimum thickness/size were 0.012 m and 0.0024 m, respectively. Note, for investment simulations, Zirconia would need to be selected for the material option that would appear if investment casting was toggled on in Figure 55(a). Additionally, if investment casting is selected, the virtual mold option would need to be toggled off shown in Figure 55(c).

After the simulations are complete, Analysis Explorer is presented that offers ample options for analyzing results as shown in Figure 56. These results are based on Filling and Solidifications stages that were simulated. They will be elaborated in the RESULTS section.

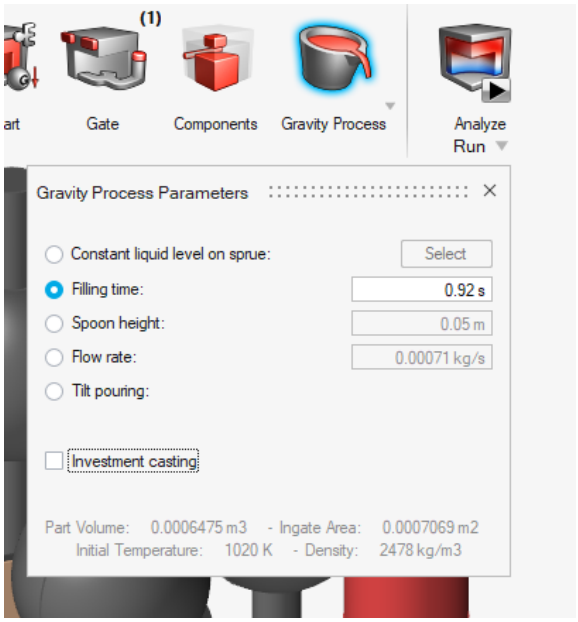

(a)

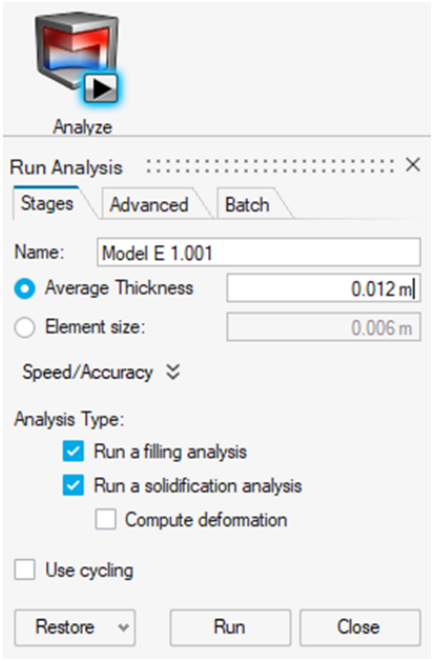

(b)

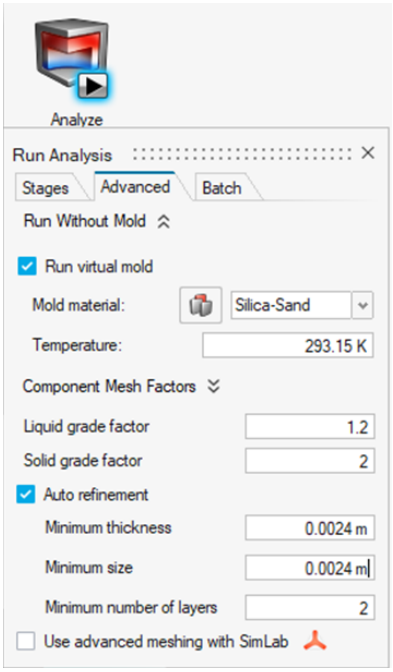

(c)

Figure 55: Inspire Cast Process Setup. (a) Process set up those entails defining a gravity fed process, where investment casting can be selected. Dimensional specifications of the (b) average thickness and (c) minimum thickness/size was pertinent for successful simulations

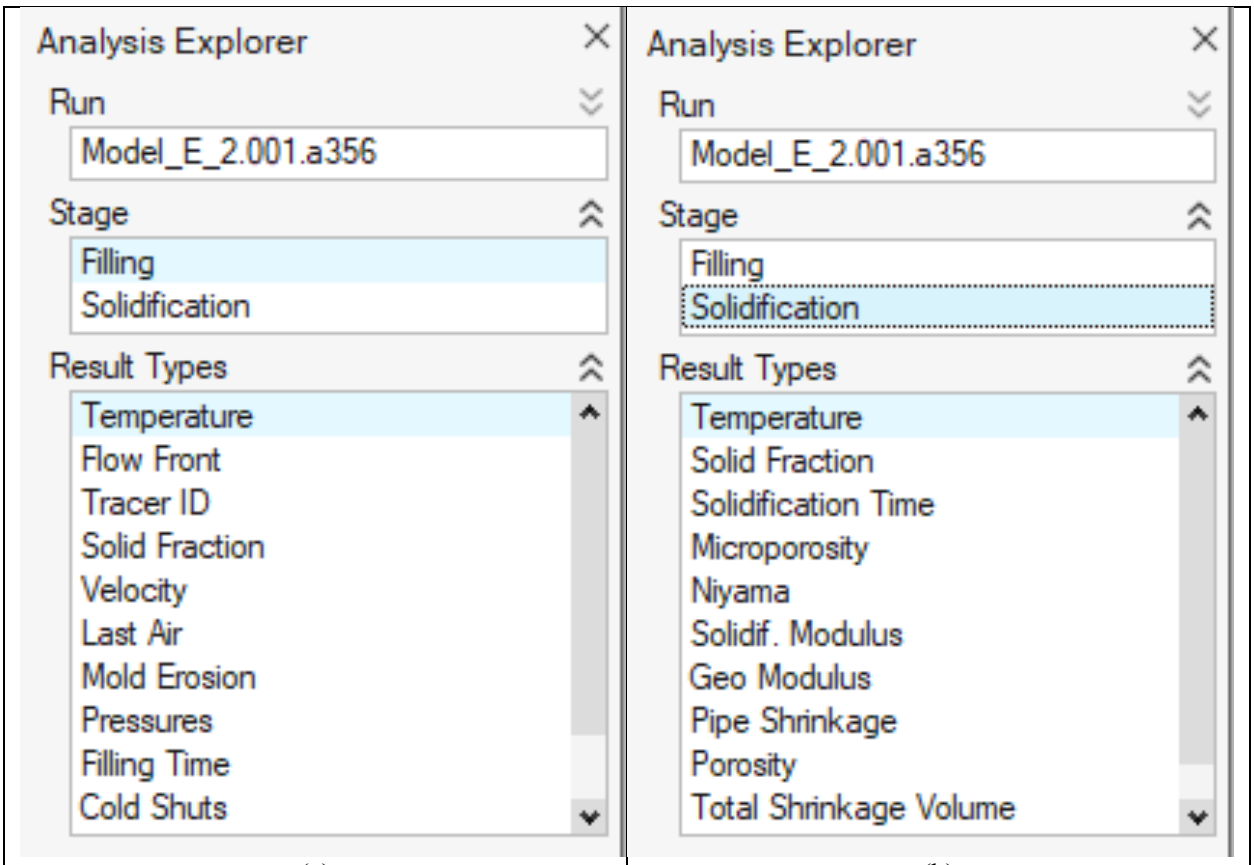

Figure 56: Inspire Cast Analysis Explorer. Analysis Explorer for (a) Filling results and (b) Solidification results. There are several types of results available for viewing. "Air Flow" and "Displacement" are two options that are at the bottom of the Filling results and "Displacement" is an option at the bottom of the Solidification results.

CHAPTER V

RESULTS

Initial Designs

Creating these was the end goal of the project. They were constructed based on evaluation and total redesigning of multiple poorly constructed rigging systems. After all the design models and iterations, the following designs shown in Figure 57 were confirmed as the initial rigging designs for sand and investment casting. Examples of slight modifications to initial mold designs were considered, such as core holes for sand molds and positions of inlets for investment molds. These rigging systems, except for Figure 57(c) due to similarity with Figure 57(a), were setup for further modifications using Generative Design (GD) to compare the design efficiency of AI to that of a human.

Generative Design Criteria

There is always room for improvement in rigging designs by either referencing industrial literature or by assigning an AI to interpret real time fluid behavior and modify the mesh boundary conditions to achieve a desired output velocity and/or pressure. Each GD simulation comprised of five studies that varied based on volumetric design criteria, which was discussed in Figure 50 and Figure 51. Figure 58 shows the GD setup for three initial designs using high resolution synthesis to increase the accuracy of pressure and velocity variations in respect to volume. The studies with optimal flow behavior were selected for simulated comparisons to the human designed models.

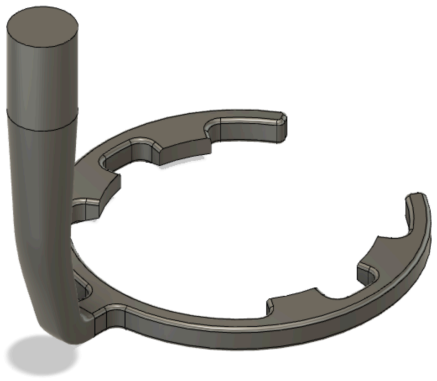

(a)

(b)

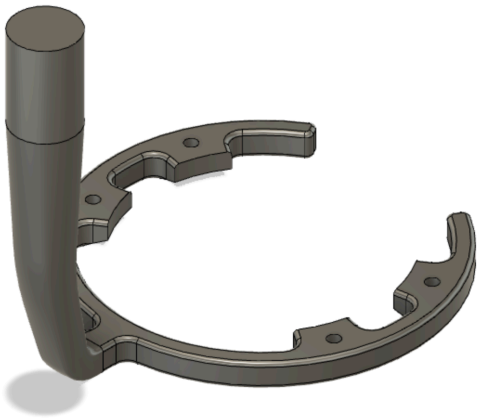

(c)

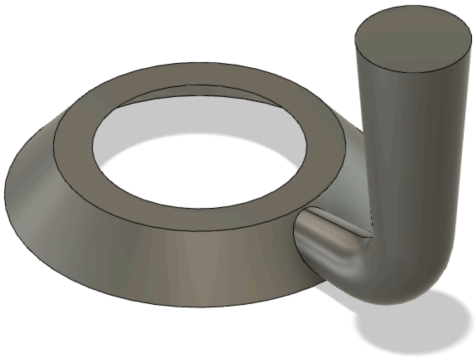

(d)

Figure 57: Initial Rigging Designs. Initial designs for rigging systems used for (a) sand molds and (b) investment molds. Small modifications can be made to each that can improve casting efficiency. Examples of small modifications can be (c) the application of core holes for sand casting or (d) repositioning of the inlet for investment casting. These designs chosen for GD processing except for the modified rigging system for sand casting shown in (c) because the GD results were substantially similar to the initial design.

Volumetric Conditions

Figures 59-61 show the resultant pressure-drop and maximum velocity values as a function of volume change for the design criteria for the GD models. The fluid dynamic data provided a baseline for the optimal

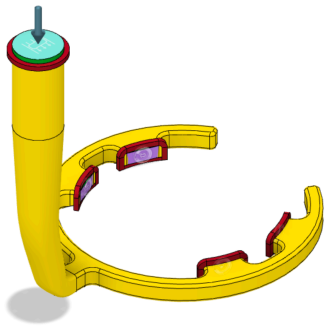

(a)

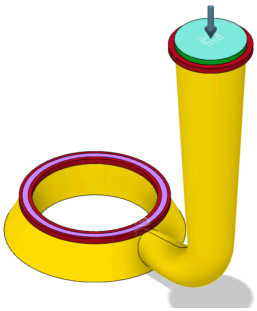

(b)

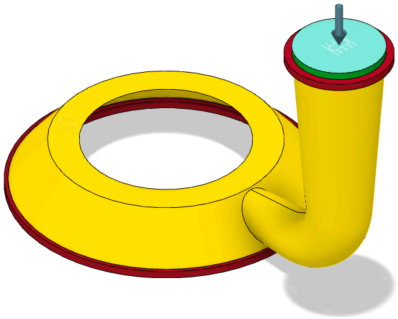

(c)

Figure 58: Generative Design Setup for Initial Designs. GD setup for initial designs developed for (a) sand and (b),(c) investment rigging systems and their corresponding velocity-volume plots on the right side of each setup. The investment rigging systems were compared between (b) bottom fed and (c) top fed inlets. The GD models that reached the lowest velocities (top right corners) were chosen for casting simulations.

GD designs that were used in the casting simulations, which are compared to their original human designs in Figure 62.

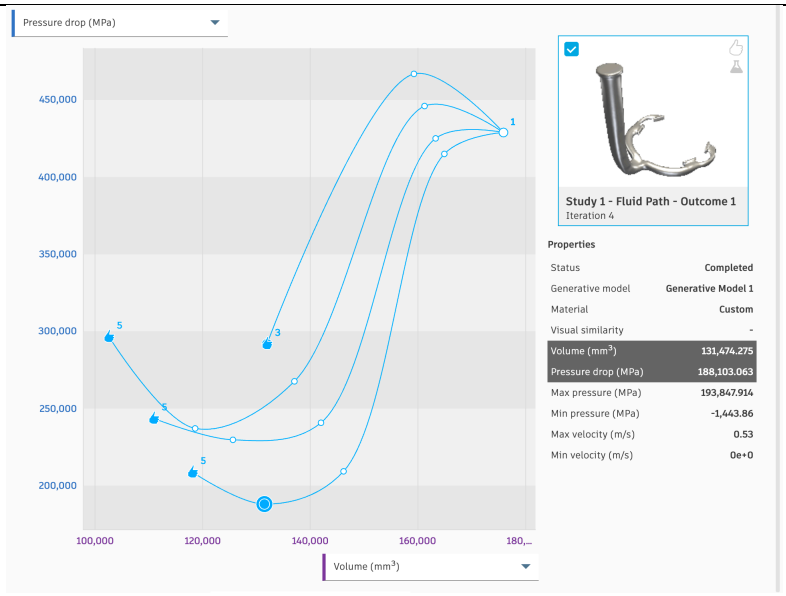

(a)

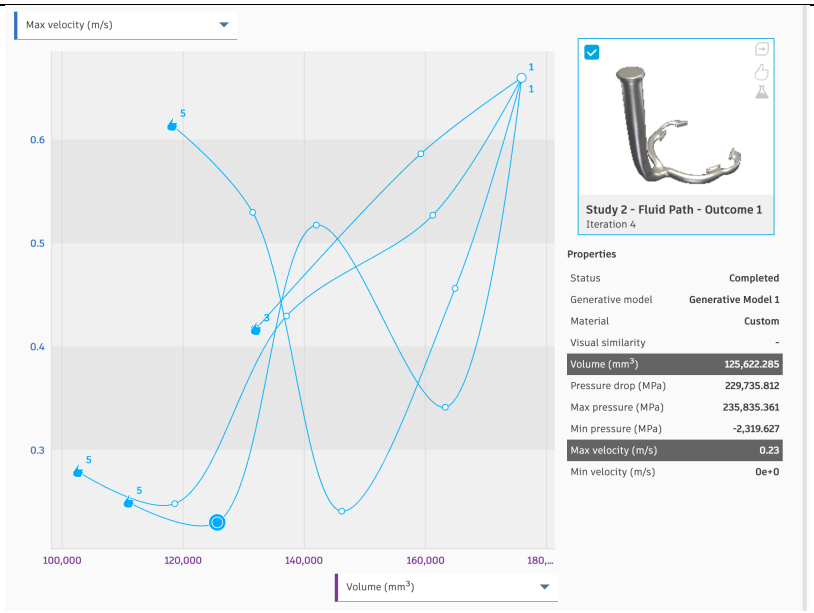

(b)

Figure 59: Fluid Dynamic Data for Model_B_10.003. Fluid dynamic data for GD model for sand casting (Model_B_10.003). (a) Pressure-drop as a function of volume change showed that Study 1 (25% of Target Volume) had the lowest pressure value and Study 5 had the highest. (b) The maximum velocity-volume change plot showed that Study 2 exhibited the lowest value, which would be the most favorable to minimize turbulence inside the cavity.

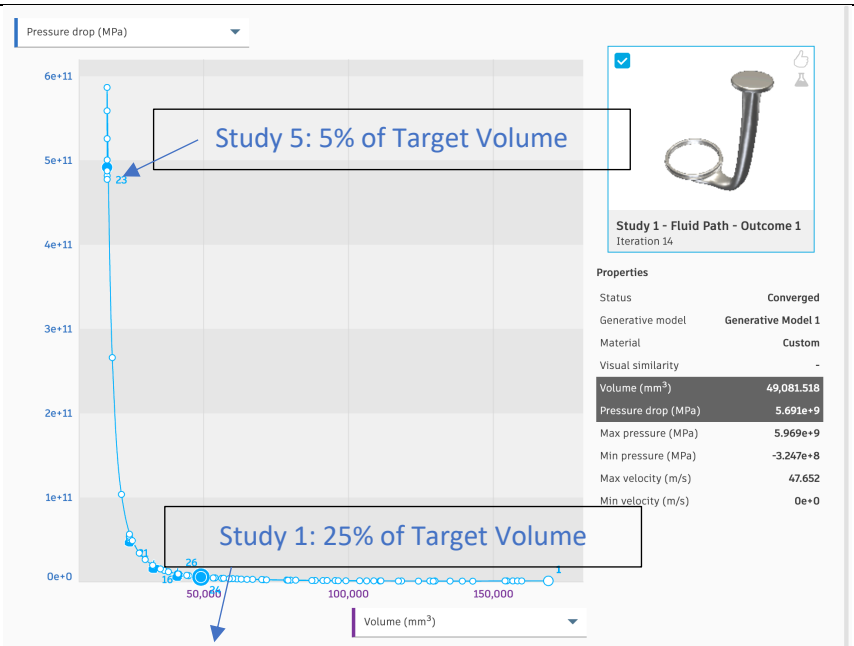

(a)

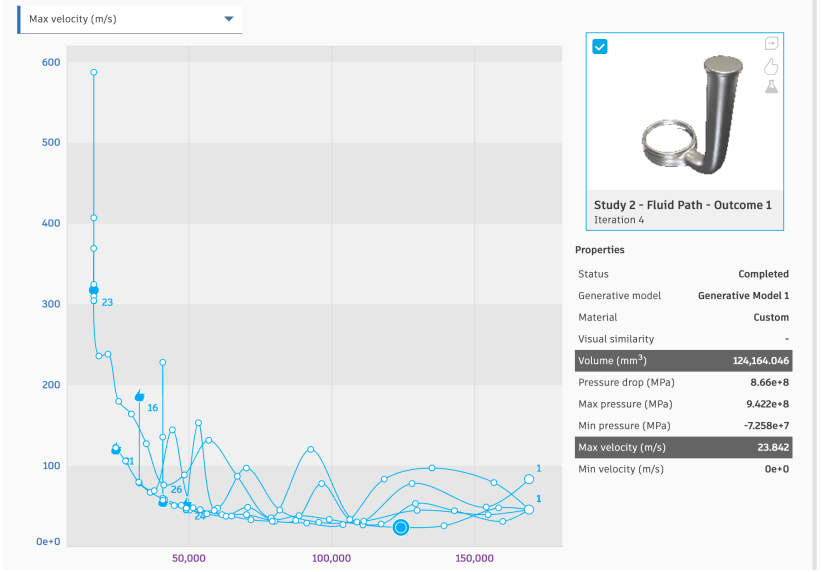

(b)

Figure 60: Fluid Dynamic Data for Model_Di_1.003. Fluid dynamic data for GD model for bottom fed investment casting (Model_Di_1.003). (a) Pressure-drop values exhibited exponential increase of pressure drop as the volumetric design criteria of target volume decreased. (b) Study 2 (20% of Target Volume) exhibited the lowest velocity and was used in the casting simulations.

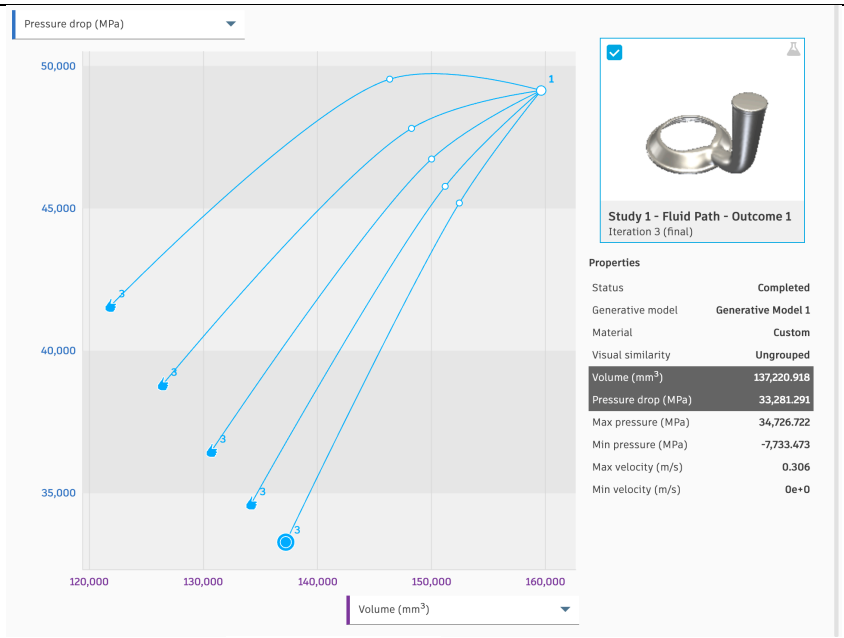

(a)

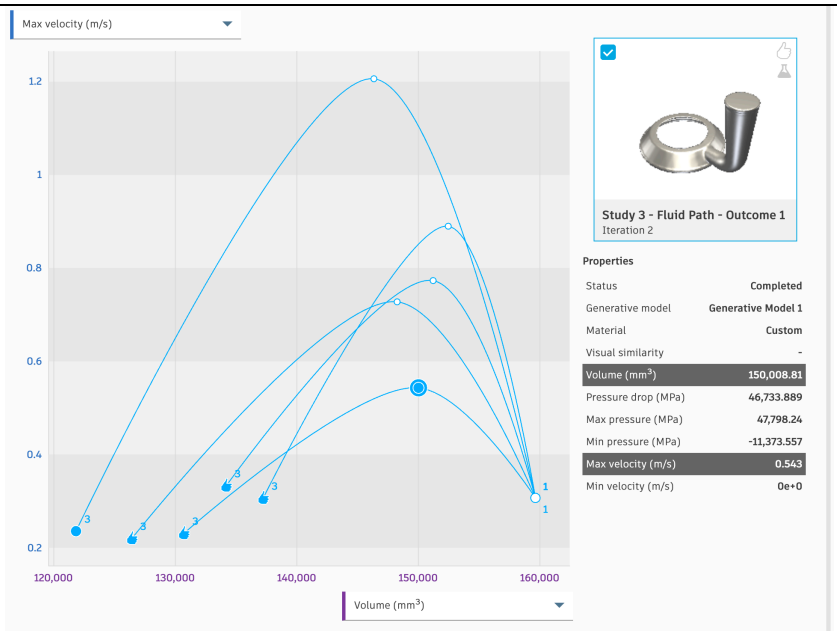

(b)

Figure 61: Fluid Dynamic Data for Model_Gi_1.003. Fluid dynamic data for GD model for top fed investment casting (Model_Gi_1.003). (a) The pressure-drops decreased with increasing target volume increased. (b) Study 3 (15% of Target Volume) exhibited the lowest velocity, which was why it was selected for casting simulations.

(a) (b) (c) (d) (e) (f)

Figure 62: Comparison of Initial Designs to Generative Designs. (a),(c),(e) Initial designs that were designed by humans and (b),(d),(f) GD modified designs feature a change of morphology, which involves shape optimization in critical locations where fluid will interact with the mold upon pouring.

Casting Simulations

InspireCast was an efficient tool for rapidly modeling vast numbers of real world casting operations. It allowed the designers to test each preliminary model design to determine the most effective based on filling and solidification analysis. This greatly sped up the development of the initial designs. Not all analysis were necessary for discussion because some of them could be directly correlated with each other, such as velocity and porosity.

Filling analysis was used to inspect filling time, velocity, mold erosion, and global pressures. Since ambient environments might be colder, filling time was monitored using flow front analysis to determine which mold design will complete filling the cavity first. An example of an incomplete filling is shown in Figure 63, which seemed to happen at the gusset closest to the sprue for each of the sand cast simulations. Figure 64 shows the last places to get filled for investment casting designs occurred at the tops for bottom fed designs and right below the sprue outlet for bottom fed designs. Velocity is known to increase turbulence, which increases risk for casting defects [20]. Mold erosion was monitored because it identifies zones where mold failure is most likely to occur as well as entrainment of sand particles can become an issue [58]. Pressures were considered because a higher pressure may be desired in thin walled and/or uniform sections since no modifications could be made to the Bearing Housing dimensions [21], [28].

For the solidification analysis, microporosity analysis was inspected because it varied substantially between designs, where the porosity analysis did not. Microporosity is related to the Niyama criterion. However, Niyama criterion factors in the effect that the mold materials have on risks of shrinkage, which was an additional factor to stay aware of at critical areas.

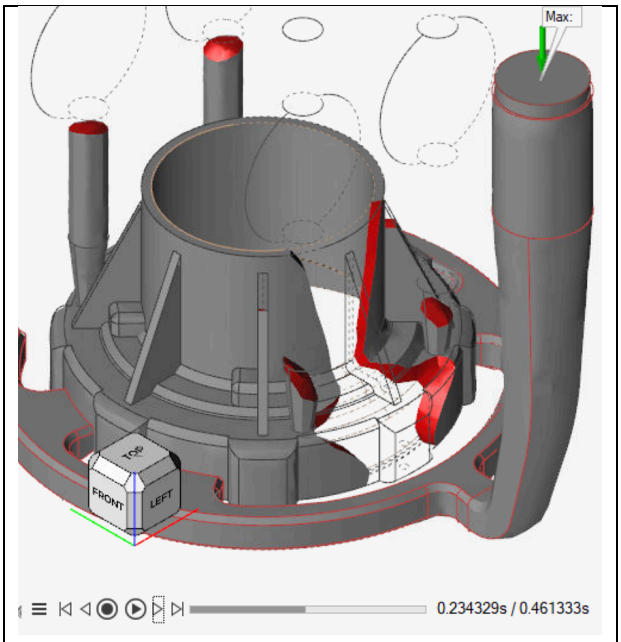

Figure 64: Flow Front - Investment Casting. Flow front indicating an incomplete filling. This is likely to happen in colder environment or if the metal was not heated enough before pouring.

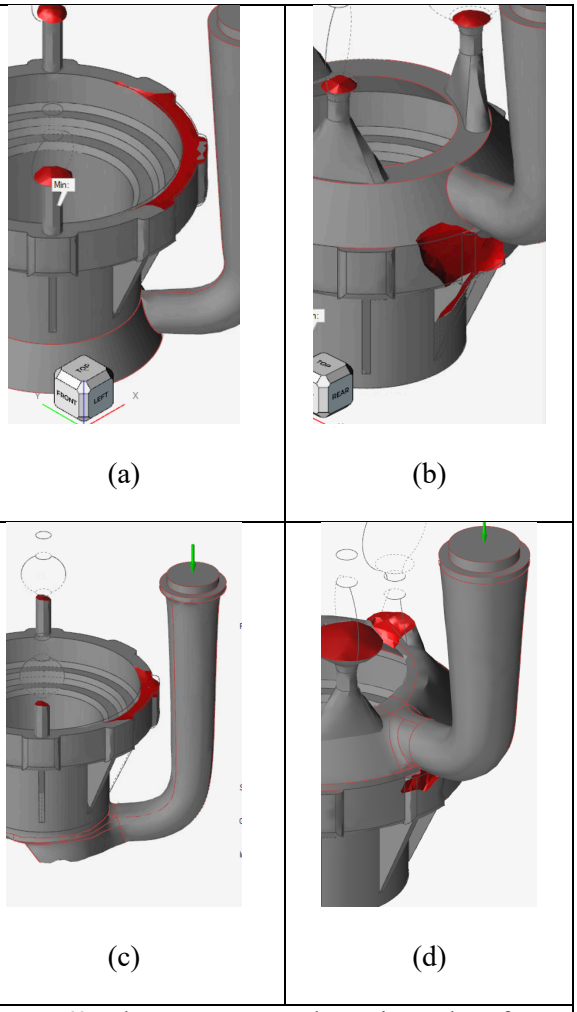

(a) (b)

(c) (d)

Figure 63: Flow Front - Sand Casting. Flow front indicating incomplete filling of investment casting designs. It occurred at the (a),(c) top of the cavity for bottom fed designs and (b),(d) underneath the sprue inlet gate for the top fed designs. The human designed models are shown in (a) and (b) while the GD models are shown in (c) and (d).

Filling Time Simulations

The time steps were paused right at the point where filling of the final gusset was complete for each simulation as shown in Figure 65 for sand casting and Figure 66 for investment casting. Results are presented with zoomed in images of the timelines.

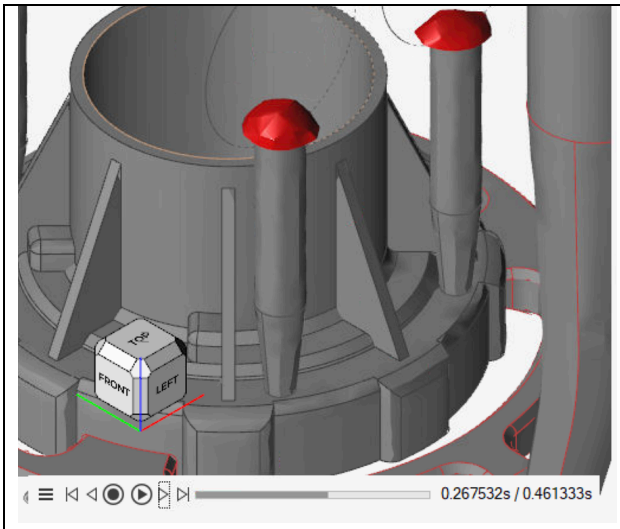

(a)

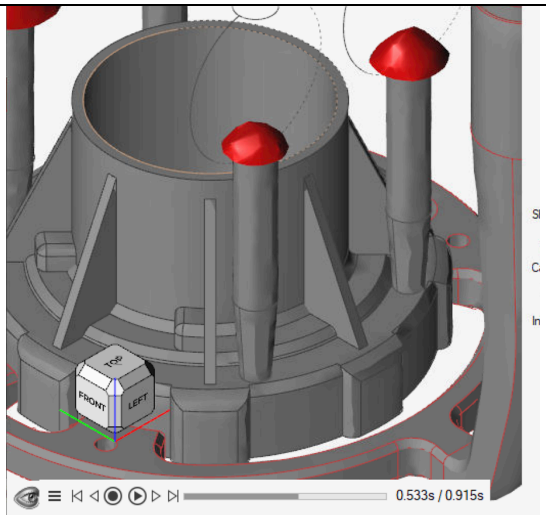

(b)

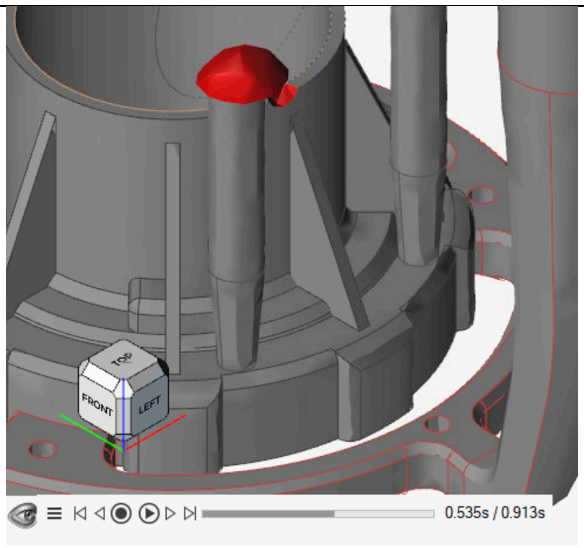

(c)

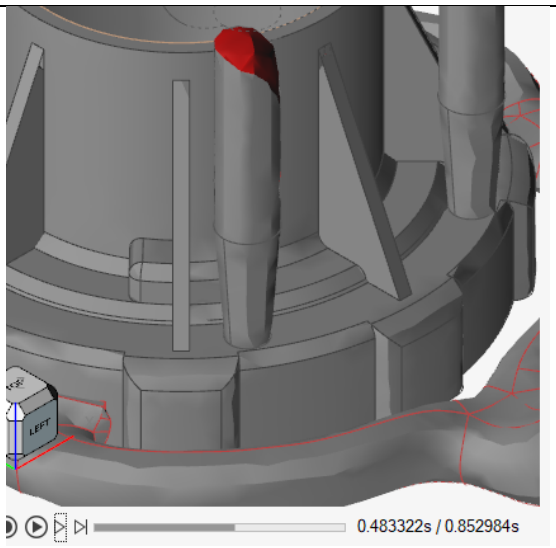

(d)

Figure 65: Filling Times - Sand Casting. Filling times for sand casting molds. (a) The initial design without core was the first to fill at 0.267s timestep. The modified design with core holes finished at about the same time of 0.53s timestep. (d) The GD modified mold finished at the 0.483s timestep.

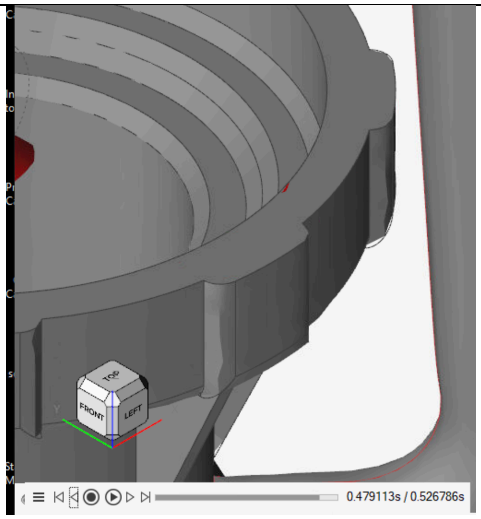

(a)

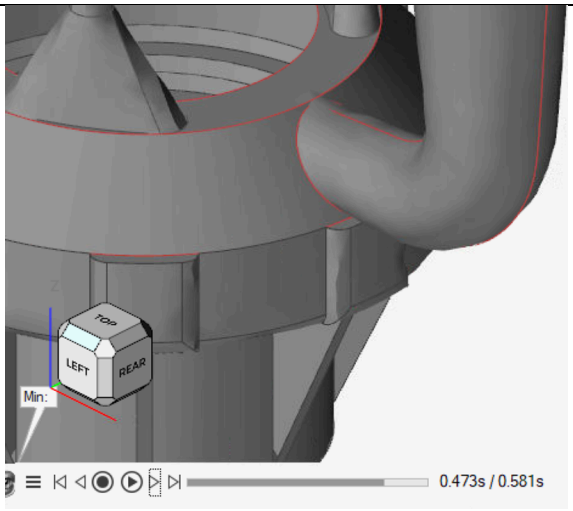

(b)

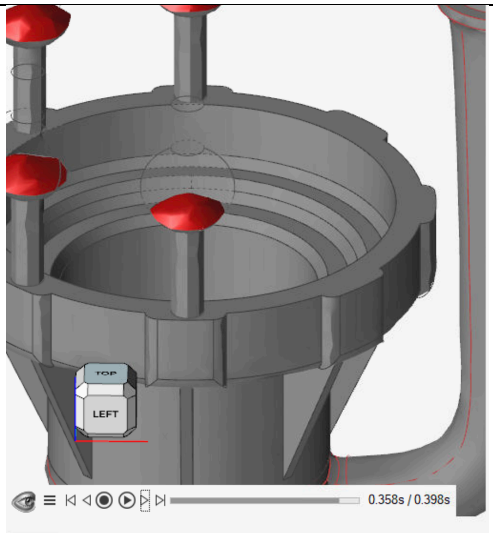

(c)

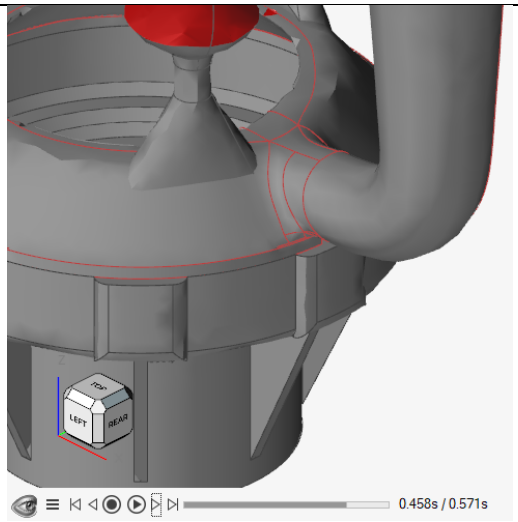

(d)

Figure 66: Filling Times - Investment Casting. Fill time simulations for investment molds. (a) The human designed bottom fed mold finished at the 0.479s timestep. (b) The human designed top fed mold finished at the 0.473s timestep. (c) The GD bottom fed mold finished at the 0.358s timestep and (d) the GD top fed mold finished at the 0.462s timestep.

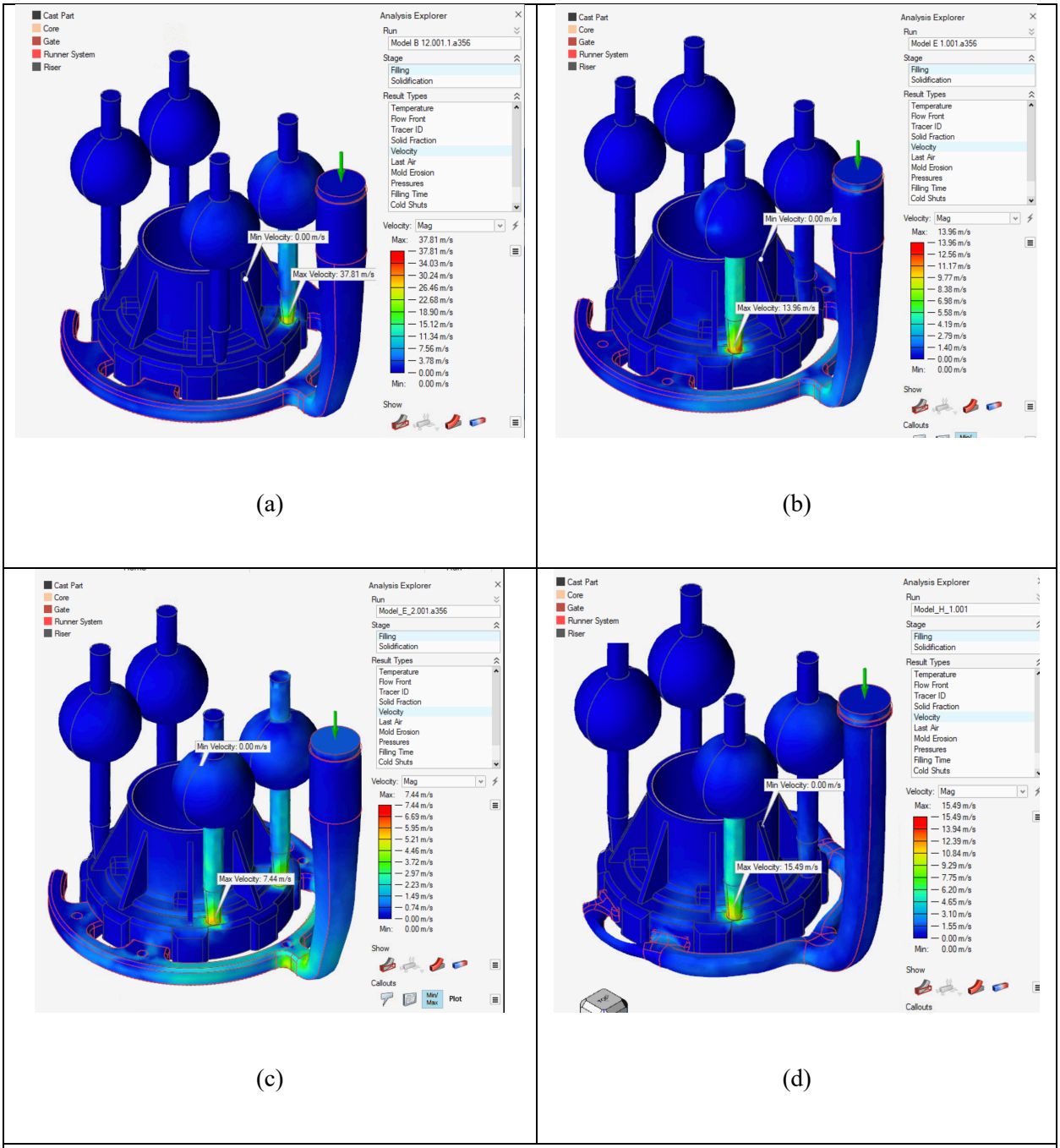

Figure 67: Velocity Simulations - Sand Casting. Velocity simulations for sand mold designs. (a) Initial design without core holes exhibited the highest velocity of 38 m/s located at the riser gates. This was the highest velocity compared to all other modified designs. (b),(c) Human modified initial designs with core holes exhibited highest velocities of 14 m/s and 7 m/s at the riser gates respectively. The model with an additional core hole at the sprue-runner T-junction exhibited the lowest velocity of all modified designs. (d) The GD modified design exhibited a velocity of 16 m/s at the riser gate, which was higher in comparison to the core-hole modified designs.

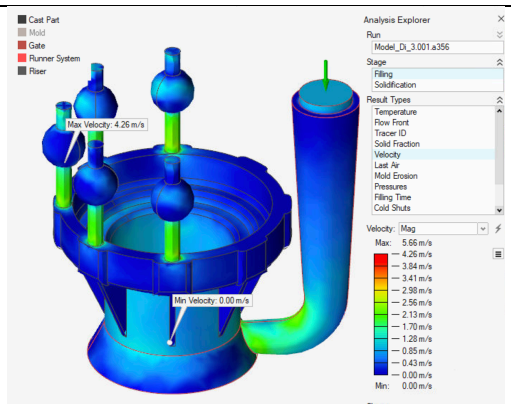

(a)

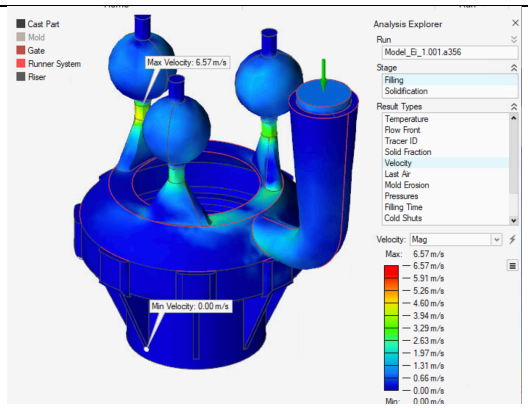

(b)

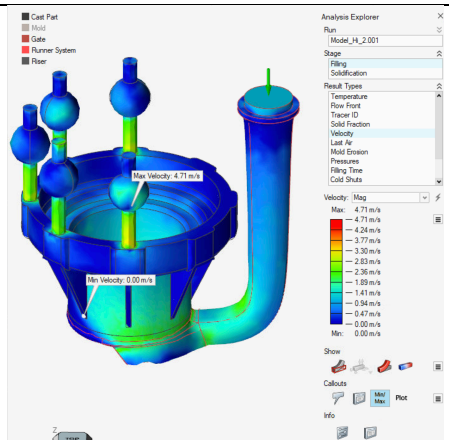

(c)

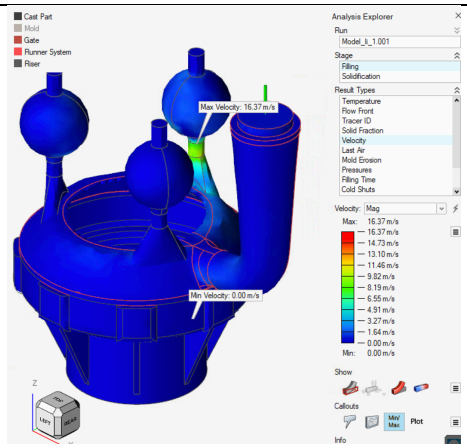

(d)

Figure 68: Velocity Simulations - Investment Casting. Velocity simulations of initial designs for investment casting. (a) The human designed bottom fed system had a maximum velocity of 3.29 m/s located at the base of the inlet. (b) The human modified top fed system had a maximum velocity of 5 m/s and 7 m/s located at the riser gates. (c) The GD bottom fed system had a maximum velocity of 4.71 m/s located at the sprue outlet (d) The GD top fed system had a maximum velocity of 16.4 m/s, which was the highest of the four located at the top of the riser.

Velocity Simulations

Velocity analysis of the sand models are presented in Figure 67. Velocity variations from the sand models proved that core holes applied at all T-junctions, including the sprue-runner junction was the best for minimizing velocity, and potential turbulence inside the cavity. Velocity analysis for investment castings is shown in Figure 68. Visually, the highest velocities were exhibited in the GD bottom fed model for investment casting at the metal entry point. Quantitatively, the highest velocity was exhibited at the riser section of the GD top fed model for investment casting.

Mold Erosion Simulations

It has been demonstrated in Figure 42 that mold erosion can happen anywhere in a mold design, but this result is more tolerable in some zones than others, depending on the selected riser location. Figure 69 shows the resultant mold erosion simulations for the sand molds. Likewise, the resultant mold erosion for investment casting is shown in Figure 70.

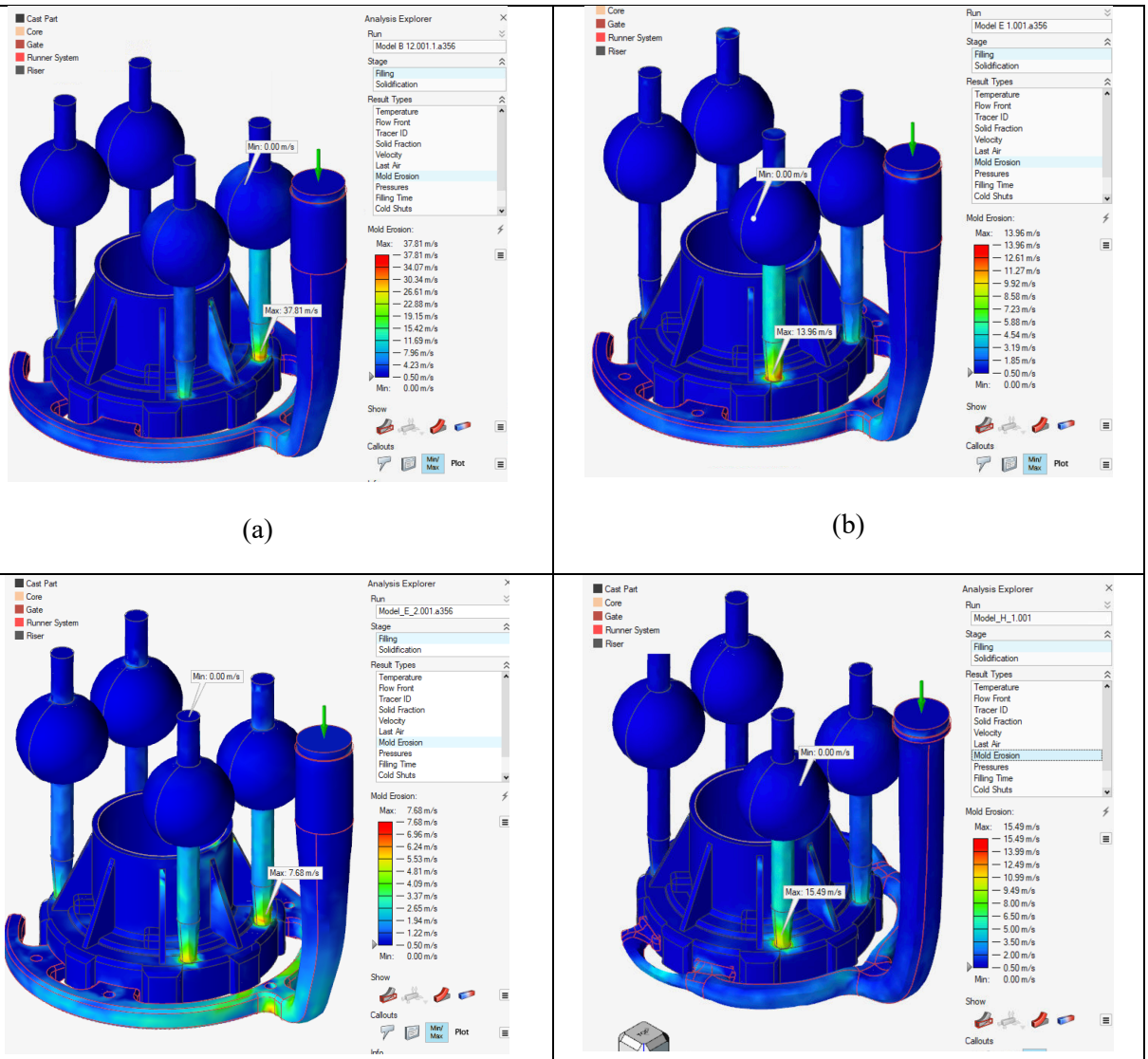

Figure 69: Mold Erosion Simulations - Sand Casting. Mold erosion simulations of initial designs for sand casting. (a)-(c) Qualitative analysis has shown that most mold distortion occurred at the riser inlets that was positioned at the top portion of the Housing base positioned closest to the sprue. Quantitative analysis has shown that the maximum distortion occurred in the (d) GD model at a gusset located opposite of the sprue.

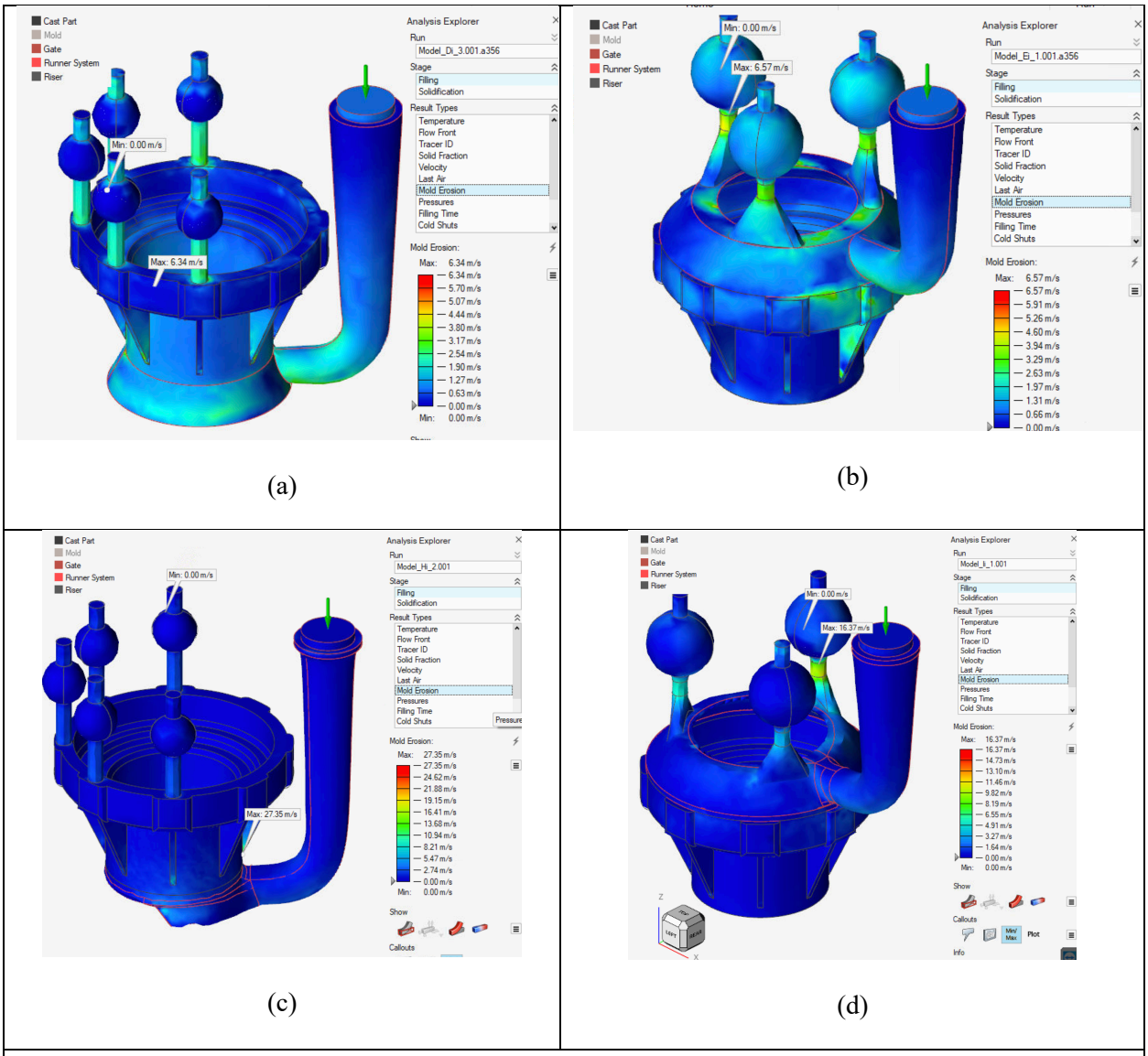

Figure 70: Mold Erosion Simulations - Investment Casting. Mold erosion simulations of initial designs for investment casting varied drastically from each model. (a) The bottom fed, human designed model indicated most of the distortion occurred at the gussets. (b) The bottom fed, GD model suggested majority of mold distortion occurred at the base of the sprue.

Pressure Simulations

Figure 71 shows the results for pressure variations within the sand casting cavities. Contrary to predictions, the highest pressurized regions were observed in the initial design without core modifications. Figure 72 shows the pressure results for investment casting, where the highest pressures occurred in the top fed designs, which may be favorable if complete filling of the gussets was difficult to achieve.

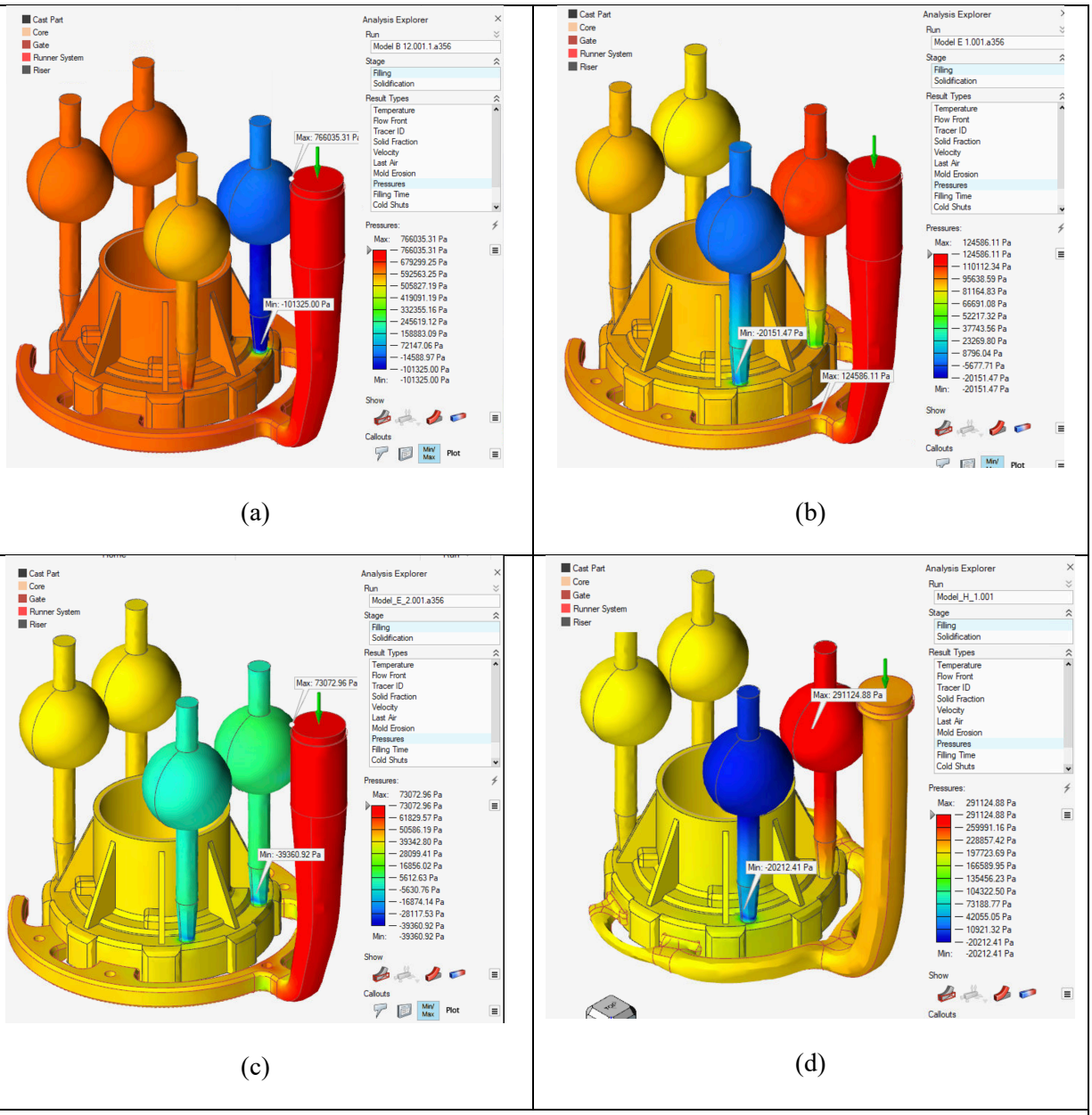

Figure 71: Pressure Simulations - Sand Casting. Pressure simulations of initial designs for sand casting were questionable because the high pressure was observed in the (a) initial design. There are times where increased pressure is favorable to fill uniform and/or thin sections.

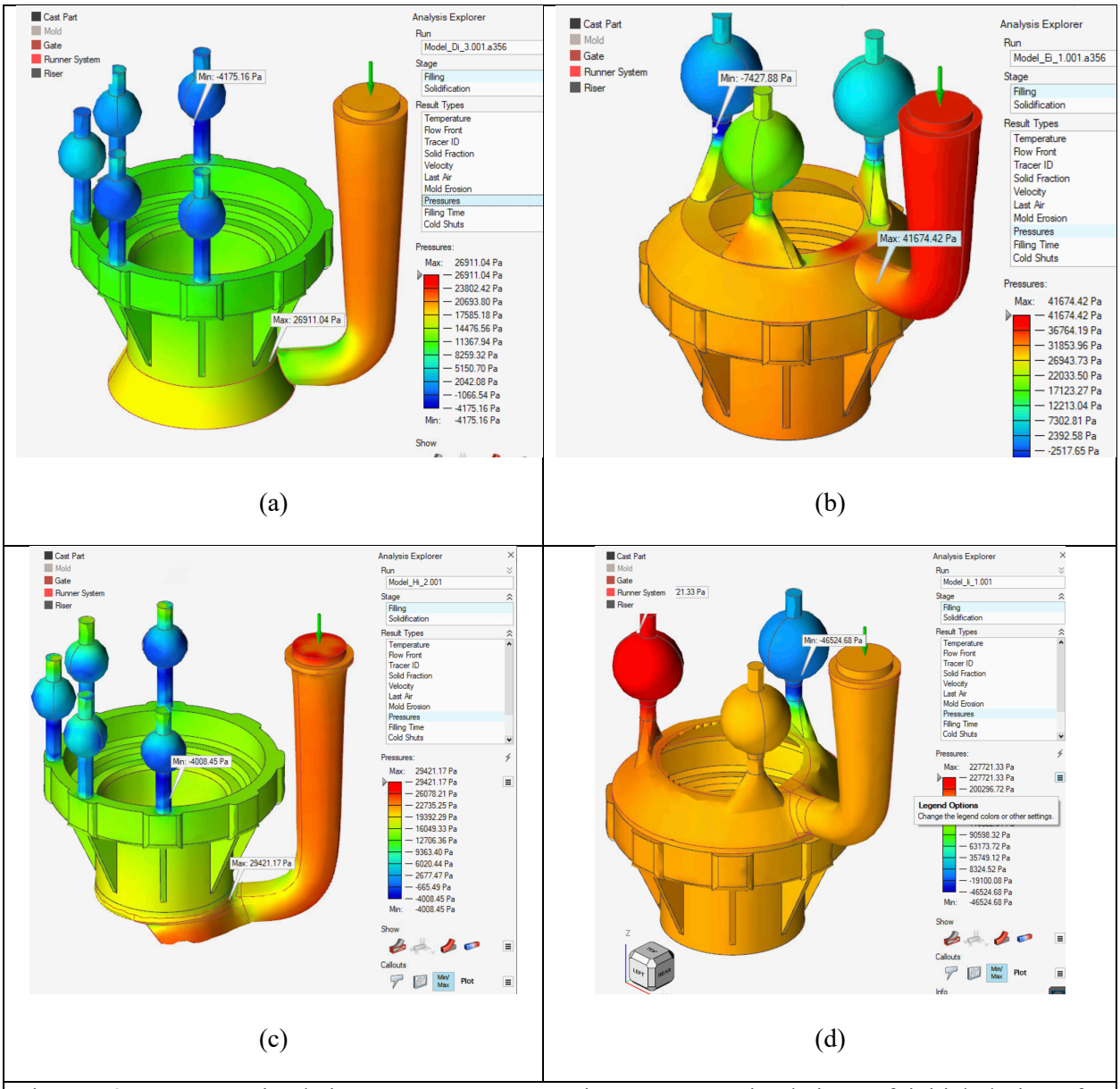

Figure 72: Pressure Simulations - Investment Casting. Pressure simulations of initial designs for investment casting. Lower pressure was observed in both (a),(c) bottom fed designs in comparison to the two (b),(d) top fed designs.

Microporosity Simulations

Figure 73 presents the microporosity formation that occurred in the sand casting simulations and Figure 74 shows microporosity for investment casting. The initial design exhibited the least amount of microporosity, which is a consideration to compare with Niyama values.

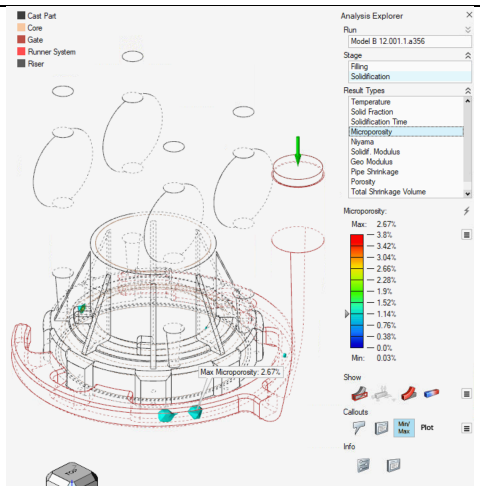

(a)

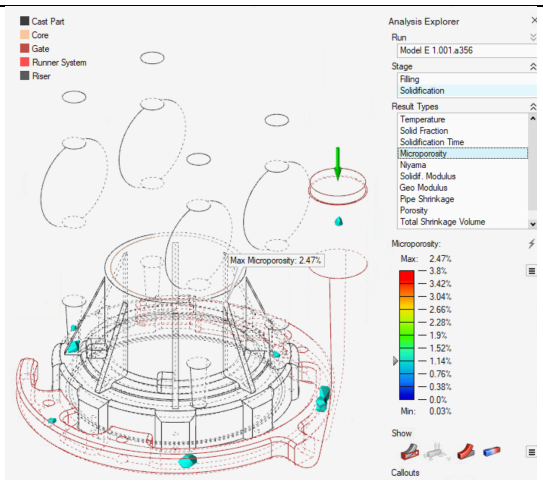

(b)

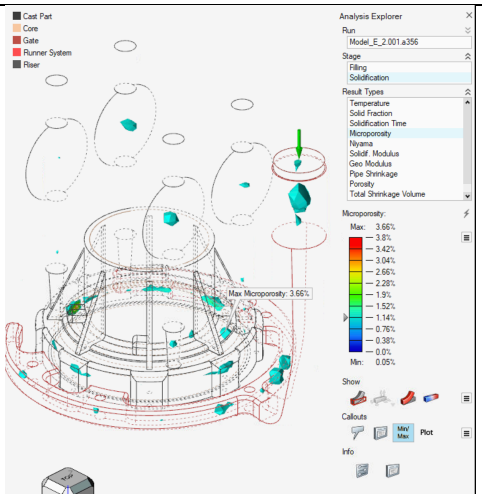

(c)

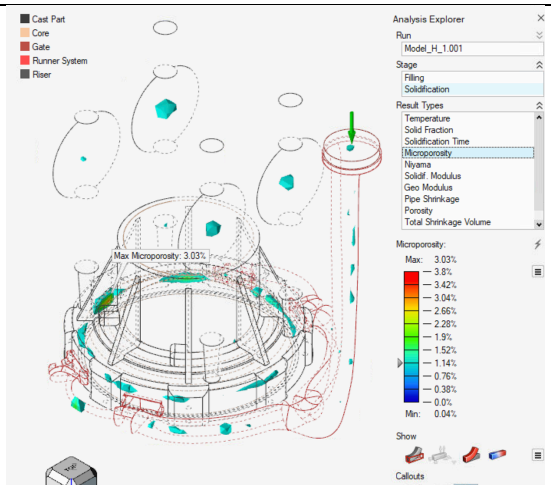

(d)

Figure 73: Microporosity Simulations - Sand Casting. Microporosity simulations of initial designs for sand casting (a) The initial design without core modification exhibited the least amount of microporosity in comparison to the model with (b) core holes at the gate entrances and (c) core hole at the sprue-runner junction. (d) Surprisingly enough, a significant increase of microporosity was observed in the GD design for sand casting.

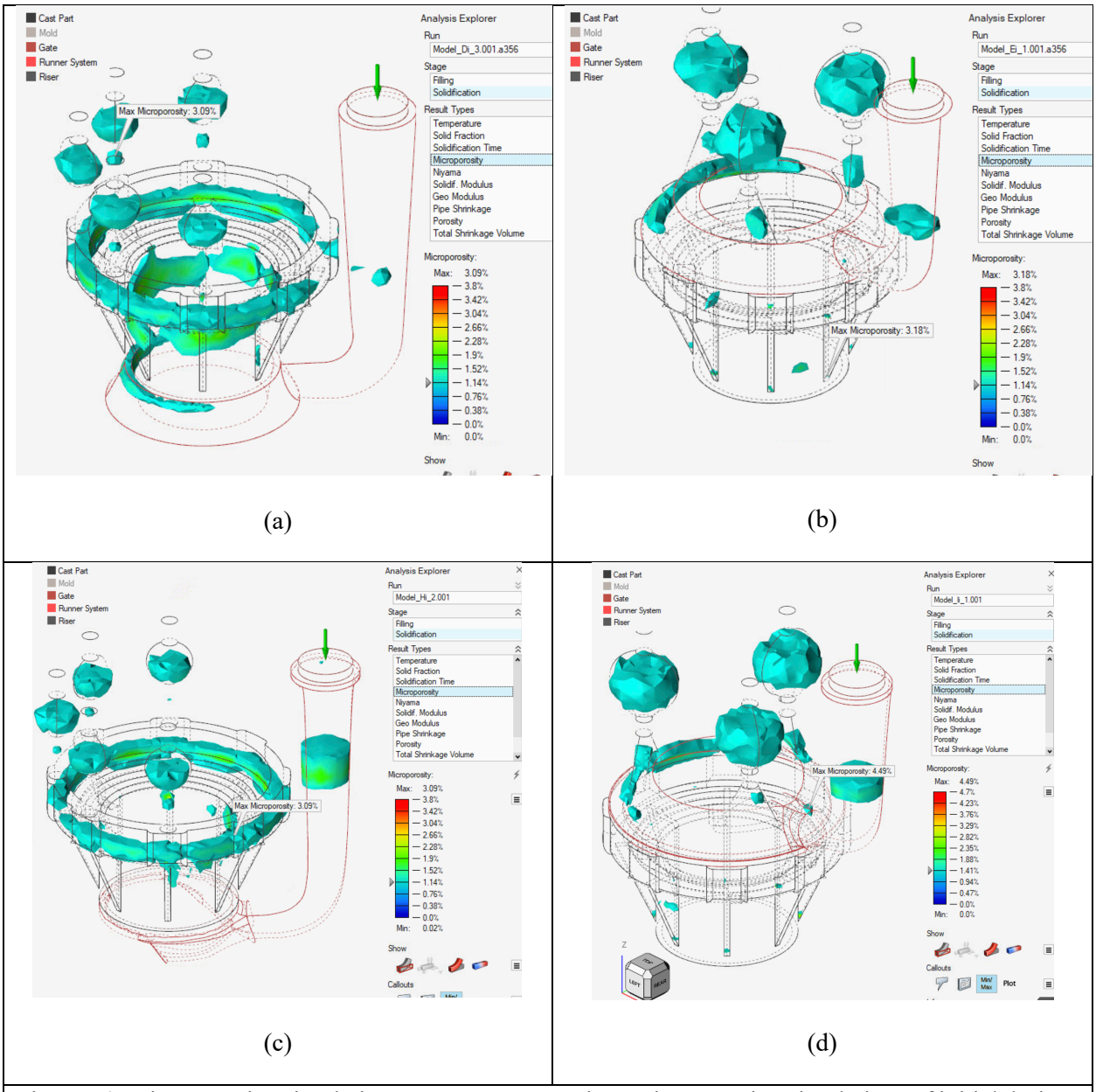

Figure 74: Microporosity Simulations - Investment Casting. Microporosity simulations of initial designs for investment casting. (a),(c) Bottom fed molds generally exhibited more porosity than the (b),(d) top fed molds. The GD top fed design exhibited the least amount of microporosity.

Shrinkage Evaluation using Niyama Simulations

As mentioned before in the THEORY section, it is favorable to have a high Niyama value because it is indicative of lower shrinkage and porosity. Figure 75 shows the highest Niyama values were exhibited in the human designed molds for sand casting. This is a notable concern for utilizing GD for casting mold

designing. However, this is the opposite case for investment casting shown in Figure 76. Higher Niyama values are exhibited in GD designed molds, which should result in lower shrinkage content.

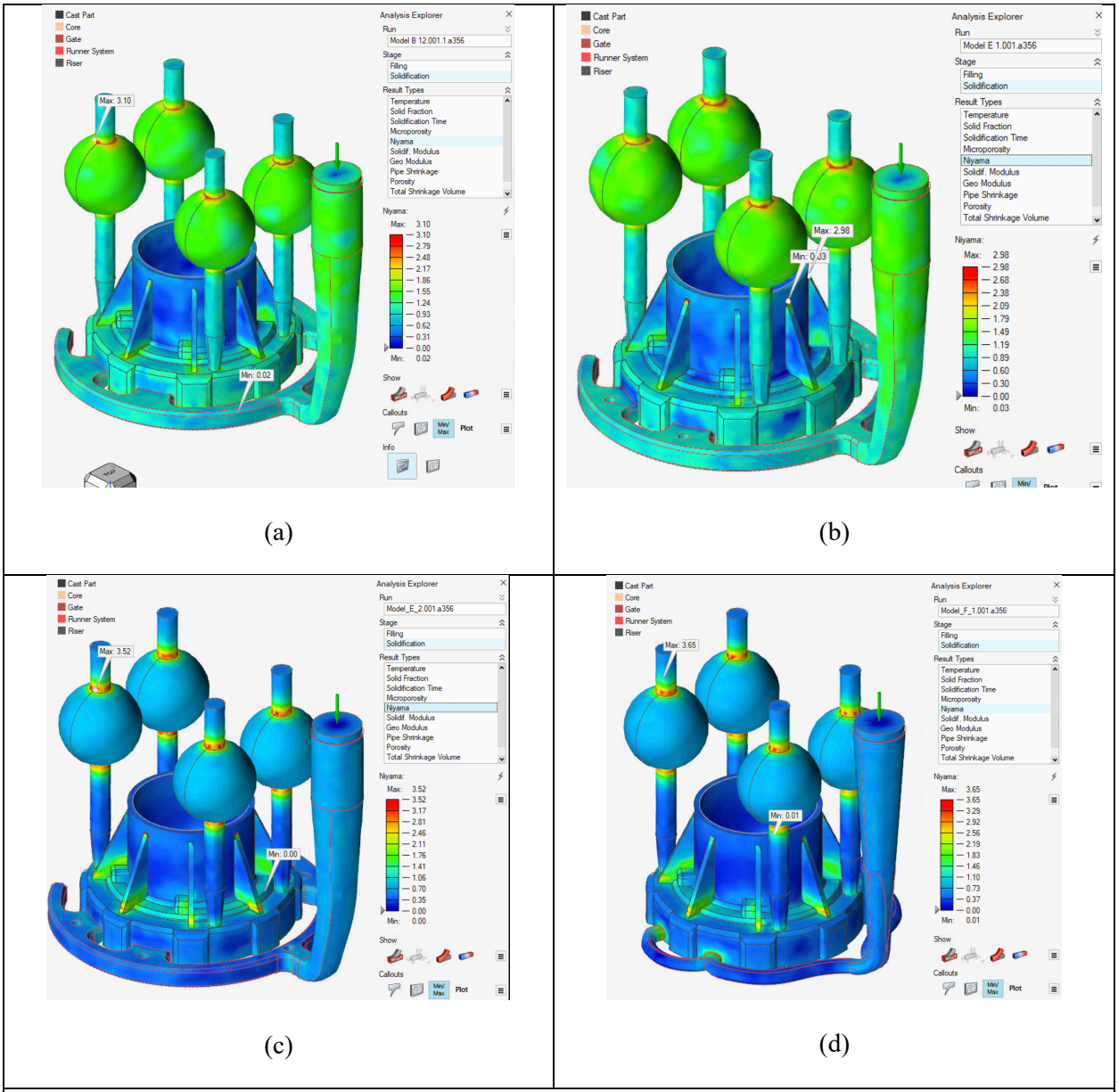

Figure 75: Niyama Criterion Simulations - Sand Casting. Niyama criterion simulations of initial designs for sand casting. (a),(b) Human designed models exhibited higher Niyama values, which was considered to be favorable to minimize shrinkage and porosity [40].

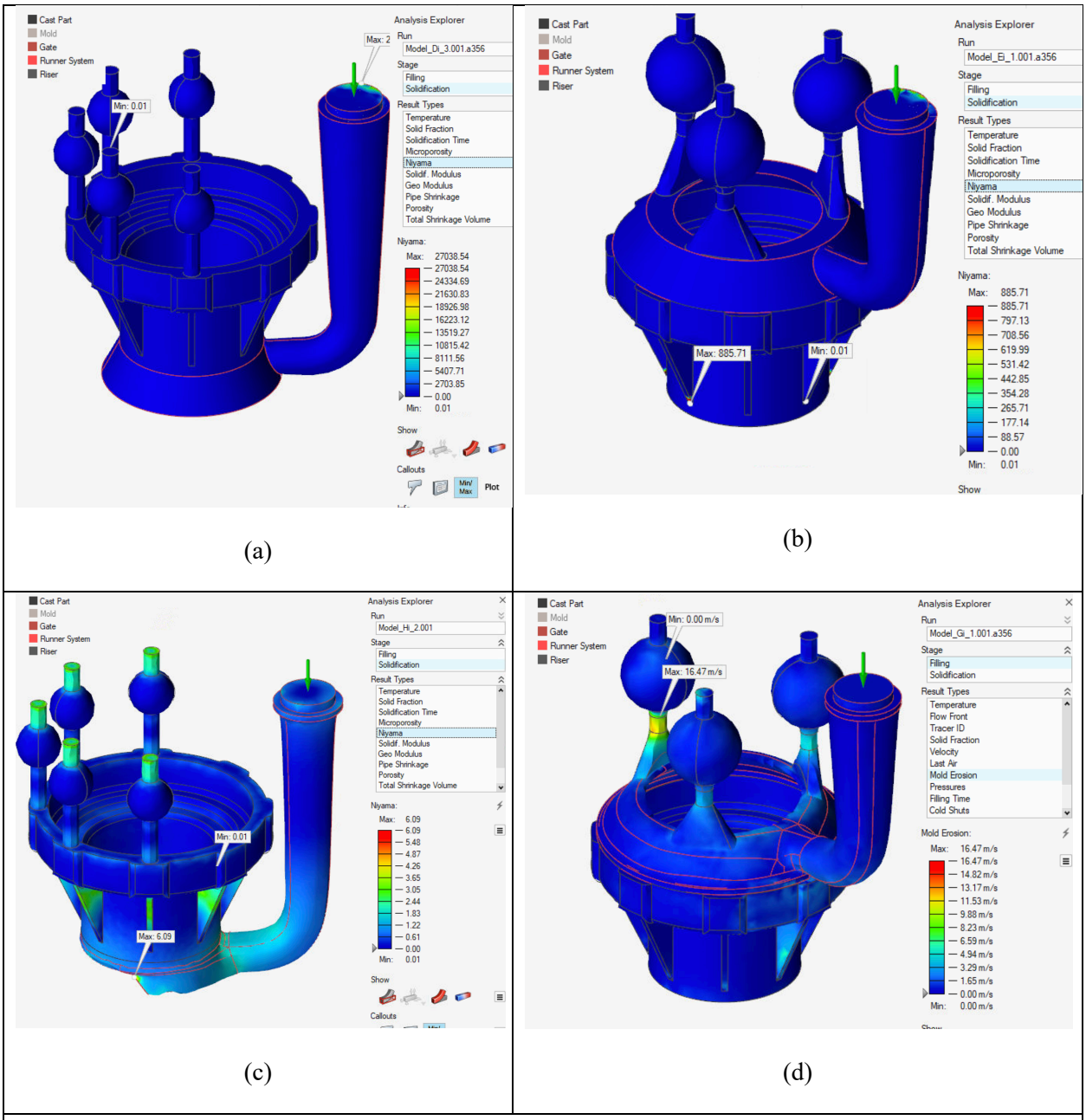

Figure 76: Niyama Criterion Simulations - Investment Casting. Niyama criterion simulations of initial designs for investment casting. (c),(d) Higher Niyama values were exhibited in the GD designs, which was considered to be favorable to minimize shrinkage and porosity [40].

CHAPTER VI

CONCLUSION

This project has demonstrated that the metal casting industry benefits markedly from modern engineering tactics using computer simulation techniques for phase prediction and thermal-fluid conditions that should be employed before additive manufacturing and real world casting operations. This increases the rate of production and improves quality output of casted products given the optimal design can be determined much quicker using these techniques, which decreases labor time. Industrial literature was referenced to improve the design of rigging systems for sand and investment casting, which is a human approach to design optimization. It was then shown that artificial intelligence can be used for design improvement that references real time fluid dynamic data. This project only scratches the surface of what can be employed in real world conditions. The next step would be to print these virtual models and administer a casting operation.

REFERENCES

[1] M. Gwyn, “Casting Design and Geometry,” in ASM Handbook Vol. 15 (Casting) - Casting Design and Performance, 2009, pp. 101–119. doi: 10.31399/asm.hb.v15.a0009020.

[2] S. Ahmed and M. K. Gupta, “Investigations on motorbike frame material and comparative analysis using generative design and topology optimization,” Mater Today Proc, pp. 1440–1446, 2022, doi: 10.1016/j.matpr.2021.12.040.

[3] Z. Jiang, H. Wen, F. Han, Y. Tang, and Y. Xiong, “Data-driven generative design for mass customization: A case study,” Advanced Engineering Informatics, vol. 54, Oct. 2022, doi: 10.1016/j.aei.2022.101786.

[4] M. Botyarov and E. E. Miller, “Partitioning around medoids as a systematic approach to generative design solution space reduction,” Results in Engineering, vol. 15, Sep. 2022, doi: 10.1016/j.rineng.2022.100544.

[5] R. H. Wilson and J.-C. Latombe, “Geometric reasoning about mechanical assembly,” Stanford, CA, 1994.

[6] B. K. Sovacool, J. C. Rogge, C. Saleta, and E. Masterson-Cox, “Transformative versus conservative automotive innovation styles: Contrasting the electric vehicle manufacturing strategies for the BMW i3 and Fiat 500e,” Environ Innov Soc Transit, vol. 33, pp. 45–60, Nov. 2019, doi: 10.1016/j.eist.2019.02.004.

[7] S. R. Sama, T. Badamo, P. Lynch, and G. Manogharan, “Novel sprue designs in metal casting via 3D sand-printing,” Addit Manuf, vol. 25, pp. 563–578, Jan. 2019, doi: 10.1016/j.addma.2018.12.009.

[8] E. Akgun, X. Zhang, T. Lowe, Y. Zhang, and M. Doré, “Fatigue of laser powder-bed fusion additive manufactured Ti-6Al-4V in presence of process-induced porosity defects,” Eng Fract Mech, vol. 259, Jan. 2022, doi: 10.1016/j.engfracmech.2021.108140.

[9] A. Mostafaei et al., “Defects and anomalies in powder bed fusion metal additive manufacturing,” Current Opinion in Solid State and Materials Science, vol. 26, no. 2. Elsevier Ltd, Apr. 01, 2022. doi: 10.1016/j.cossms.2021.100974.

[10] T. Fiegl, M. Franke, A. Raza, E. Hryha, and C. Körner, “Effect of AlSi10Mg0.4 long-term reused powder in PBF-LB/M on the mechanical properties,” Mater Des, vol. 212, Dec. 2021, doi: 10.1016/j.matdes.2021.110176.

[11] A. Soltani-Tehrani, J. P. Isaac, H. v. Tippur, D. F. Silva, S. Shao, and N. Shamsaei, “Ti-6Al-4V powder reuse in laser powder bed fusion (L-PBF): The effect on porosity, microstructure, and mechanical behavior,” Int J Fatigue, p. 107343, Oct. 2022, doi: 10.1016/j.ijfatigue.2022.107343.

[12] T. Hitchens, “Air Force To Set Up 3D Printed Supply Chain At Tinker AFB - Breaking Defense,” Breaking Defense, 2021.

[13] “GE Aviation reaches milestone with 100,000 fuel nozzle tips,” 2021. [Online]. Available: https://www.metal-am.com/mimete-and-nam-develop-

[14] “GE receives Air Force airworthiness qualification for first metal 3D-printed, critical jet engine part,” 2021.

[15] Srinath Viswanathan et al., “Casting Design and Processes,” in ASM Handbook Vol. 15 (Casting) - Casting Design and Processes, ASM International, 2009, pp. 9–36. doi: 10.31399/asm.hb.v15.a0009015.

[16] “ExOne _ Binder Jetting Technology”.

[17] A. Mostafaei et al., “Binder jet 3D printing—Process parameters, materials, properties, modeling, and challenges,” Progress in Materials Science, vol. 119. Elsevier Ltd, Jun. 01, 2021. doi: 10.1016/j.pmatsci.2020.100707.

[18] G. D. Martin, S. D. Hoath, and I. M. Hutchings, “Inkjet printing - The physics of manipulating liquid jets and drops,” J Phys Conf Ser, vol. 105, no. 1, Mar. 2008, doi: 10.1088/1742-6596/105/1/012001.

[19] D. Singh, R. Singh, and K. S. Boparai, “Development and surface improvement of FDM pattern based investment casting of biomedical implants: A state of art review,” Journal of Manufacturing Processes, vol. 31. Elsevier Ltd, pp. 80–95, Jan. 01, 2018. doi: 10.1016/j.jmapro.2017.10.026.

[20] H. W. Stoll, “Casting Design Issues and Practices,” in ASM Handbook Vol. 15 (Casting) - Casting Design Issues and Practices, ASM International, 2009, pp. 1–8. doi: 10.31399/asm.hb.v15.a0009014.

[21] “Design Problems Involving Uniform Sections,” in ASM Hanbook Vo. 15 (Casting) - Design Problems Involving Uniform Sections, ASM International, 2009, pp. 133–138. doi: 10.31399/asm.hb.v15.a0009022.

[22] Properties and Selection: Nonferrous Alloys and Special-Purpose Materials, vol. ASM Handbook Vol. 15. ASM International, 1990. doi: 10.31399/asm.hb.v02.9781627081627.

[23] J. Campbell, “Dimensional Accuracy,” in Complete Casting Handbook, Elsevier, 2015, pp. 893–926. doi: 10.1016/b978-0-444-63509-9.00018-2.

[24] “Design Problems Involving Distortion,” in ASM Handbook Vol. 15 (Casting) - Design Problems Involving Distortion, ASM International, 2009, pp. 155–161. doi: 10.31399/asm.hb.v15.a0009025.

[25] J. Campbell, “The 10 Rules for Good Castings,” in Complete Casting Handbook, Elsevier, 2015, pp. 535–638. doi: 10.1016/b978-0-444-63509-9.00010-8.

[26] E. J. Paul DeGarmo T Black Ronald A Kohser Solutions Manual by Barney E Klamecki, “Solutions Manual to Accompany MATERIALS AND PROCESS IN MANUFACTURING Ninth Edition,” 2003.

[27] “Design Problems Involving Junctions,” in ASM Hanbook Vo. 15 (Casting) - Design Problems Involving Junctions, ASM International, 2009, pp. 147–153. doi: 10.31399/asm.hb.v15.a0009024.

[28] “Design Problems Involving Thin Sections,” in ASM Hanbook Vo. 15 (Casting) - Design Problems Involving Thin Section, ASM International, 2009, pp. 121–132. doi: 10.31399/asm.hb.v15.a0009021.

[29] J. Campbell, “Complete Casting Handbook, Second Edition Metal Casting Processes, Metallurgy, Techniques and Design - Chapter 1: The Melt,” in Complete Casting Handbook, Elsevier, 2015, pp. 3–15. doi: 10.1016/b978-0-444-63509-9.00001-7.

[30] Richard J. Fruehan and Prince N. Anyalebechi, “Gases in Metals,” in ASM Handbook Vol. 15 (Casting) - Gasses in Metals, ASM International, 2009, pp. 64–73. doi: 10.31399/asm.hb.v15.a0005192.

[31] J. M. Zeng, L. W. Tang, and S. Y. Lin, “Experimental study on hydrogen diffusion in molten aluminum,” 2013.

[32] K. Richardson, “Using Casting Simulation to Ensure Better-Quality Pumps and Valves,” American Institute of Chemical Egngineers, 2013.

[33] “Riser Design,” in ASM Handbook Vol. 15 (Casting) - Riser Design, ASM International, 2009, pp. 61–72. doi: 10.31399/asm.hb.v15.a0009016.

[34] A. L. Kearney, “Properties of Cast Aluminum Alloys,” in ASM Metals Handbook Vol. 2 - Properties and Selection: Nonferrous Alloys and Special-Purpose Materials, ASM International, 2018, pp. 152–177. doi: 10.31399/asm.hb.v02.a0001062.

[35] “Gating Design,” in ASM Handbook Vol. 15 (Casting) - Gating Design, ASM International, 2009, pp. 73–80. doi: 10.31399/asm.hb.v15.a0009017.

[36] Q. Han and S. Viswanathan, “Microstructure Prediction in A356 Alloy Castings.”

[37] M. O. Shabani and A. Mazahery, “Prediction of mechanical properties of cast A356 alloy as a function of microstructure and cooling rate,” Archives of Metallurgy and Materials, vol. 56, no. 3, pp. 671–675, 2011, doi: 10.2478/v10172-011-0073-1.

[38] Guang Ran, Jingen Zhou, and Q.G. Wang, “The Effect of Hot Isotactic Pressing on the Microstructure and Tensile Properties of an Unmodified A356-T6 Cast Aluminum Alloy,” 2005.

[39] N. Jain, K. D. Carlson, and C. Beckermann, “Round Robin Study to Assess Variations in Casting Simulation Niyama Criterion Predictions,” 2007.

[40] K. D. Carlson and C. Beckermann, “Use of the Niyama Criterion To Predict Shrinkage-Related Leaks in High-Nickel Steel and Nickel-Based Alloy Castings,” 2008.

[41] E. Clouet, “Modeling of Nucleation Processes,” in Fundamentals of Modeling for Metals Processing, ASM International, 2018, pp. 203–219. doi: 10.31399/asm.hb.v22a.a0005410.

[42] R. Kobayashi, “Modeling and numerical simulations of dendritic crystal growth,” 1993.

[43] A. Ito, N. Kenmochi, and N. Yamazaki, “A Phase-Field Model of Grain Boundary Motion,” 2008.

[44] T. F. Flint, Y. L. Sun, Q. Xiong, M. C. Smith, and J. A. Francis, “Phase-Field Simulation of Grain Boundary Evolution In Microstructures Containing Second-Phase Particles with Heterogeneous Thermal Properties,” Sci Rep, vol. 9, no. 1, Dec. 2019, doi: 10.1038/s41598-019-54883-8.

[45] D. Mukherjee, H. Larsson, and J. Odqvist, “Phase field modelling of diffusion induced grain boundary migration in binary alloys.,” Comput Mater Sci, vol. 184, p. 109914, Nov. 2020, doi: 10.1016/J.COMMATSCI.2020.109914.

[46] B. Echebarria, R. Folch, A. Karma, and M. Plapp, “Quantitative phase-field model of alloy solidification,” Phys Rev E Stat Phys Plasmas Fluids Relat Interdiscip Topics, vol. 70, no. 6, p. 22, 2004, doi: 10.1103/PhysRevE.70.061604.

[47] L. Wu et al., “A new method for computing the anisotropic free energy of the crystal-melt interface,” Comput Mater Sci, vol. 210, Jul. 2022, doi: 10.1016/j.commatsci.2022.111481.

[48] M. M. Makhlouf and H. v Guthy, “The aluminum-silicon eutectic reaction: mechanisms and crystallography.” [Online]. Available: www.elsevier.com/locate/lightmetals

[49] Ch.-A. Gandin and I. Steinbach, “Direct Modeling of Structure Formation,” in ASM Handbook Vo. 15 (Casting) - Direct Modeling of Structure Formation, ASM International, 2009, pp. 435–444. doi: 10.31399/asm.hb.v15.a0005236.

[50] N. T. Brown, E. Martinez, and J. Qu, “Interfacial free energy and stiffness of aluminum during rapid solidification,” Acta Mater, vol. 129, pp. 83–90, May 2017, doi: 10.1016/j.actamat.2017.02.033.

[51] D. A. Kessler, J. Koplik, and H. Levine, “Geometrical models of interface evolution. III. Theory of dendritic growth,” 1985.

[52] Mark Horstemeyer, “Integrated Computational Materials Engineering (ICME) for Metals: Using Multiscale Modeling to Invigorate Engineering Design with Science - Phase-field methods,” pp. 229–232, 2012.

[53] R. Yan, S. D. Ma, W. Z. Sun, T. Jing, and H. B. Dong, “The solid–liquid interface free energy of Al: A comparison between molecular dynamics calculations and experimental measurements,” Comput Mater Sci, vol. 184, Nov. 2020, doi: 10.1016/j.commatsci.2020.109910.

[54] Reza Abbaschian, Lara Abbaschian, and Robert E. Reed-Hill, “Physical Metallurgy Principles,” 2009.

[55] Porter D. A., Easterling K. E., and Sherif M. Y., “Phase Transformations in Metals and Alloys Third Edition, Solidification,” 2009.

[56] Porter D. A., Easterling K. E., and Sherif M. Y., “Phase Transformations in Metals and Alloys,” 2009.

[57] F. Delannay, L. Froyen, and A. Deruyttere, “The wetting of solids by molten metals and its relation to the preparation of metal-matrix composites,” 1987.

[58] J. Campbell, “Complete Casting Handbook, Second Edition Metal Casting Processes, Metallurgy, Techniques and Design - Chapter 2: Entrainment,” in Complete Casting Handbook, Elsevier, 2015, pp. 17–90. doi: 10.1016/B978-0-444-63509-9.00002-9.

[59] B. G. Thomas and M. Bellet, “Modeling of Stress, Distortion, and Hot Tearing,” in ASM Handbook Vo. 15 (Casting) - Modeling of Stress, Distortion, and Hot Tearing, ASM International, 2009, pp. 449–461. doi: 10.31399/asm.hb.v15.a0005238.

[60] A. T. Dinsdale and P. N. Quested, “The viscosity of aluminium and its alloys - A review of data and models,” in Journal of Materials Science, Dec. 2004, vol. 39, no. 24, pp. 7221–7228. doi: 10.1023/B:JMSC.0000048735.50256.96.

[61] A. L. Kearney, “Properties of Cast Aluminum Alloys,” in Properties and Selection: Nonferrous Alloys and Special-Purpose Materials, ASM International, 2018, pp. 152–177. doi: 10.31399/asm.hb.v02.a0001062.

[62] Y. Birol and Y. Birol, “Production of Al-7Si-0.3Mg slurry for Rheocasting via internal cooling of the melt below the liquidus temperature,” 2009. [Online]. Available: https://www.researchgate.net/publication/286723887

VITA

Mikael Andrew Garcia

Candidate for the Degree of

Master of Science

Thesis: MODERN PROCESS PLANNING FOR ADDITIVE MANUFACTURING ASSISTED A356 ALUMINUM CASTING

Major Field: Materials Science and Engineering

Biographical:

Education:

Completed the requirements for the Master of Science in Materials Science and Engineering at Oklahoma State University, Stillwater, Oklahoma in May, 2023.

Completed the requirements for the Bachelor of Science in Mechanical Engineering at University of Texas at El Paso, El Paso, Texas in 2019.

Completed the requirements for the Bachelor of Science in Metallurgical and Materials Engineering at University of Texas at El Paso, El Paso, Texas in 2017.

Professional Memberships:

Material Advantage, 2014-2019

American Foundry Society, 2014-Present